High-Energy-Density Astrophysics in the Laboratory

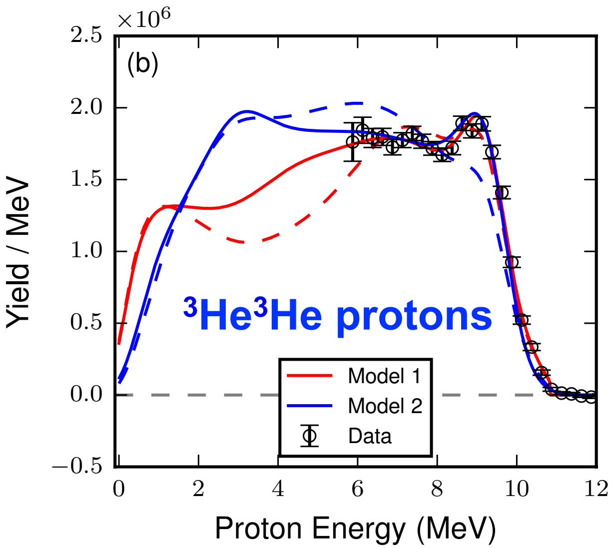

Plasma Nuclear Science

Hydrodynamic Instabilities

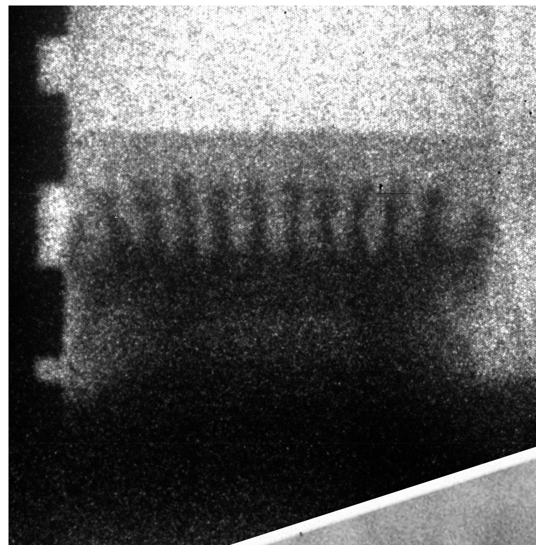

Pair Plasmas

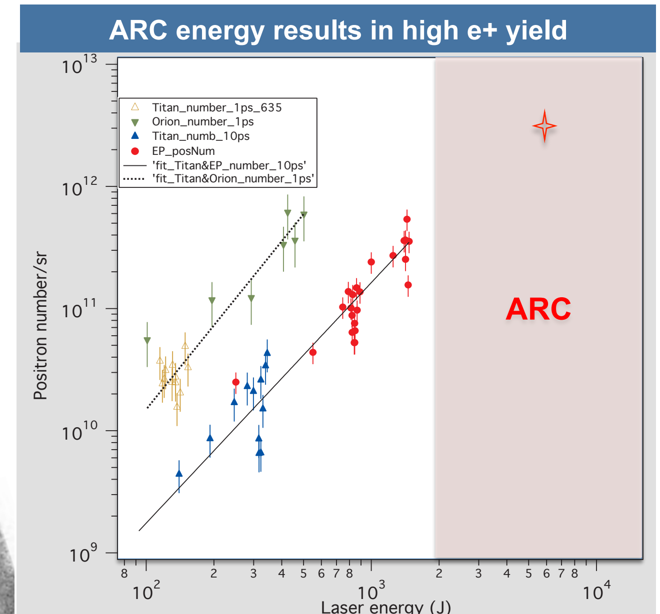

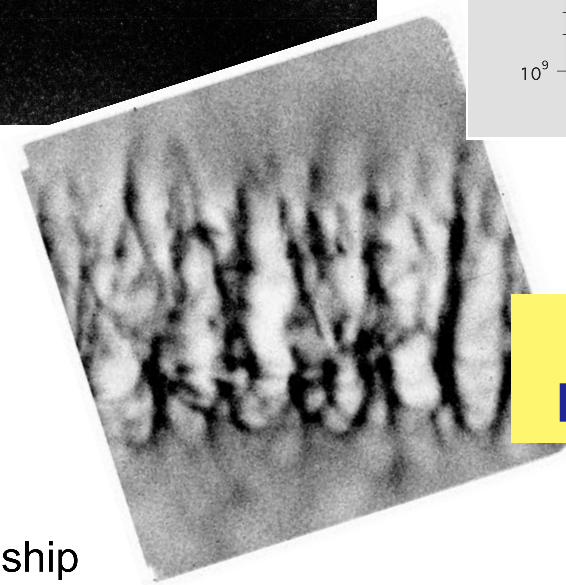

Magneto-Hydrodynamics

Mario Manuel
General Atomics

Science Undergraduate Laboratory Internship
June 15th, 2017

Laboratory experiments provide a complimentary technique to investigate some astrophysical systems

- High-power laser facilities provide a versatile environment to generate physical conditions similar to those in multiple astrophysical systems

- Laboratory results are directly scalable when similarity and geometric conditions hold between the two systems

- Experiments also allow for detailed benchmark comparisons with numerical calculations in relevant dynamic regimes

Outline

- High-Energy-Density (HED) Plasma
  - US facilities

Zylstra et al. (LANL)

- Plasma Nuclear Science using ICF-like implosions
  - p-p chain at relevant Gamow energies

Drake, Kuranz et al. (UM)

- Laser-produced Magnetohydrodynamics
  - similarity conditions
  - Rayleigh-Taylor growth in core-collapse SNe

Park, Huntington et al. (LLNL) ←

- Laser-produced Jets
  - 'collisionless' shocks
  - supersonic jet dynamics

→ Manuel, et al. (GA)

Chen et al. (LLNL)

- Pair-Plasma Production
  - relativistic jets

- Summary

High-energy-density (HED) physics involves the study of systems having pressures > 1 Mbar

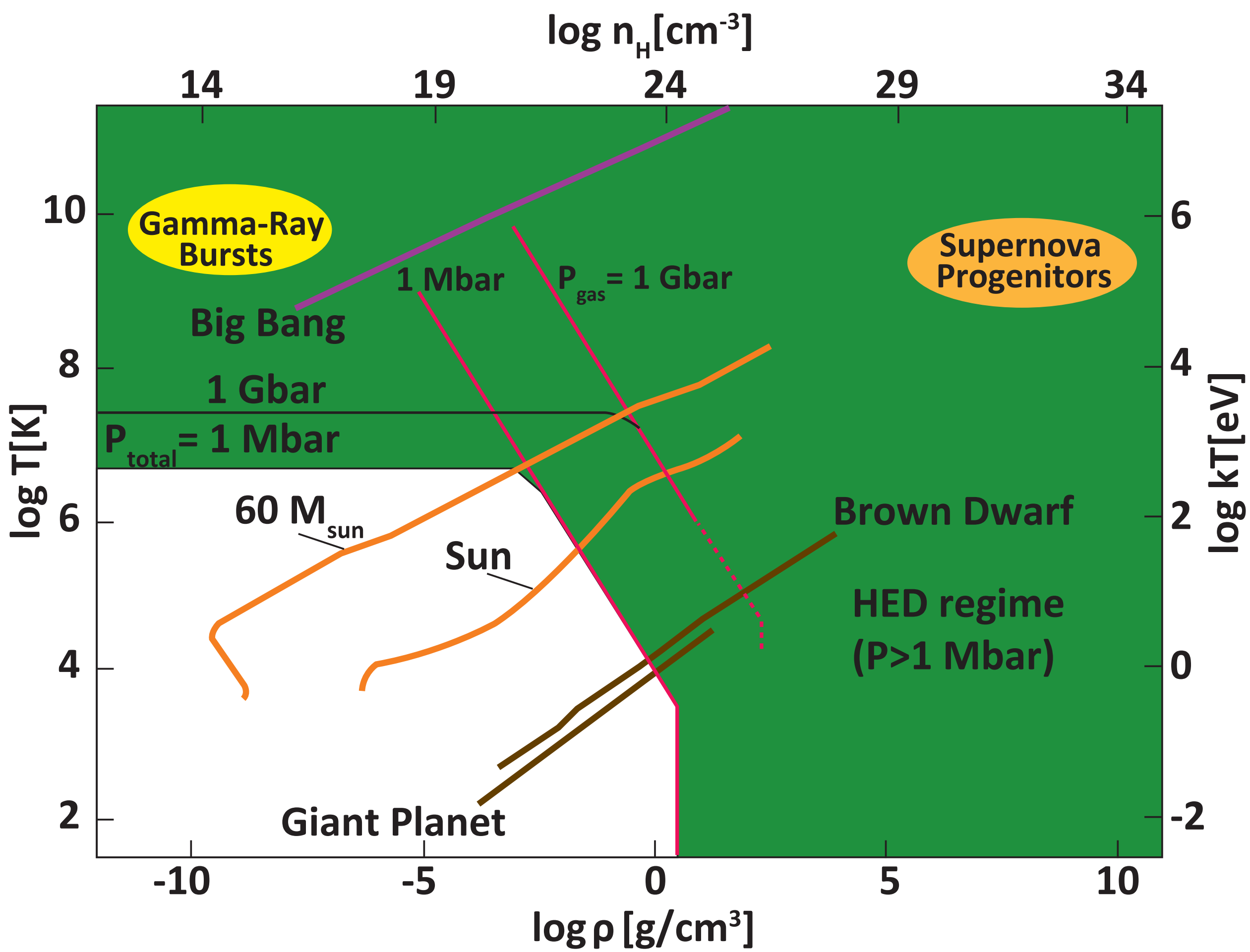

*Adapted from NRC committee on HEDP (2003)

Present-day laser facilities access a unique region in HED-relevant parameter space

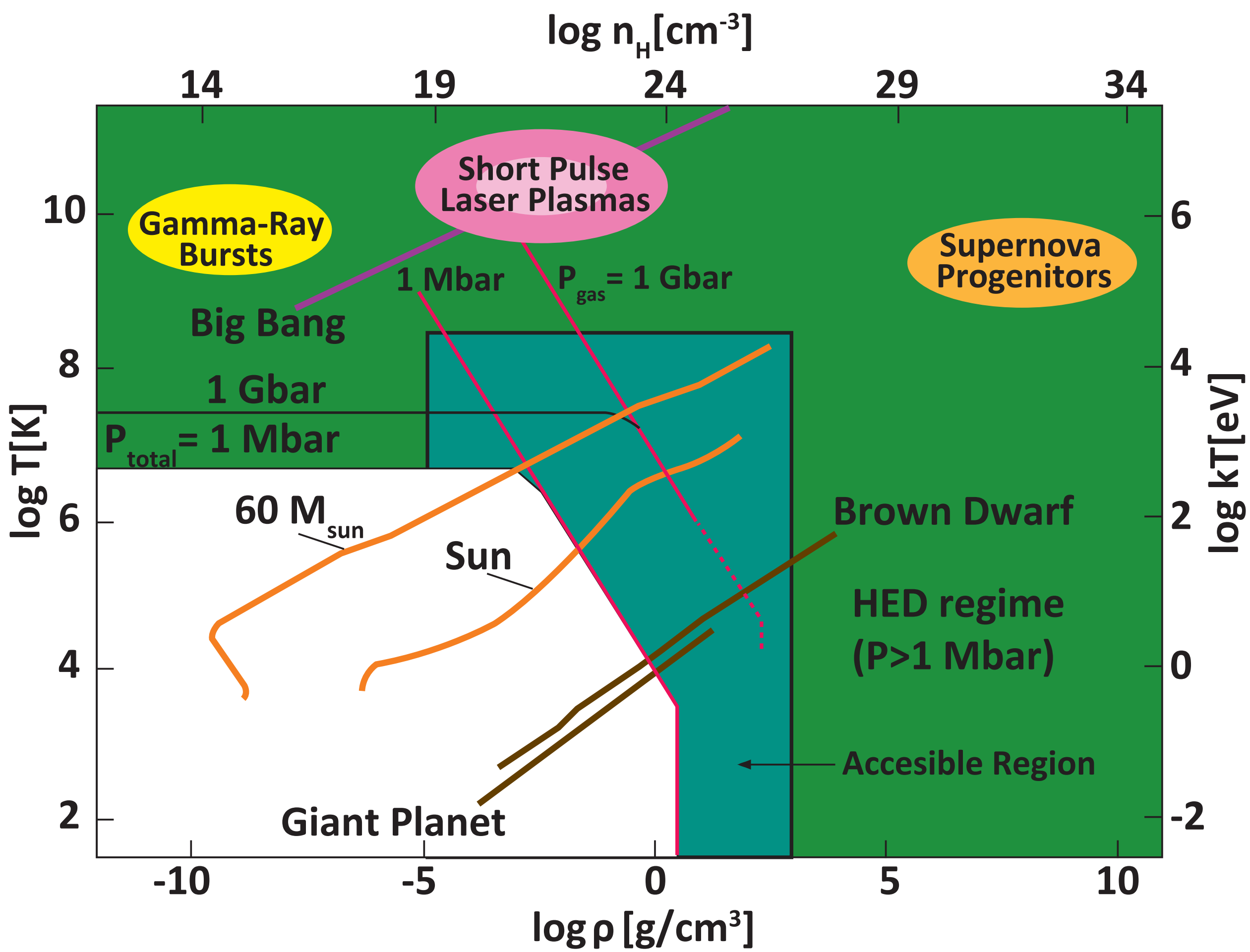

*Adapted from NRC committee on HEDP (2003)

Many experiments take place at the Omega Laser Facility

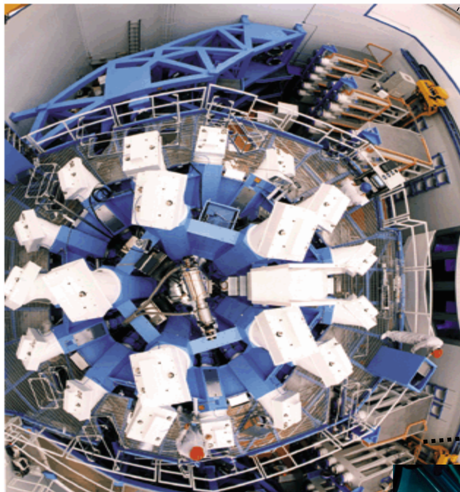

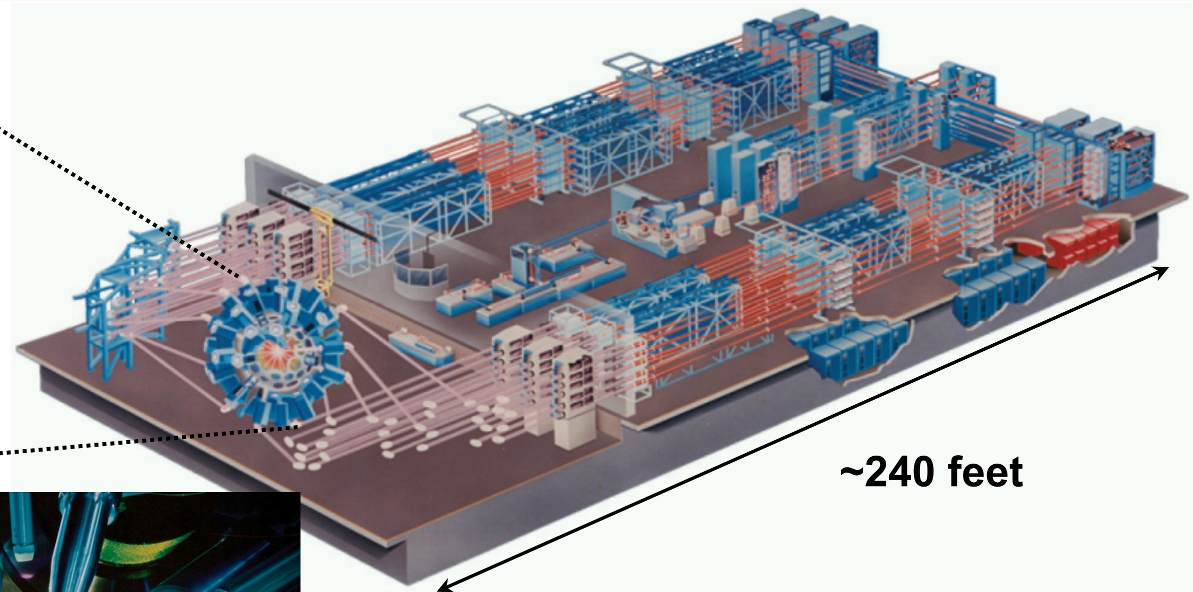

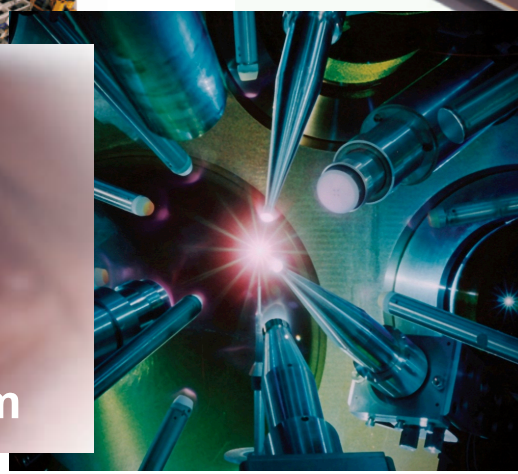

- **60 laser beams**
- **30 kJ on target ~1 ns (~30 TW)**
- **flexible laser pulses and timing**
- **Shot cycle ~1/hr**
- **1-2% irradiation nonuniformity**

---

*Boehly, Optics Comm. 133 (1997)

Next-gen experiments take place at the National Ignition Facility

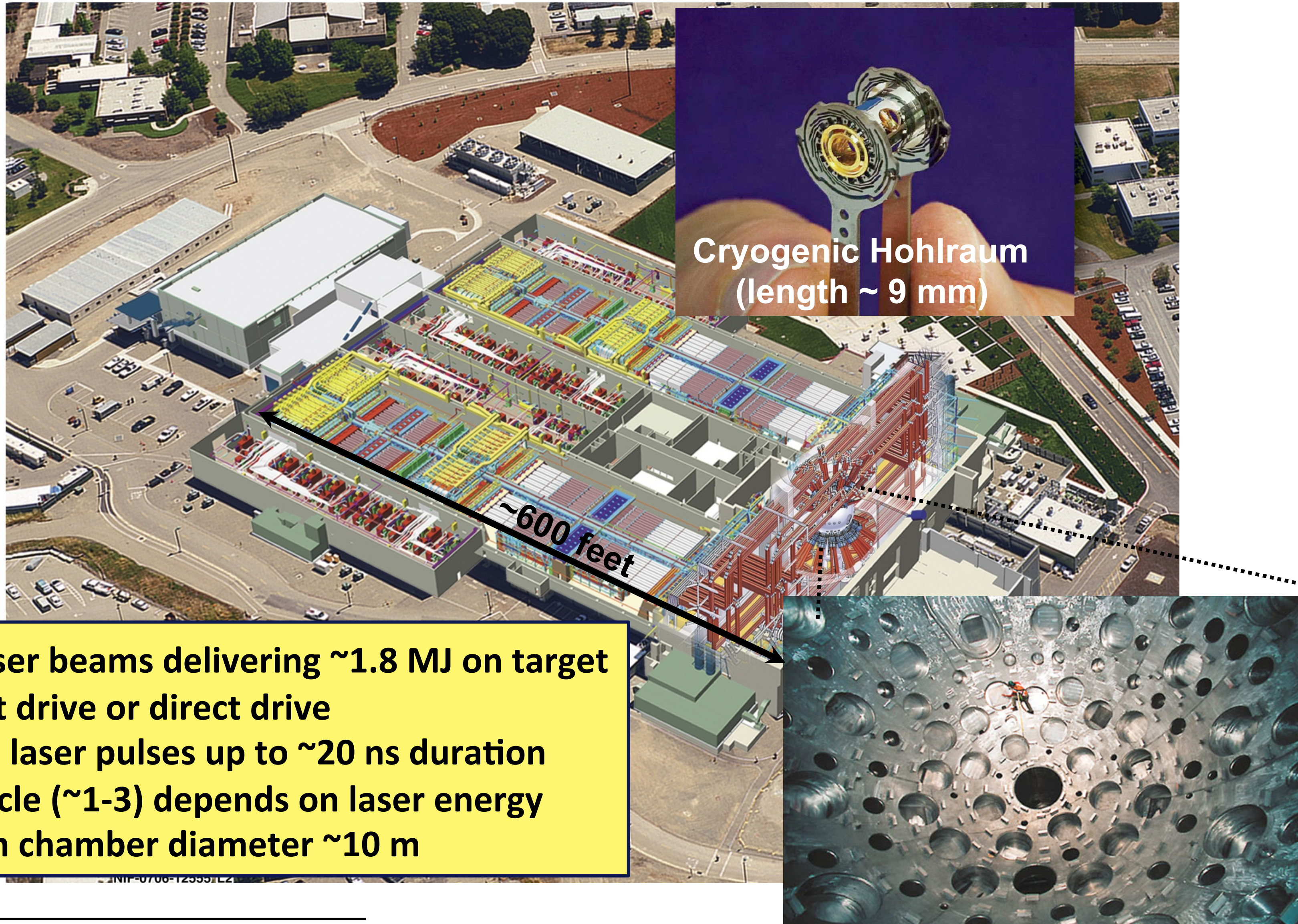

- 192 laser beams delivering ~1.8 MJ on target
- Indirect drive or direct drive
- flexible laser pulses up to ~20 ns duration
- shot cycle (~1-3) depends on laser energy
- vacuum chamber diameter ~10 m

*Miller, Nuclear Fusion 44 (2004)

Outline

- High-Energy-Density (HED) Plasma
  - US facilities

Zylstra et al. (MIT)

- Plasma Nuclear Science using ICF-like implosions
  - p-p chain at relevant Gamow energies

Drake, Kuranz et al. (UM)

- Laser-produced Magnetohydrodynamics
  - similarity conditions
  - Rayleigh-Taylor growth in core-collapse SNe

Park, Huntington et al. (LLNL) ← 'collisionless' shocks

Manuel, Kuranz et al. (UM) ← supersonic jet dynamics

- Laser-produced Jets
  - 'collisionless' shocks
  - supersonic jet dynamics

Chen et al. (LLNL)

- Pair-Plasma Production
  - relativistic jets

- Summary

Inertial fusion utilizes high-power lasers to implode a capsule of DT fuel to ρ~1000 g/cc and T~5 keV

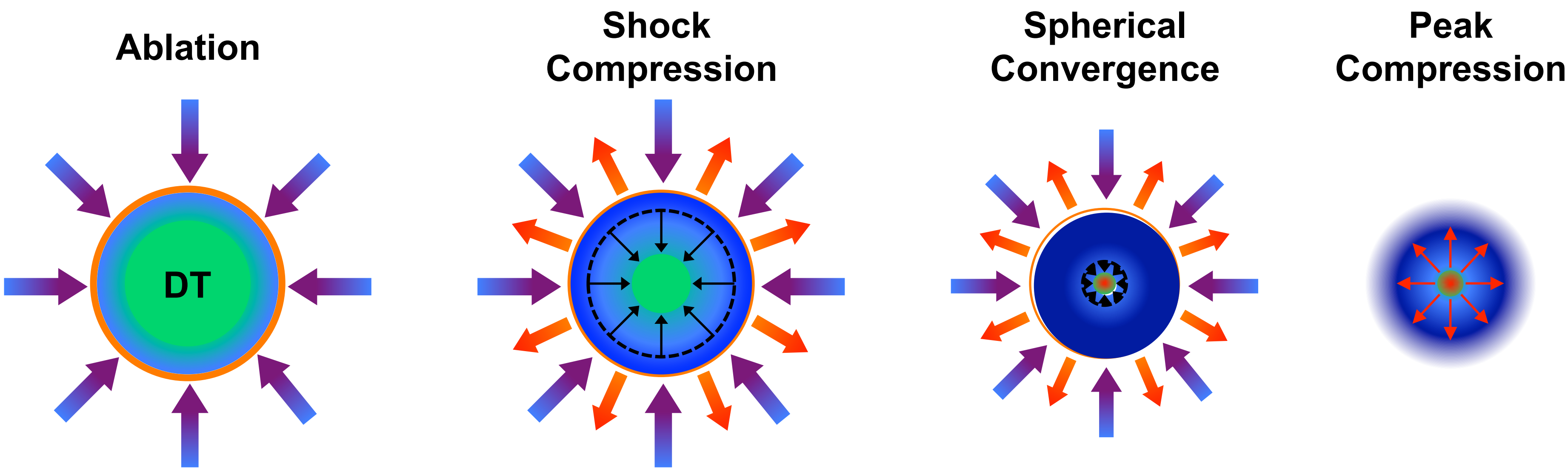

ICF requires precise understanding of many different physics processes:

- laser-plasma interactions
- hydrodynamic instabilities and shock propagation
- nuclear reactions in HED environments
- …

In contrast to accelerators, ICF facilities provide an environment for nuclear reactions in thermalized plasma

Accelerator

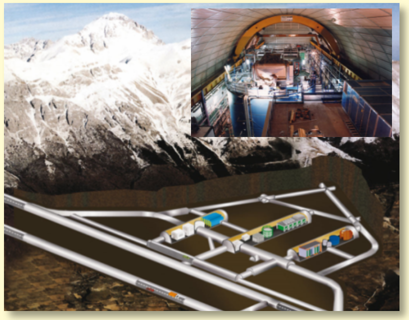

Target

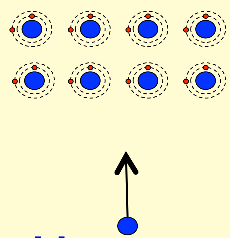

Ions
Electrons

Accelerated ion

- **Monoenergetic beam ions**
- **Bound electron screening**

Plasma

- **Thermal ions**
- **Debye electron screening**

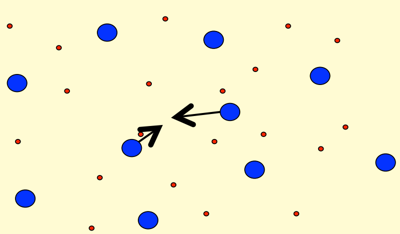

Ions
Electrons

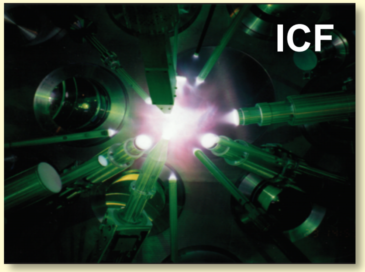

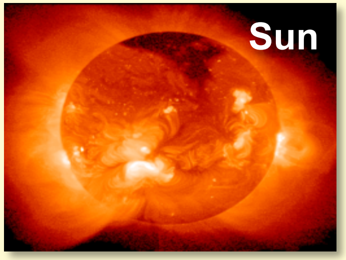

	ICF	Sun
Density:	**0.1 – 1000 g/cc**	**160 g/cc (core)**
Temperature:	**1 – 20 keV**	**1.3 keV (core)**
Mass:	**0.1 µg – 1 mg**	**2×10^{33} g**
Time (s):	**10^{-10} s**	**3×10^{17} s**

* M. Aliotta *et al*, NP A (2001), U. Schröder *et al*, NIM B (1989), H. J. Assenbaum *et al*, ZP (1987)

Laser-generated plasmas are created at similar densities and temperatures as those in stellar cores

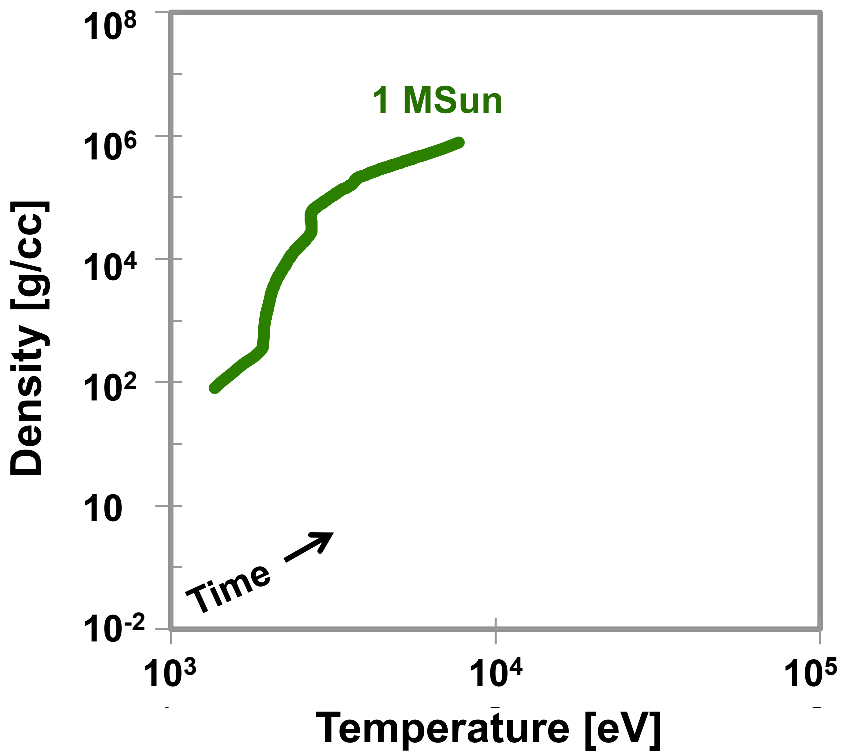

* Stellar evolution simulations by Dave Dearborn, NIF Simulations Harry Robey and Bob Tipton, OMEGA Simulation P. B. Radha

Laser-generated plasmas are created at similar densities and temperatures as those in stellar cores

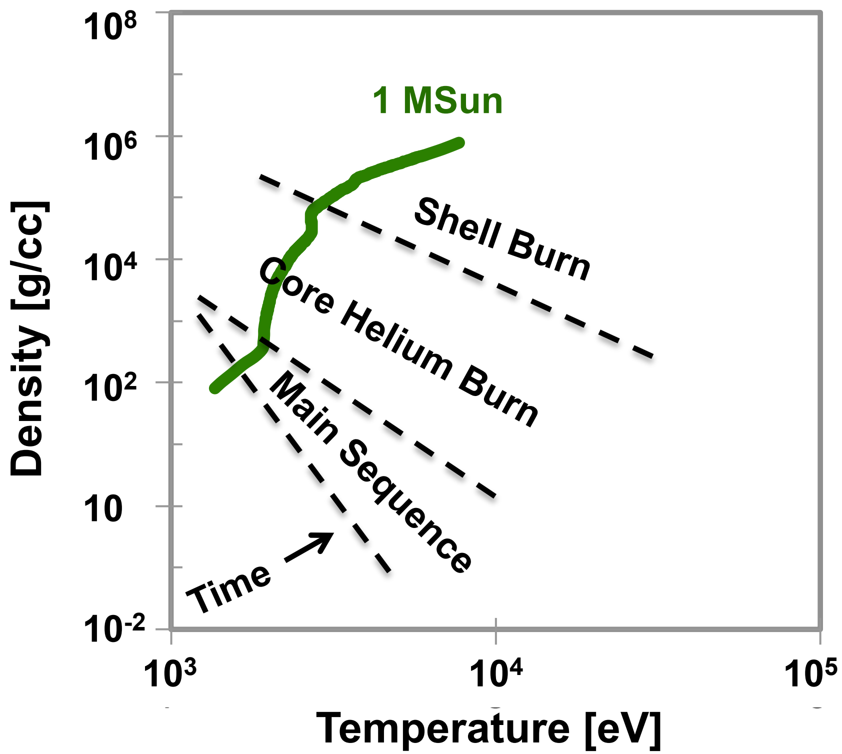

* Stellar evolution simulations by Dave Dearborn, NIF Simulations Harry Robey and Bob Tipton, OMEGA Simulation P. B. Radha

Laser-generated plasmas are created at similar densities and temperatures as those in stellar cores

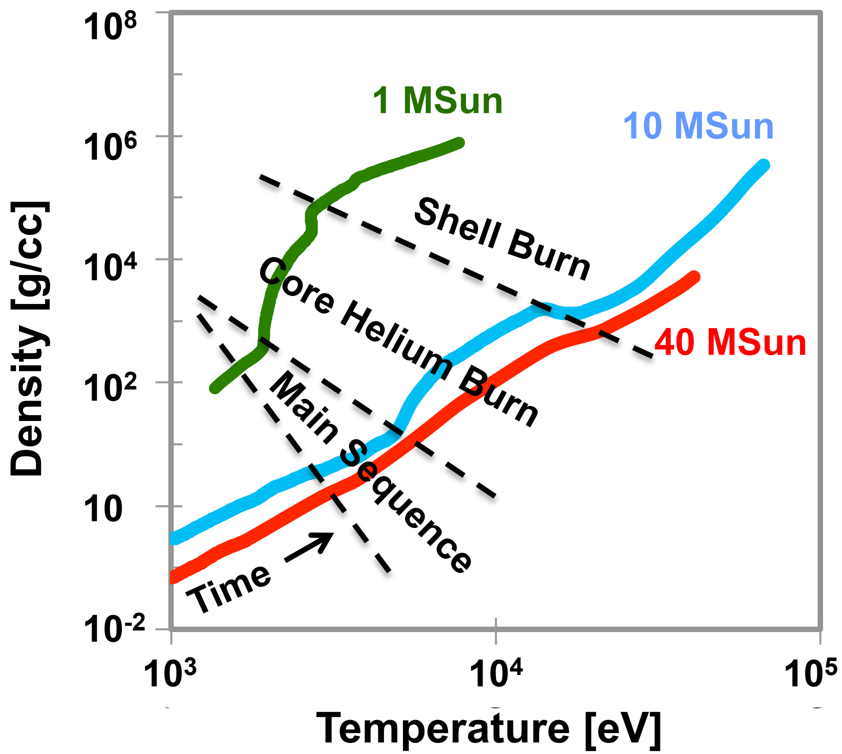

* Stellar evolution simulations by Dave Dearborn, NIF Simulations Harry Robey and Bob Tipton, OMEGA Simulation P. B. Radha

Laser-generated plasmas are created at similar densities and temperatures as those in stellar cores

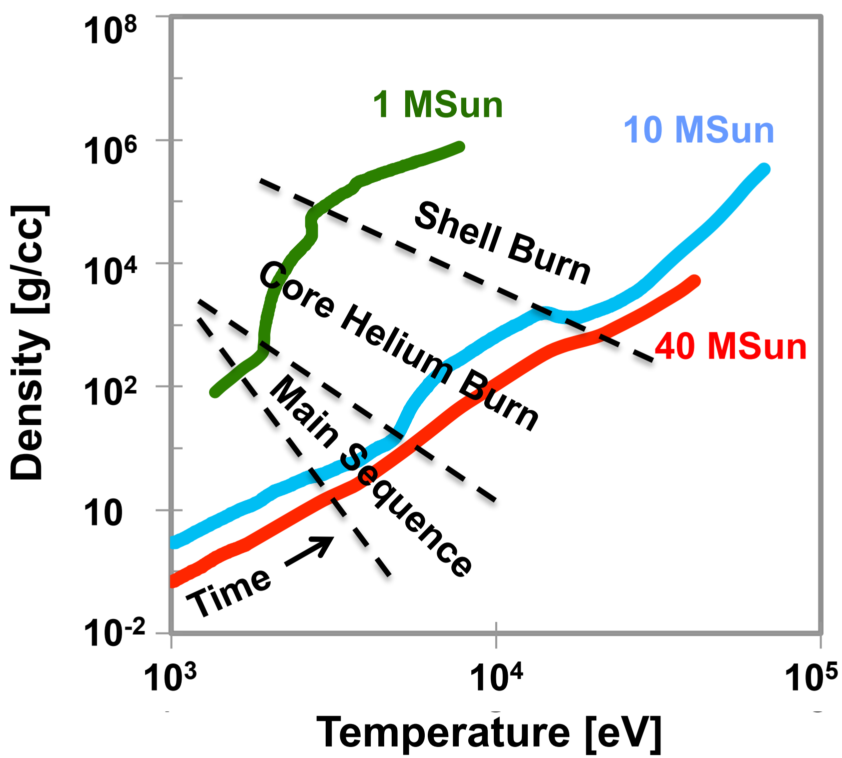

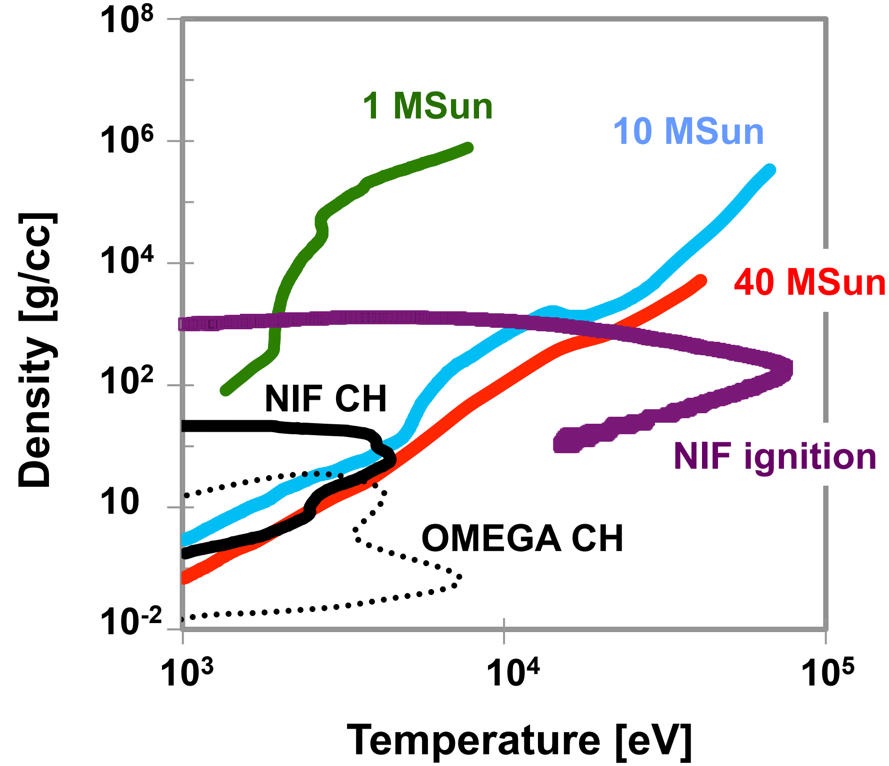

* Stellar evolution simulations by Dave Dearborn, NIF Simulations Harry Robey and Bob Tipton, OMEGA Simulation P. B. Radha

The Gamow energy for $^{3}He+^{3}He$ fusion in the sun is ~22 keV at T~1.3 keV at densities of ~160 g/cc

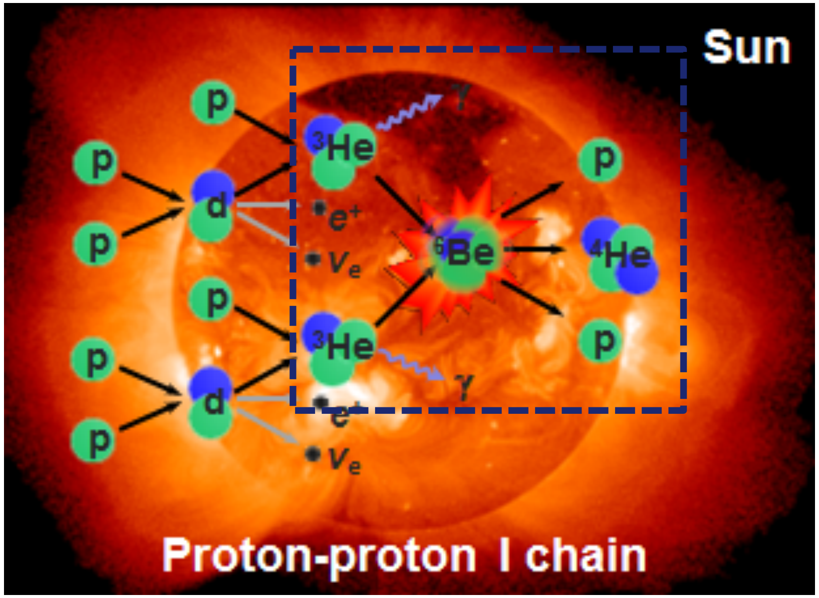

T_i ~ 1.3 keV
E_G ~ 22 keV
ρ = 160 g/cc

$E_G(^{3}He+^{3}He) \approx 18.1 \times Ti^{0.67}$ [keV]

The measured $^3He+^3He$ proton spectrum displays multiple reaction channels at a Gamow energy of ~165 keV

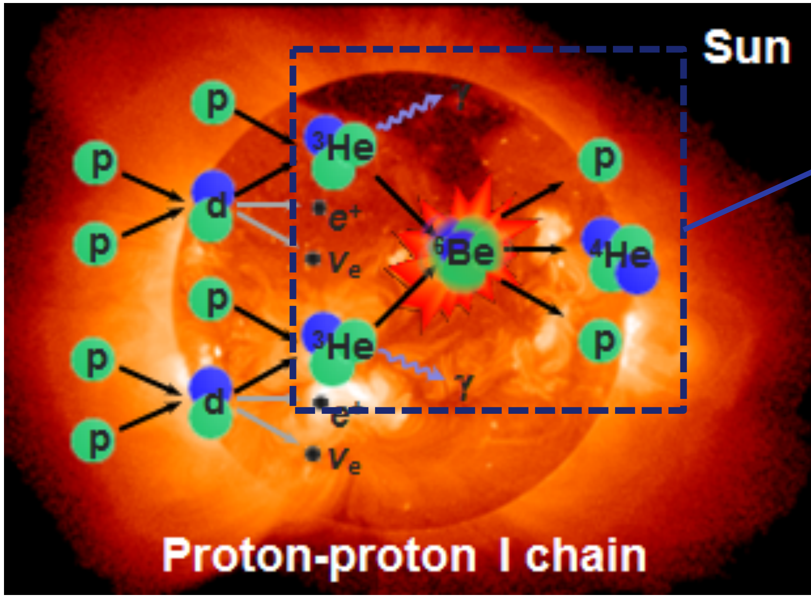

$^3He + ^3He$	→	^4He + 2p (0-10.8 MeV)
	→	^5Li + p (9.2 MeV)
	→	$^5Li^*$ + p

T_i ~ 1.3 keV
E_G ~ 22 keV
ρ = 160 g/cc

T_i ~ 27 keV
E_G ~ 165 keV
ρ = 0.1 g/cc

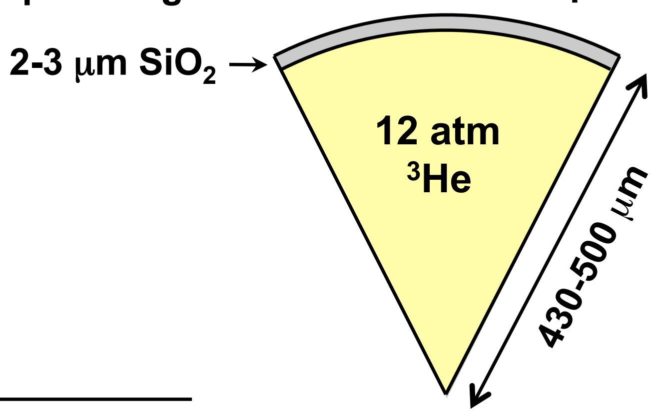

$E_G(^3He+^3He) \approx 18.1 \times Ti^{0.67}$ [keV]

The measured $^3He+^3He$ proton spectrum displays multiple reaction channels at a Gamow energy of ~165 keV

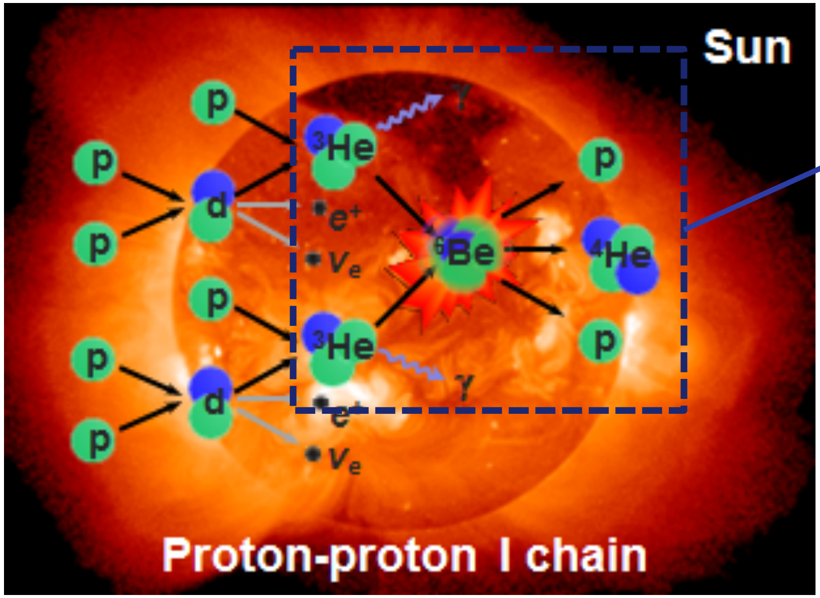

$^3He + ^3He$	→	^4He + 2p (0-10.8 MeV)
	→	^5Li + p (9.2 MeV)
	→	$^5Li^*$ + p

T_i ~ 1.3 keV
E_G ~ 22 keV
ρ = 160 g/cc

T_i ~ 27 keV
E_G ~ 165 keV
ρ = 0.1 g/cc

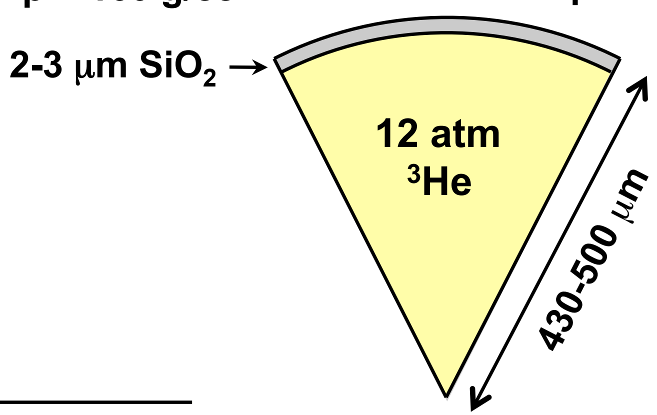

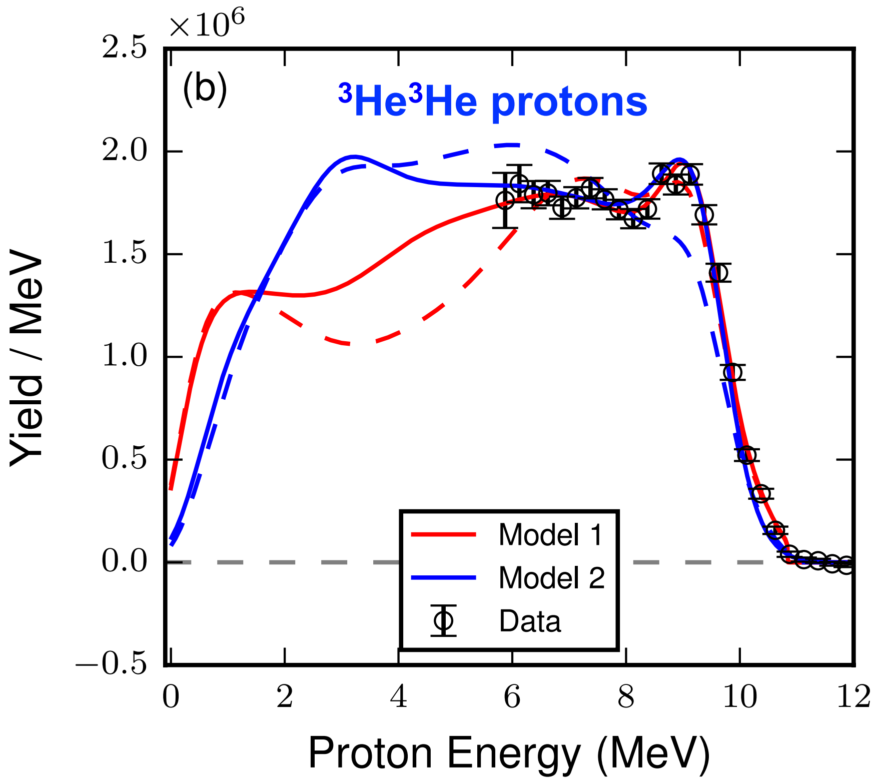

$E_G(^3He+^3He) \approx 18.1 \times Ti^{0.67}$ [keV]

To understand stars we must understand how fast they burn by measuring reactivity <$\boldsymbol{\sigma v}$> or cross section $\boldsymbol{\sigma}$

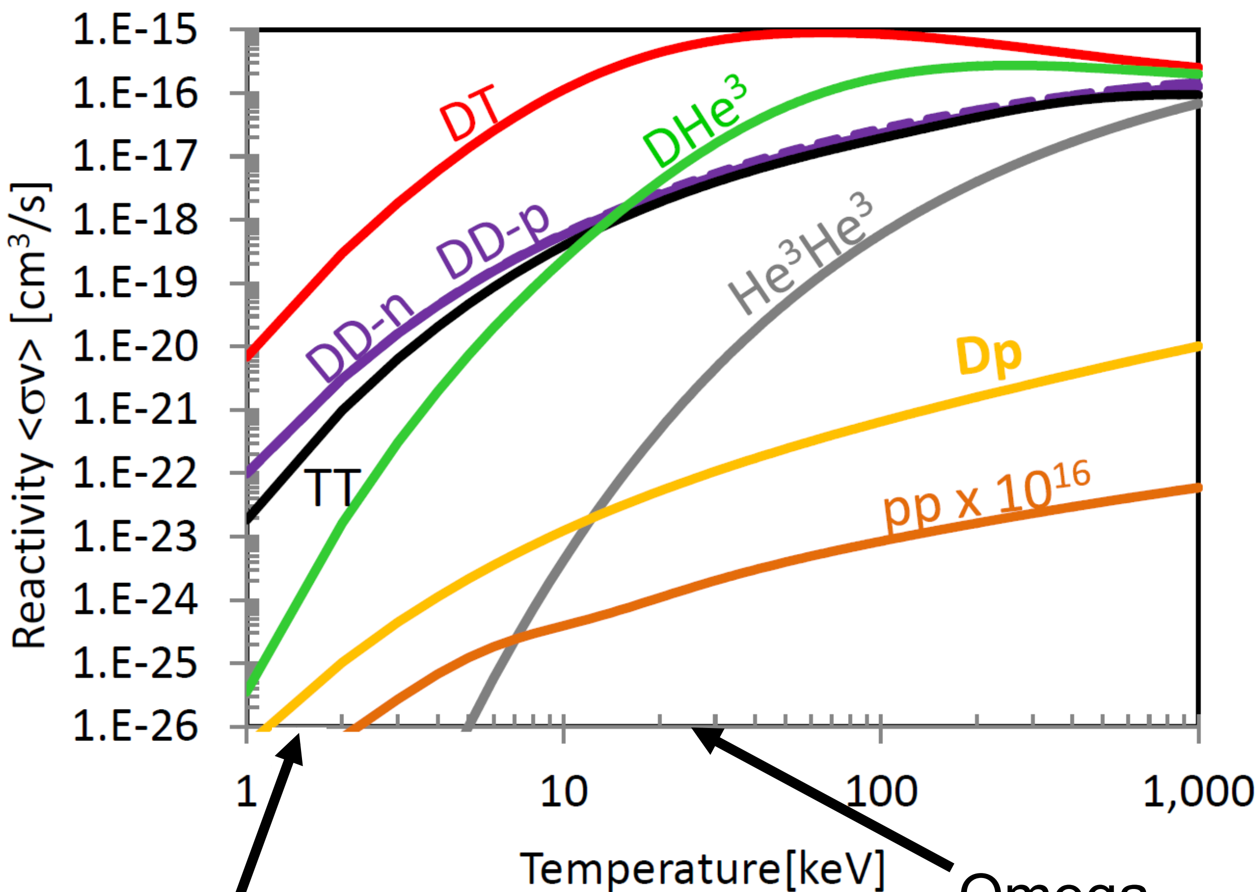

Solar Core
E_G~22 keV

Omega
E_G~165 keV

NIF experiments allow measurements at lower Gamow energies closer to the solar Gamow peak

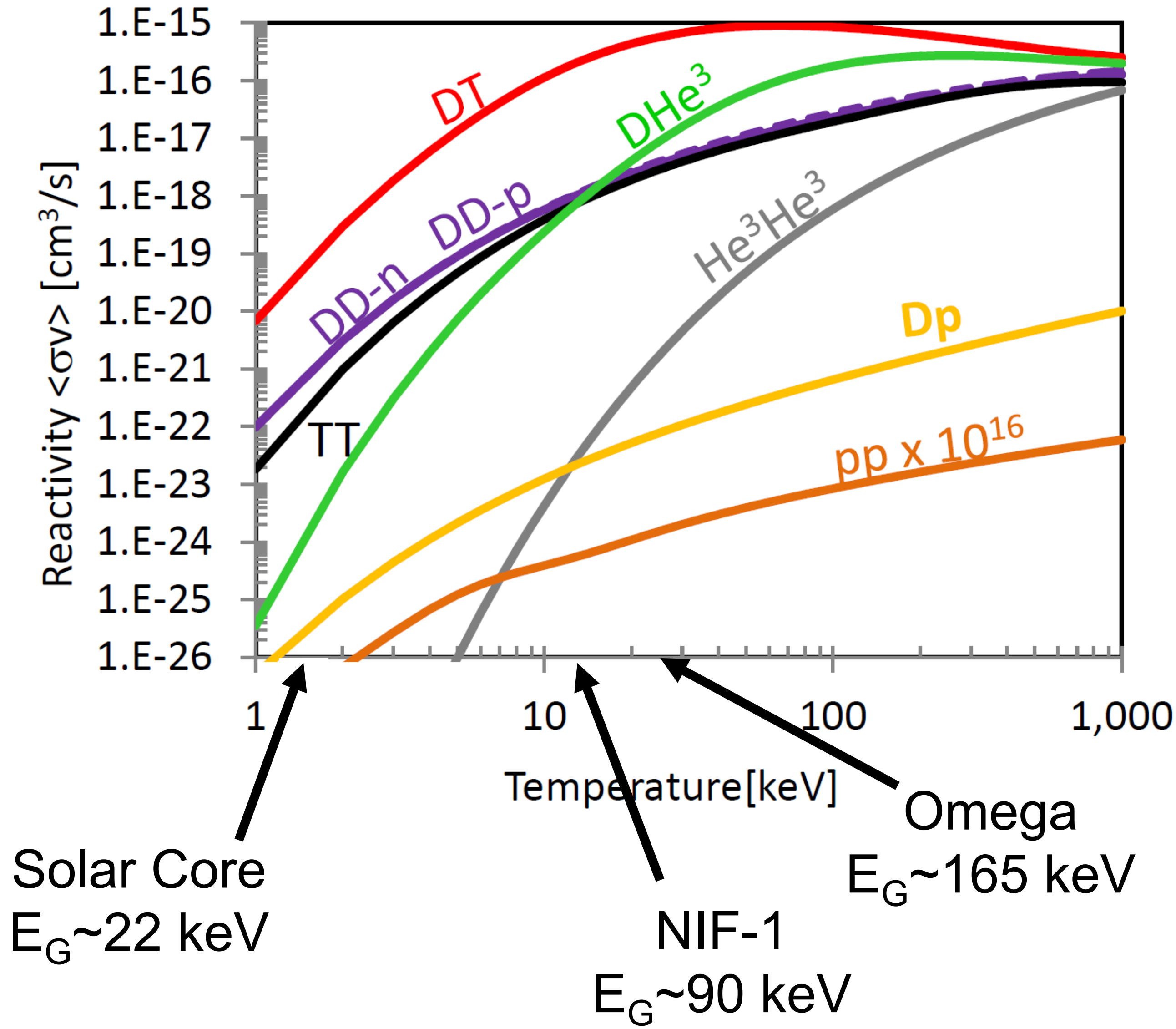

NIF experiments allow measurements at lower Gamow energies closer to the solar Gamow peak

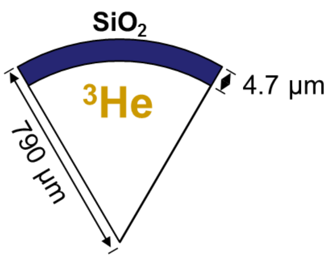

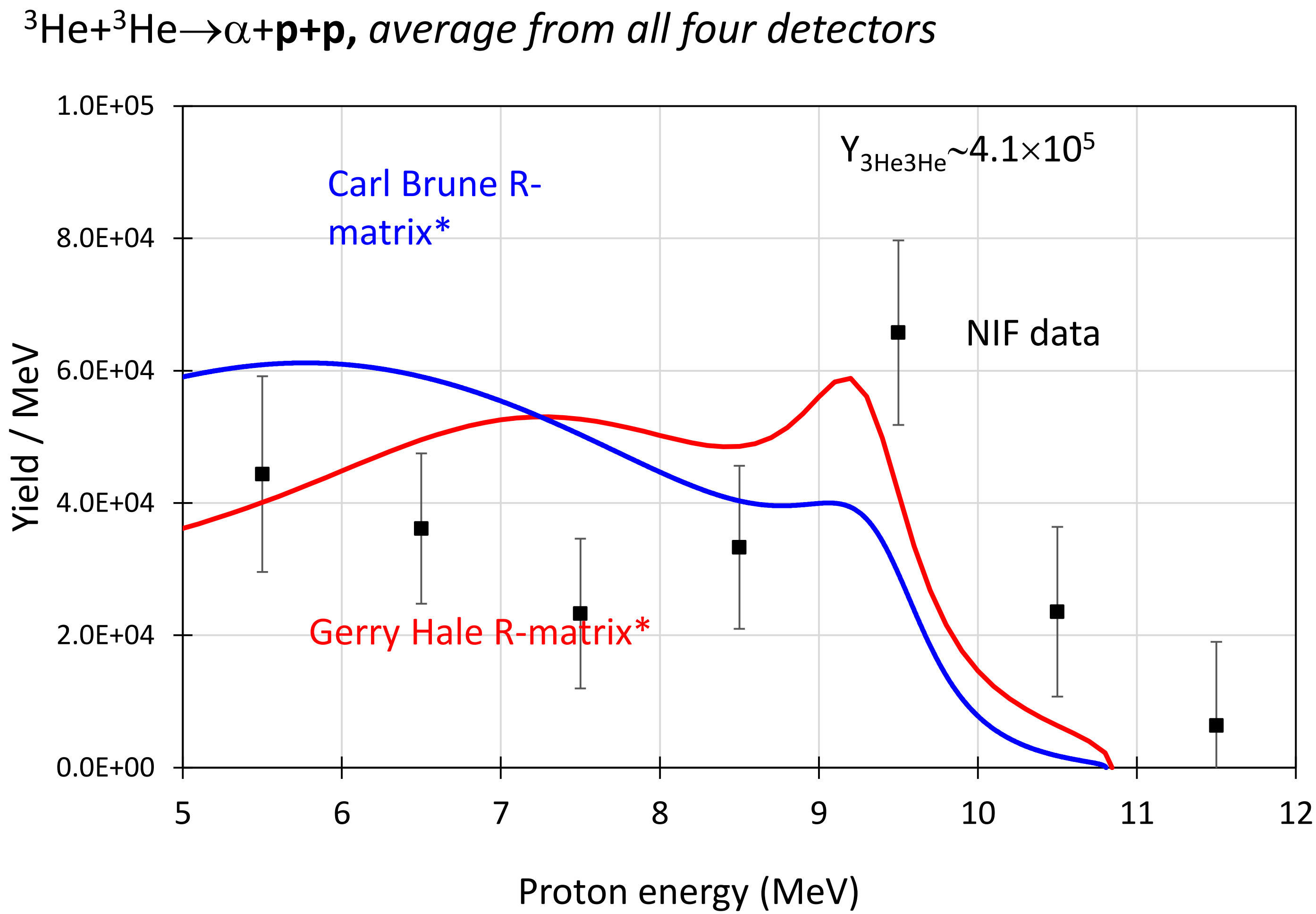

Results from Maria Gatu-Johnson
R-matrix spectra not broadened by ion temperature or instrument response

NIF experiments allow measurements at lower Gamow energies closer to the solar Gamow peak

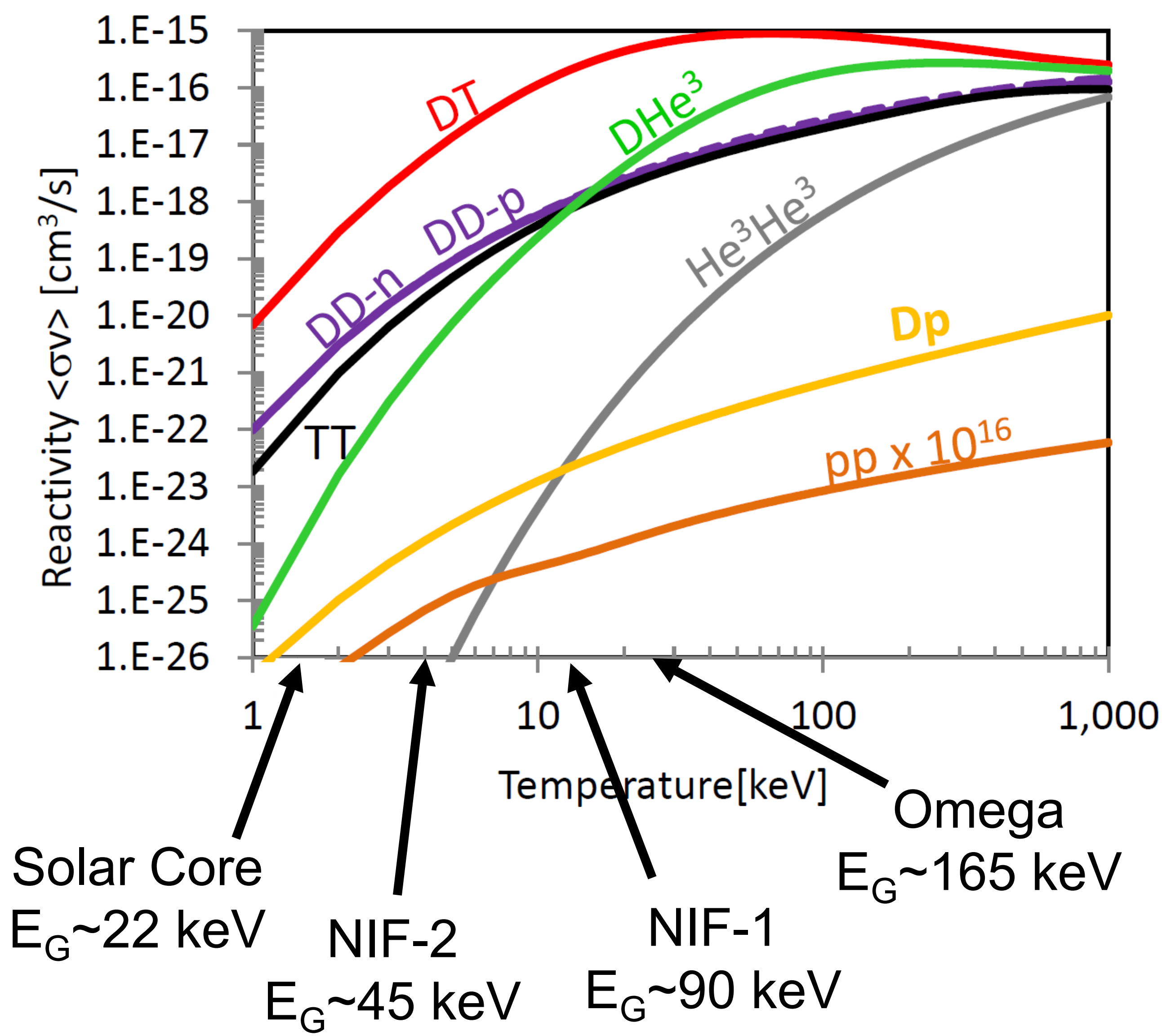

There is a rich set of opportunities to study nuclear reactions at OMEGA and the NIF

Current work

Charged-particle induced reactions:

- **T(t,2n)^{4}He** (analogue to ^{3}He(^{3}He,2p)^{4}He).
- **T(^{3}He,np)^{4}He, T(^{3}He,d) ^{4}He, T(^{3}He,γ)^{6}Li** (impact BBN?).
- **^{3}He(^{3}He,2p)^{4}He** (pp-I).
- **D(p,γ)^{3}He** (Brown dwarfs, protostars).
- **^{6}Li(p,α)^{3}He**
- **^{7}Li(p,α)^{4}He**
- **^{7}Be(p,γ)^{8}B** (pp-III).
- **^{11}B(p,α)^{8}Be** (non-Maxwellian ion distributions).
- **^{15}N(p,α)^{12}C** (last step of CNO).
- **^{12}C(α,γ)^{16}O** ?

Neutron-induced reactions:

- **n-d and n-T** at 14 MeV
- **D(n,2n)** at 14 MeV
- **T(n,2n)** at 14 MeV
- Various (n,γ), (n,2n) processes?

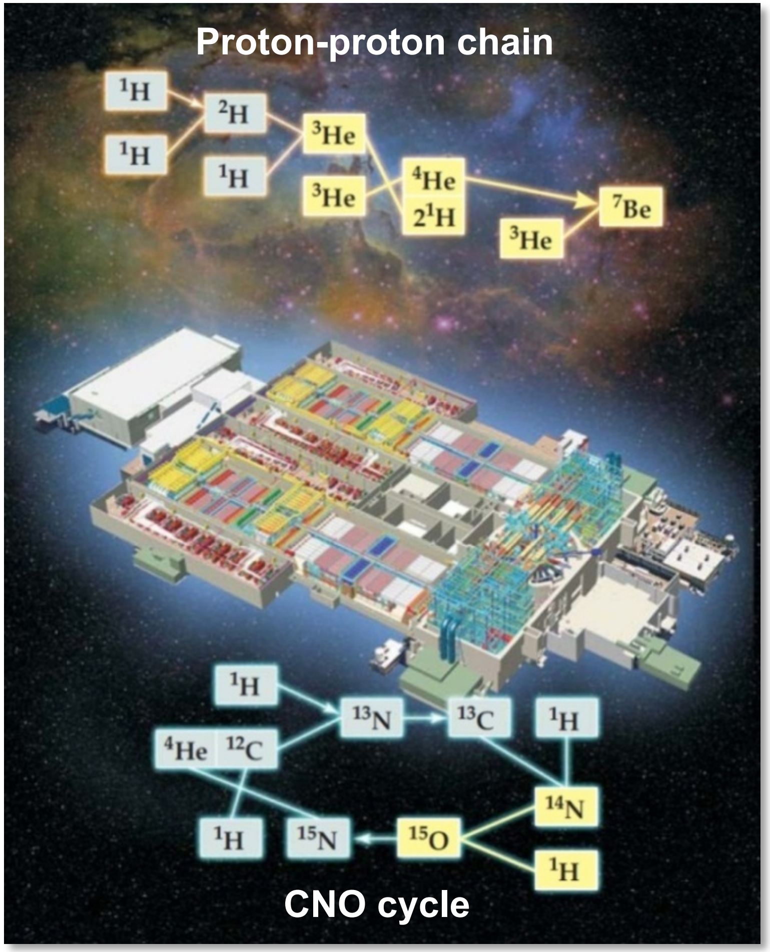

Outline

- ➢ High-Energy-Density (HED) Plasma
  - US facilities

Zylstra et al. (MIT)

- ➢ Plasma Nuclear Science using ICF-like implosions
  - p-p chain at relevant Gamow energies

Drake, Kuranz et al. (UM)

- ➢ Laser-produced Magnetohydrodynamics
  - similarity conditions
  - Rayleigh-Taylor growth in core-collapse SNe

Park, Huntington et al. (LLNL)

- ➢ Laser-produced Jets
  - ‘collisionless’ shocks
  - supersonic jet dynamics

Manuel, Kuranz et al. (UM)

Chen et al. (LLNL)

- ➢ Pair-Plasma Production
  - relativistic jets

- ➢ Summary

Magnetohydrodynamic (MHD) equations describe both laboratory and astrophysical systems

Continuity
$$\frac{\partial \rho}{\partial t} + \nabla \cdot \rho \mathbf{v} = 0$$

Momentum
$$\rho\left(\frac{\partial \mathbf{v}}{\partial t} + \mathbf{v} \cdot \nabla \mathbf{v}\right) = -\nabla p + \frac{1}{\mu_0}\left(\nabla \times \mathbf{B}\right) \times \mathbf{B}$$

Energy
$$\frac{\partial p}{\partial t} - \gamma \frac{p}{\rho}\frac{\partial \rho}{\partial t} + \mathbf{v} \cdot \nabla p - \gamma \frac{p}{\rho} \mathbf{v} \cdot \nabla \rho = 0$$

Field Evolution
$$\frac{\partial \mathbf{B}}{\partial t} = \nabla \times \left(\mathbf{v} \times \mathbf{B}\right)$$

[1] Ryutov, ApJ 518 (1999)
[2] Ryutov, POP 8 (2001)
[3] Drake, High-energy-density physics (2006), ch 10
[4] Remington, RMP 78 (2006)
[5] Falize, ApJ 730 (2011)

Multiple dimensionless parameters determine the validity of using the MHD equations to describe system dynamics

- **The system exhibits fluid-like behavior** $l_{mfp}/L << 1$
- **Energy flow by particle heat conduction is negligible** $\mathrm{Pe} >> 1$
- **Energy flow by radiation flux is negligible** $\mathrm{Pe}_{\gamma} >> 1$
- **Viscous dissipation is negligible** $\mathrm{Re} >> 1$

Astrophysical systems are large and fulfill these criteria in many cases!

Multiple dimensionless parameters determine the validity of using the MHD equations to describe system dynamics

Parameter	SN	Lab
l_{mfp}/L	4×10^{-3}	4×10^{-9}
Pe	1.1×10^{13}	5.9×10^{3}
Pe_γ	1.6×10^{16}	1.6×10^{10}
Re	1.9×10^{11}	1.4×10^{5}

$l_{mfp}/L << 1$

$Pe >> 1$

$Pe_\gamma >> 1$

$Re >> 1$

* Drake, ApJ 564 (2002) Table 1

Multiple dimensionless parameters determine the validity of using the MHD equations to describe system dynamics

Parameter	SN	Lab
l_{mfp}/L	4×10^{-3}	4×10^{-9}
Pe	1.1×10^{13}	5.9×10^{3}
Pe_{γ}	1.6×10^{16}	1.6×10^{10}
Re	1.9×10^{11}	1.4×10^{5}

$l_{mfp}/L << 1$

$\mathrm{Pe} >> 1$

$\mathrm{Pe}_{\gamma} >> 1$

$\mathrm{Re} >> 1$

Two MHD systems evolve similarly when the Euler number (Eu) and magnetization (μ) are similar.

$$\mathrm{Eu} \equiv \frac{v^*}{\sqrt{p^*/\rho^*}} \qquad \mu \equiv \frac{\left(B^*\right)^2}{p^*}$$

* Drake, ApJ 564 (2002) Table 1

Outline

- High-Energy-Density (HED) Plasma
  - US facilities

Zylstra et al. (MIT)

- Plasma Nuclear Science using ICF-like implosions
  - p-p chain at relevant Gamow energies

Drake, Kuranz et al. (UM)

- Laser-produced Magnetohydrodynamics
  - similarity conditions
  - Rayleigh-Taylor growth in core-collapse SNe

Park, Huntington et al. (LLNL) ← 'collisionless' shocks

Manuel, Kuranz et al. (UM) ← supersonic jet dynamics

- Laser-produced Jets
  - 'collisionless' shocks
  - supersonic jet dynamics

Chen et al. (LLNL)

- Pair-Plasma Production
  - relativistic jets

- Summary

SN1987a stimulated research into Rayleigh-Taylor growth in supernovae explosions

SN1987A, Hubble Space Telescope

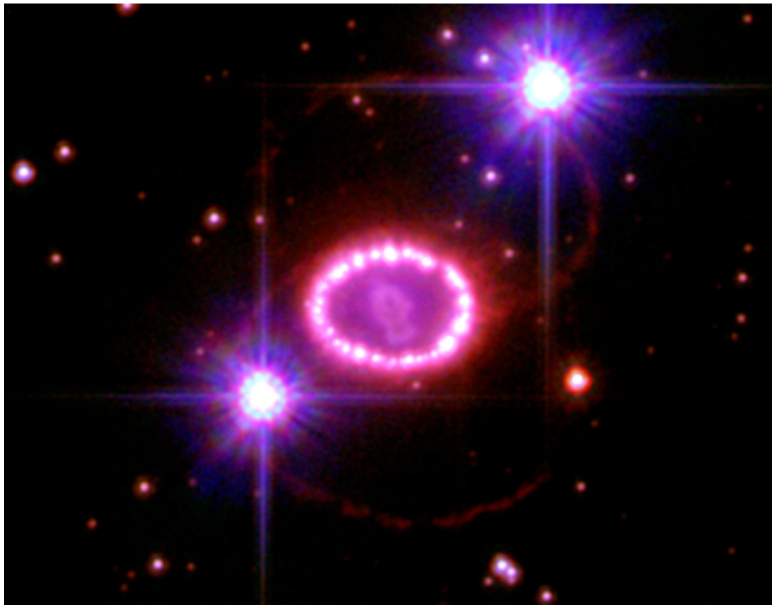

- Core-collapse supernova of a bluegiant
- Light curve data suggested* 'mixing' between stellar layers

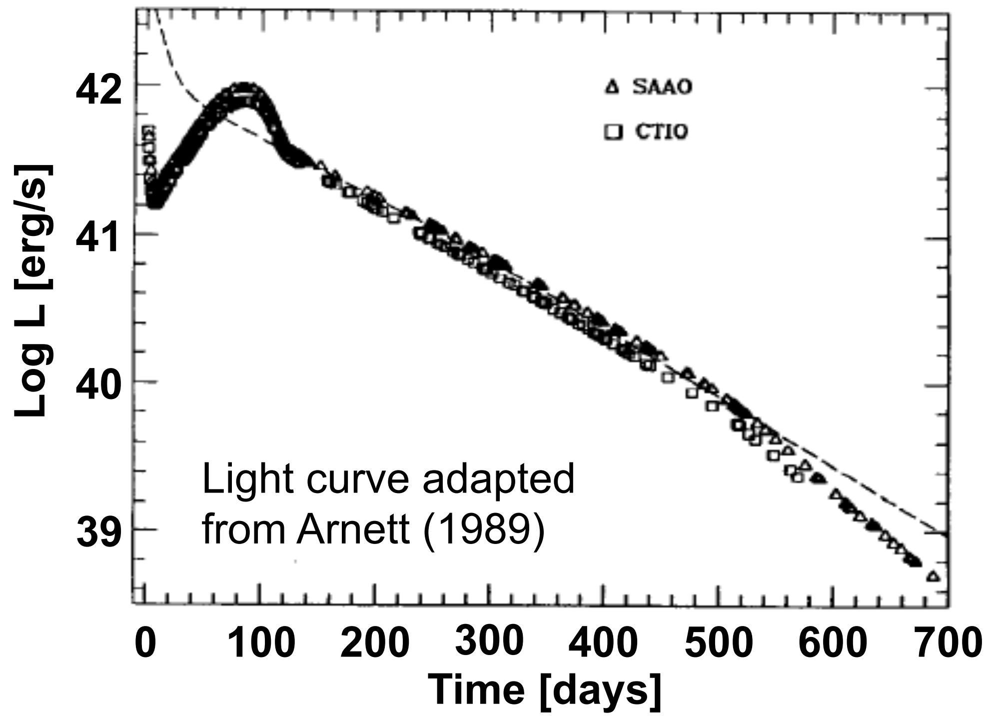

Can mixing in supernovae be investigated in the lab?

* Arnett, ARAA 27 (1989)

Simulations suggest that geometric similarities are sufficient to investigate instability growth in SNe

1D PROMETHEUS simulation
He-H interface in SN1987a

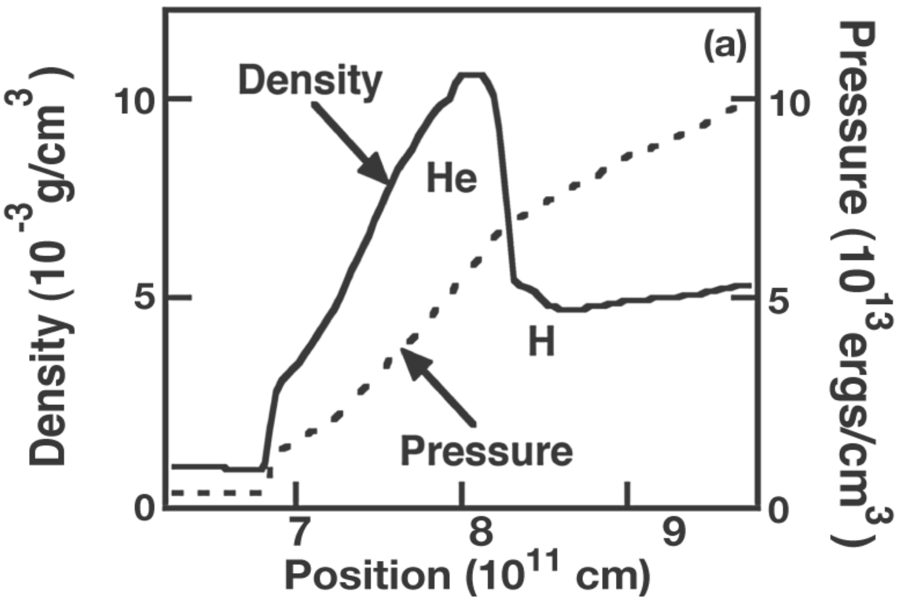

1D HYADES simulation
OMEGA experiment

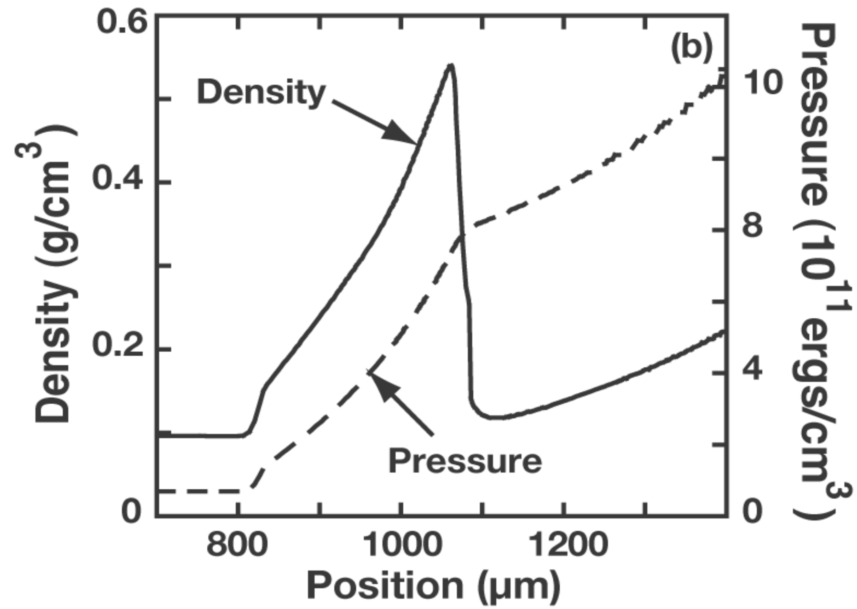

The Euler number is approximately equal between the two systems.

$$Eu_{SN} \approx 2.2 \qquad Eu_{Exp} \approx 2.3$$

* Kuranz, ApJ 696 (2009) Fig. 1

Simulations demonstrate the similarity of the interface-velocity evolution in both systems

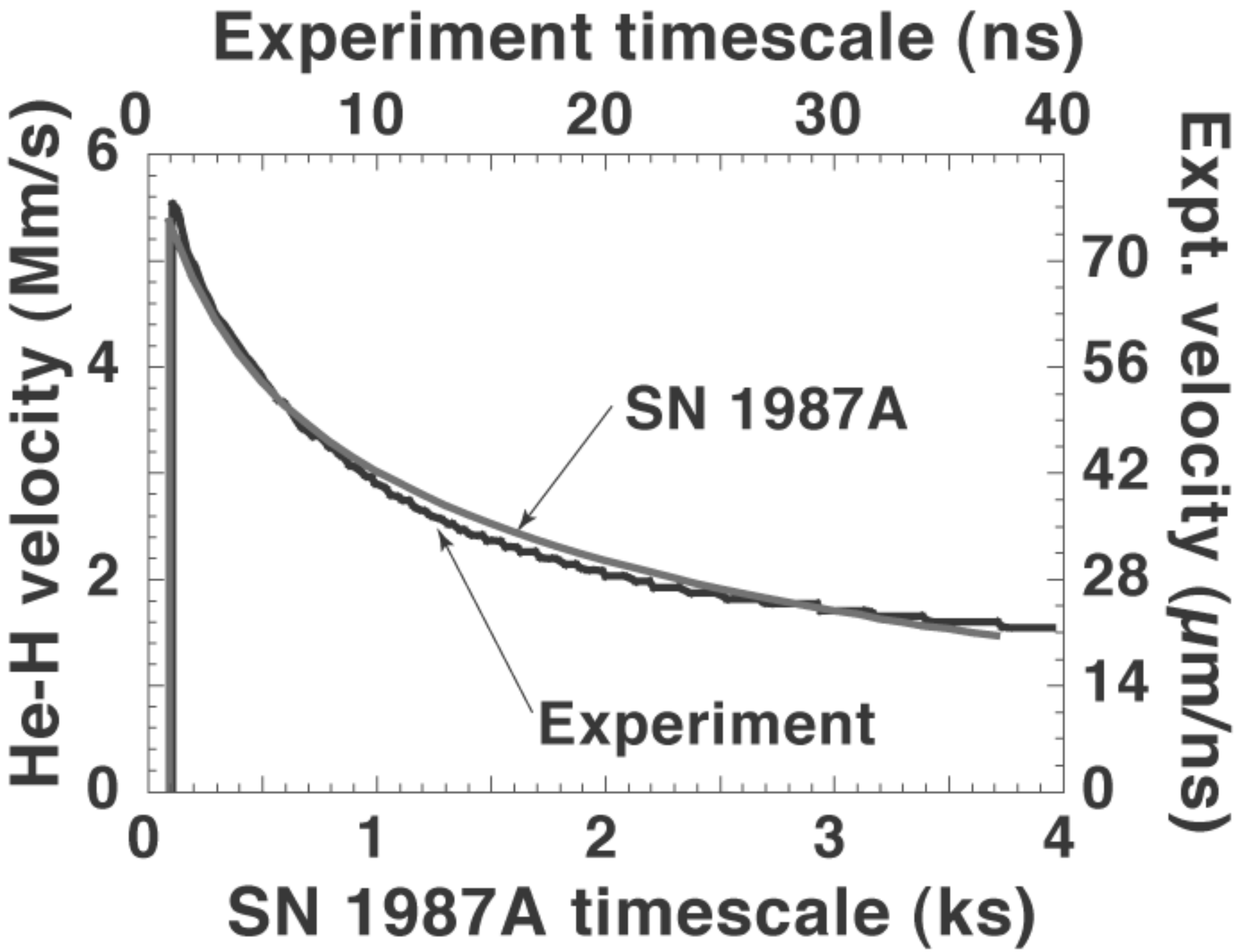

* Kuranz, ApJ 696 (2009) Fig. 1

Scaled experiments investigated instability growth at the He-H interface in supernovae at Omega

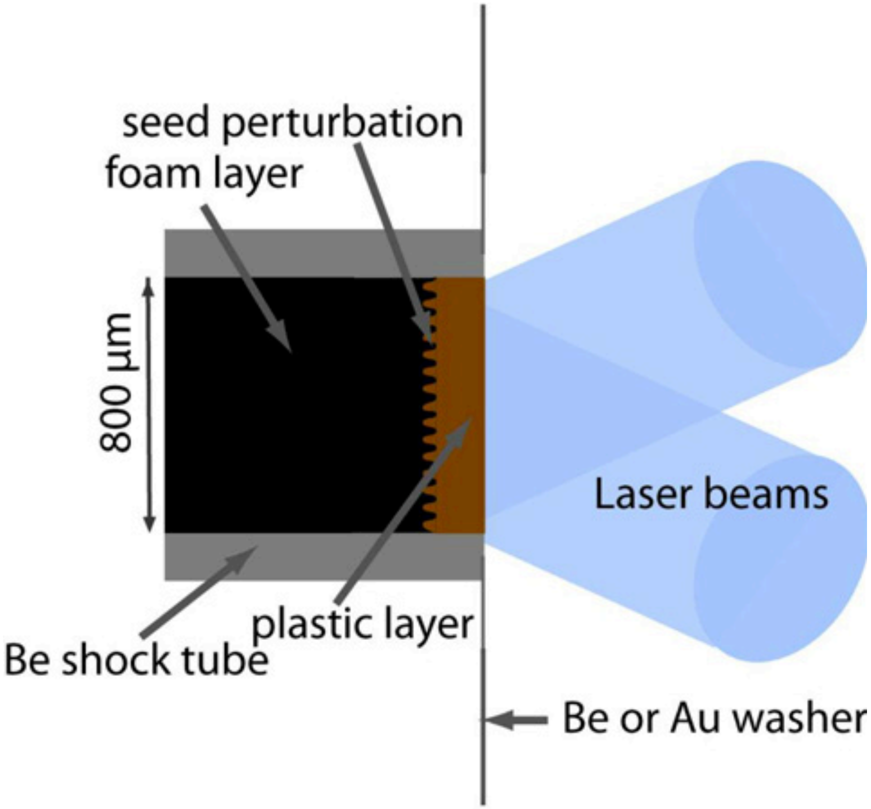

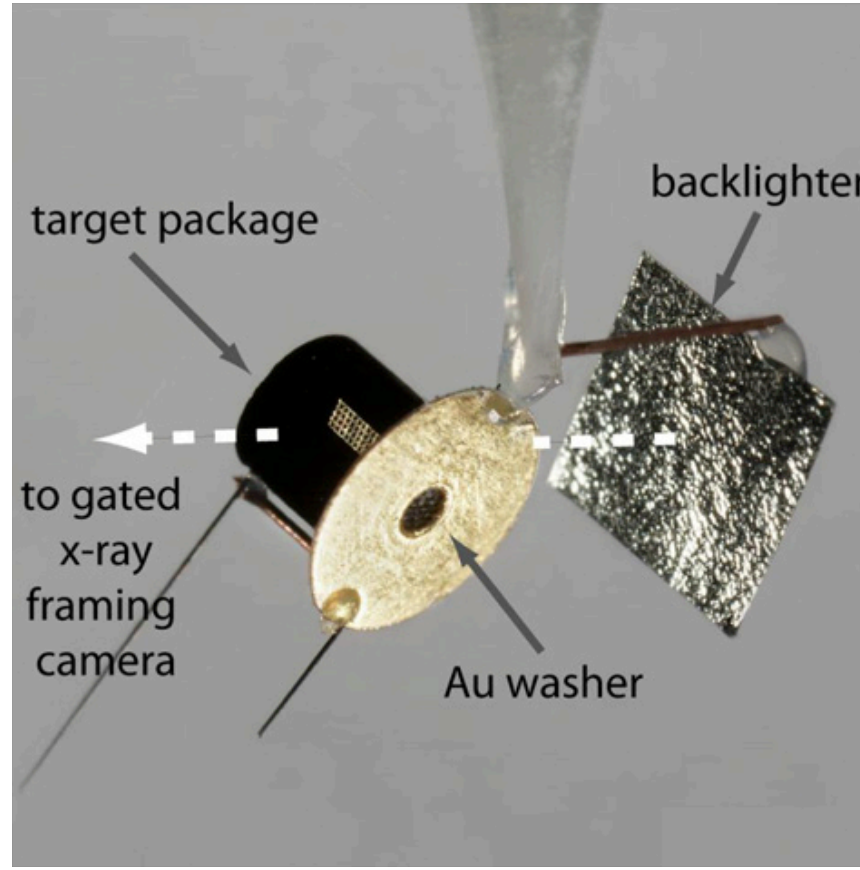

* Kuranz, ApJ 696 (2009) Fig. 2

Scaled experiments investigated instability growth at the He-H interface in supernovae at Omega

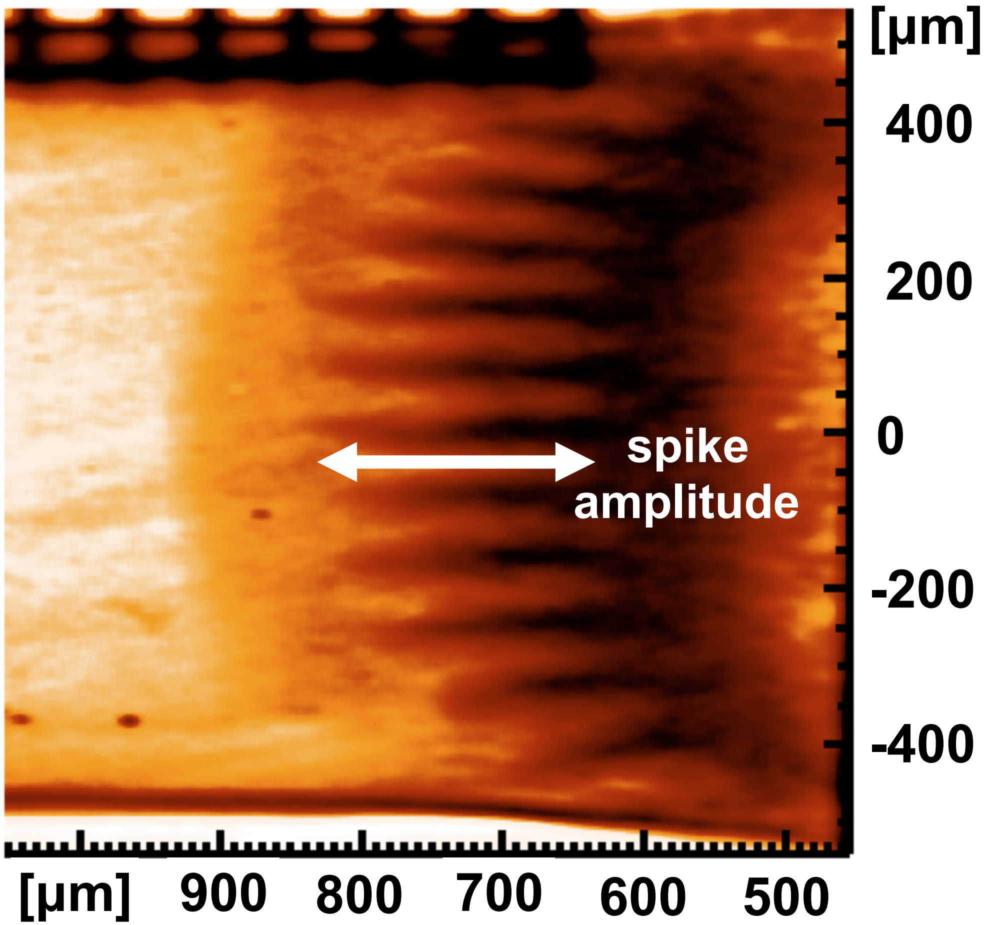

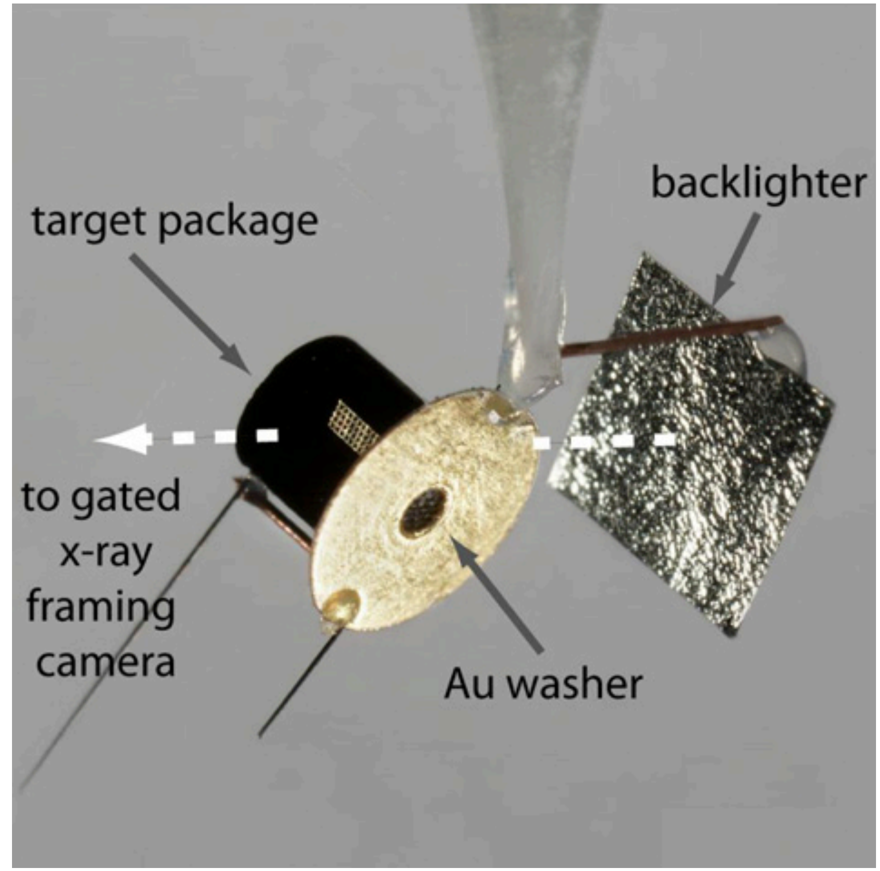

X-ray radiographs demonstrated that amplitude growth was consistent with the nonlinear 'buoyancy-drag' model.

* Kuranz, POP 16 (2009) Fig. 5

Scaled experiments investigated instability growth at the He-H interface in supernovae at Omega

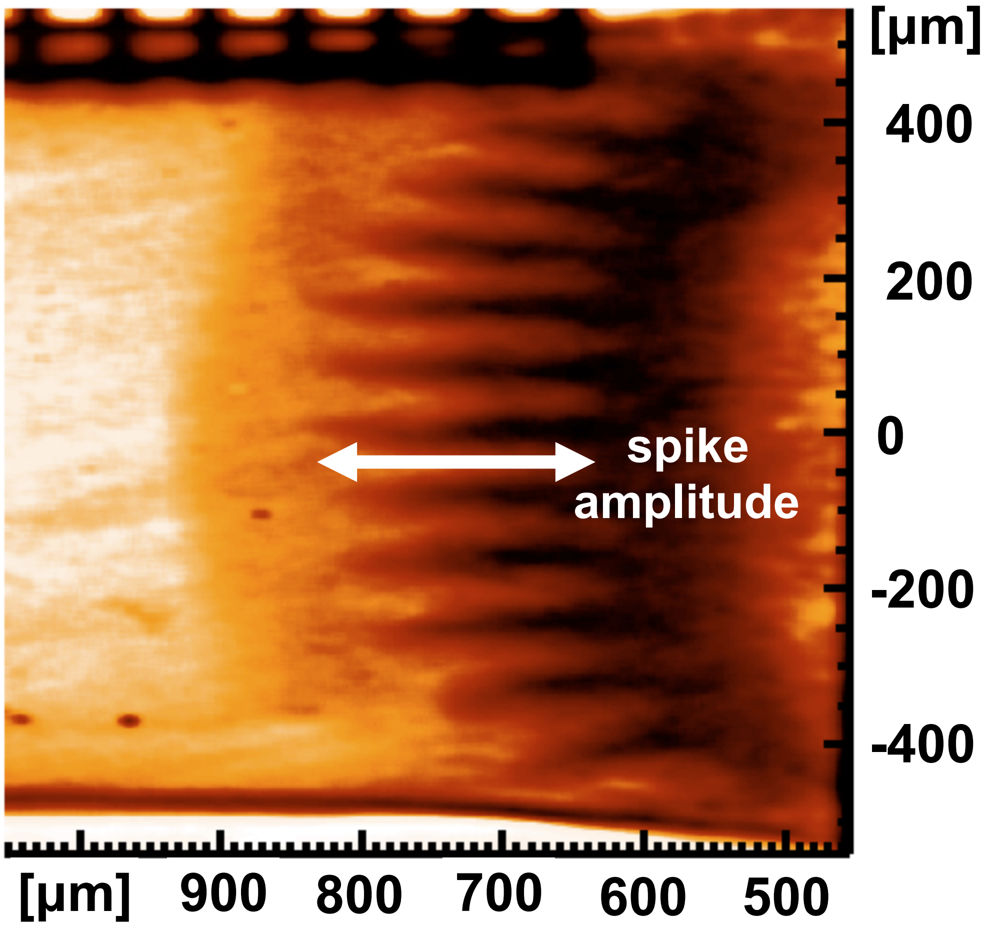

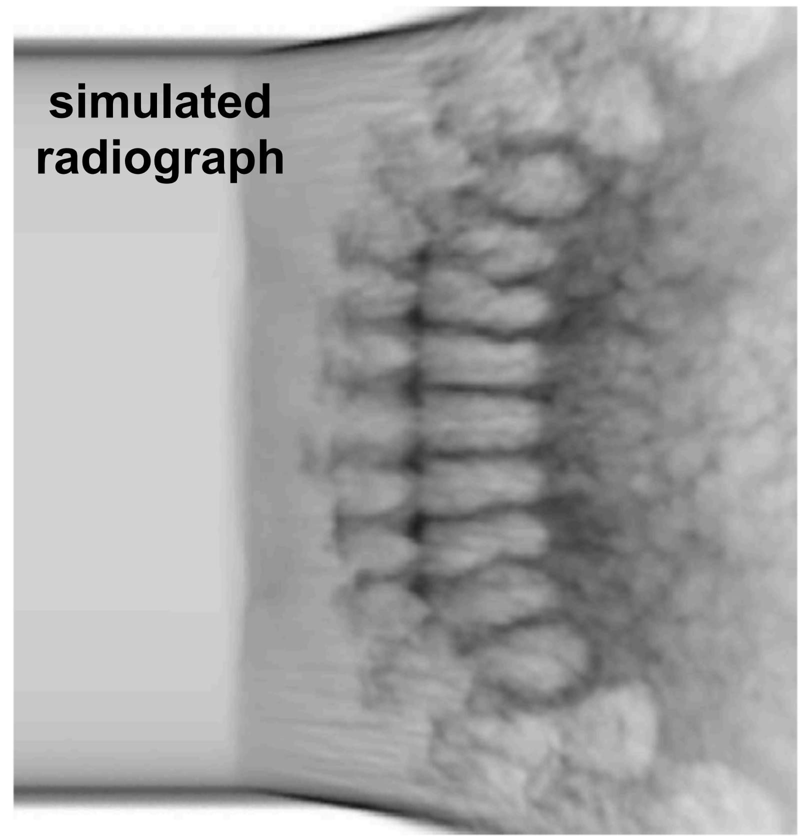

… but the detailed spike morphology is different!

* Kuranz, POP 16 (2009) Fig. 5; Kuranz POP 17 (2010) Fig. 8

The study of radiative effects on the Rayleigh-Taylor instability is relevant to core-collapse, red supergiant

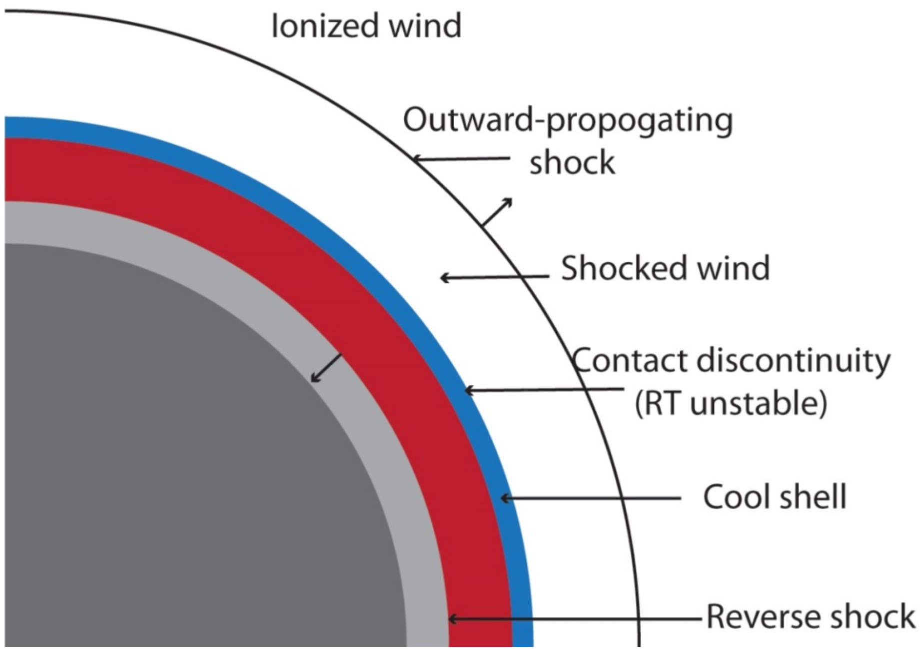

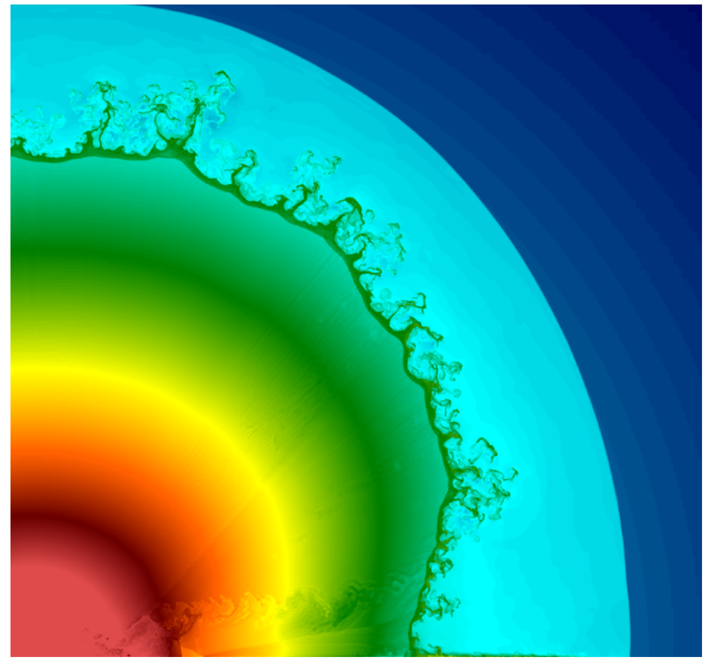

Nymark et al., Astron. & Astro. 449, 171 (2006) "X-ray emission from radiative shocks in type II supernovae"

Plewa hydrodynamic simulation of red supergiant showing RT instability develop in shocked wind region

C. Kuranz et al, Astrophys. Space Sci, 336, 207 (2011)
C. Huntington et al., PoP, 18, 112703 (2011)

Classical RT growth is expected with 230 eV drive whereas growth is stabilized at higher temperatures >325 eV

Drive temperature (keV) vs time (us)

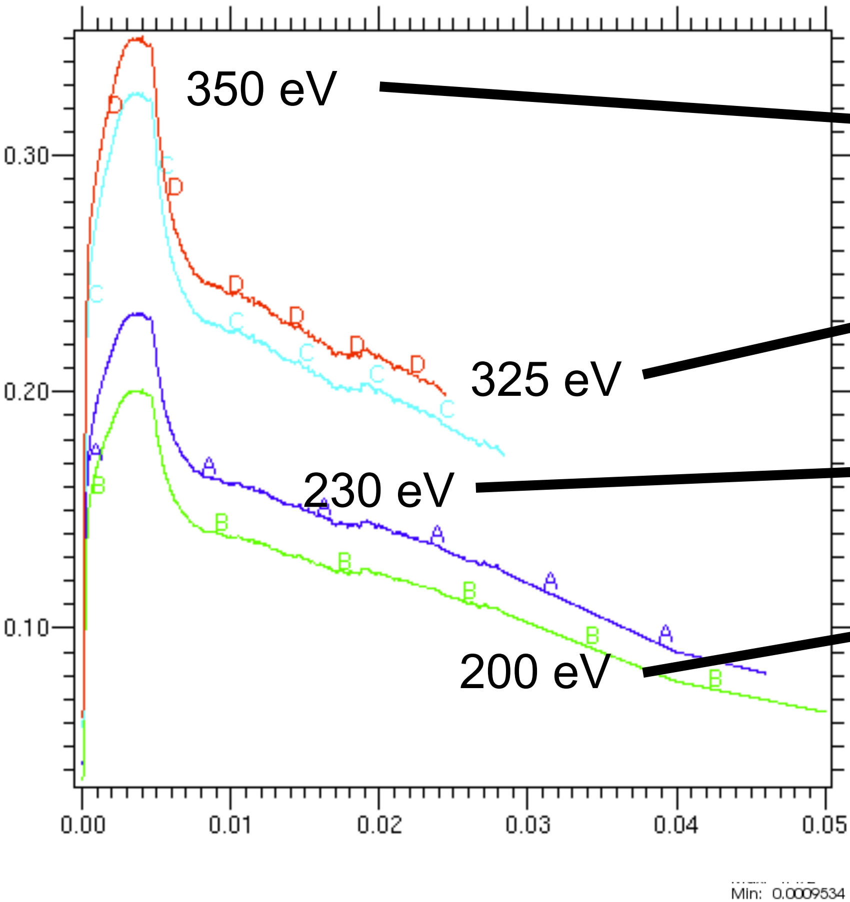

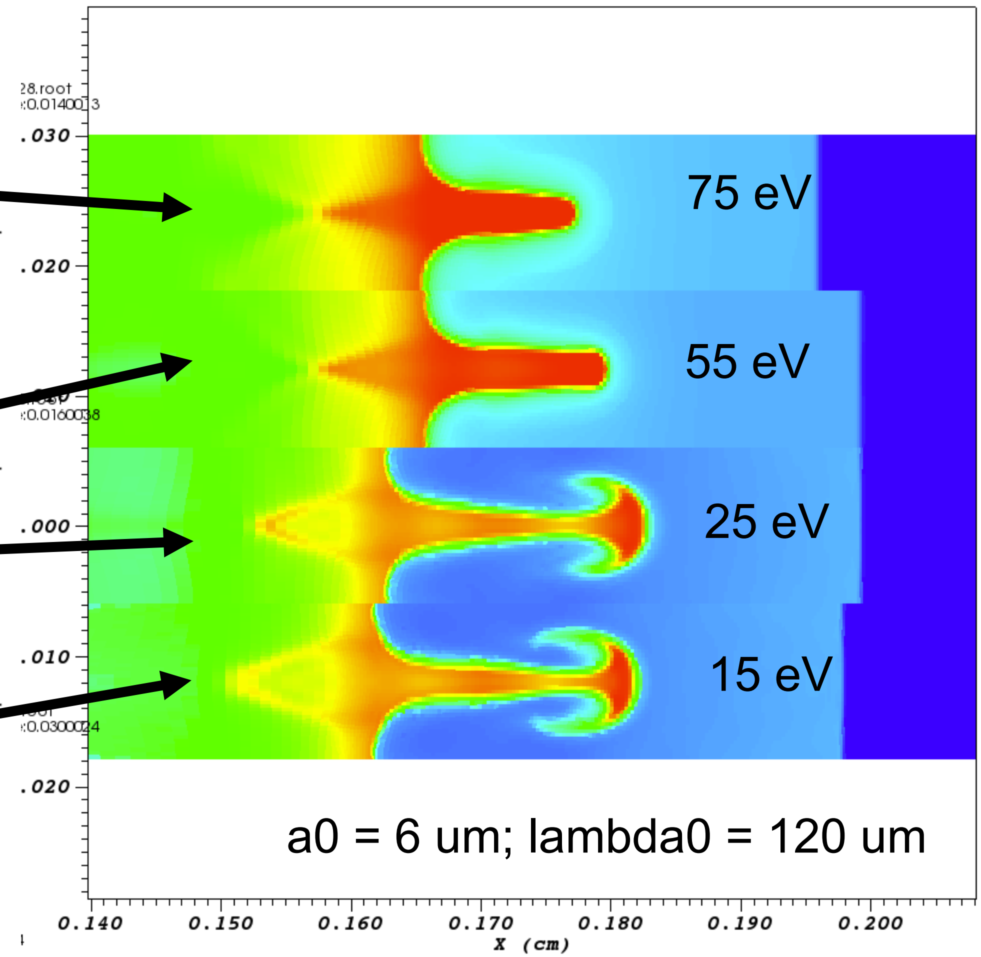

K. Raman, F. Doss, A. Miles on hydro simulations
S. MacLaren, S. Prisbrey, H. Robey on hohlraum simulations

Preliminary results from recent NIF experiments demonstrate radiatively stabilized RT growth

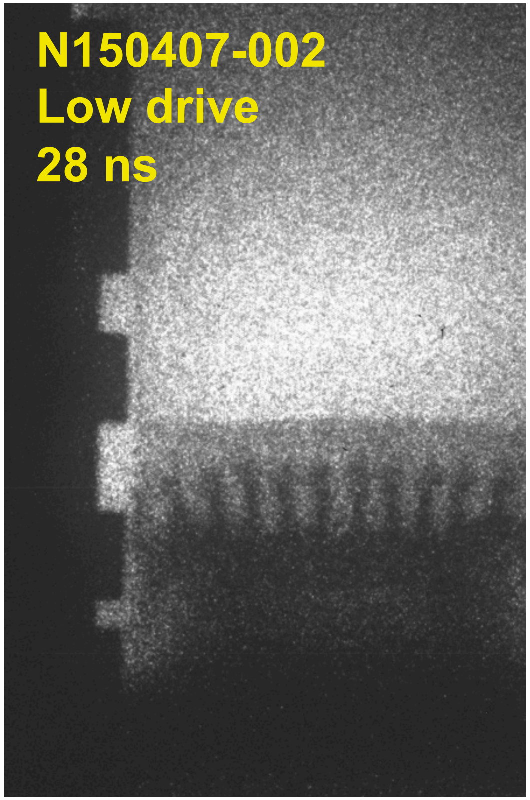

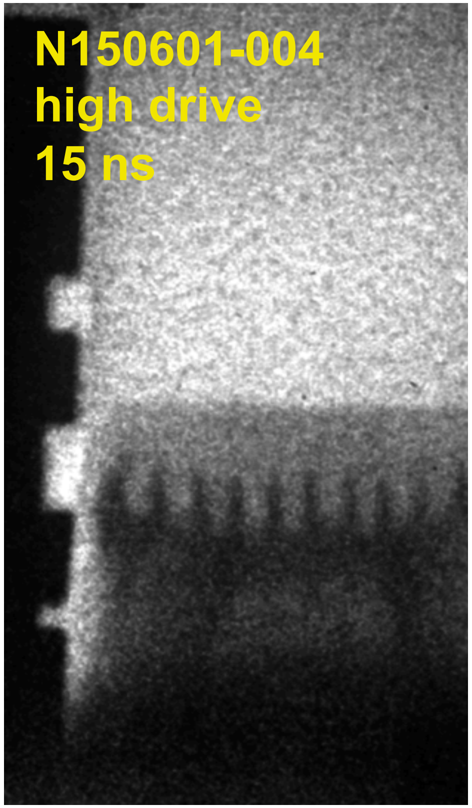

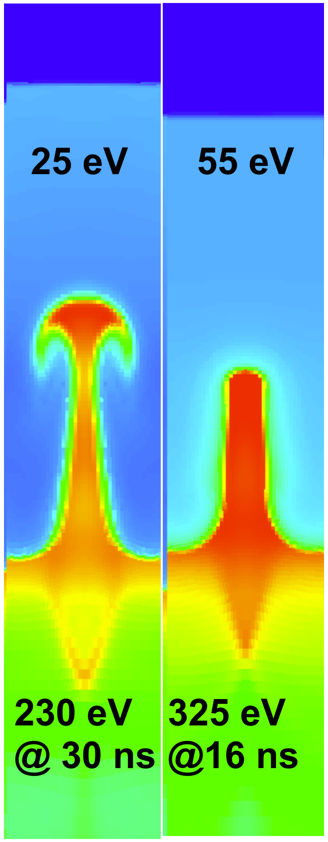

- **Compare 15 ns (high-drive) and 28 ns (low-drive) images when the distance-travelled is about the same**

C. Kuranz *et al.* submitted to Nature Communications

Outline

- High-Energy-Density (HED) Plasma
  - US facilities

Zylstra et al. (MIT)

- Plasma Nuclear Science using ICF-like implosions
  - p-p chain at relevant Gamow energies

Drake, Kuranz et al. (UM)

- Laser-produced Magnetohydrodynamics
  - similarity conditions
  - Rayleigh-Taylor growth in core-collapse SNe

Park, Huntington et al. (LLNL) ←

- Laser-produced Jets
  - 'collisionless' shocks
  - supersonic jet dynamics

→ Manuel, Kuranz et al. (UM)

Chen et al. (LLNL)

- Pair-Plasma Production
  - relativistic jets

- Summary

Shocks are formed in many astrophysical objects, but how are 'collisionless' shocks created

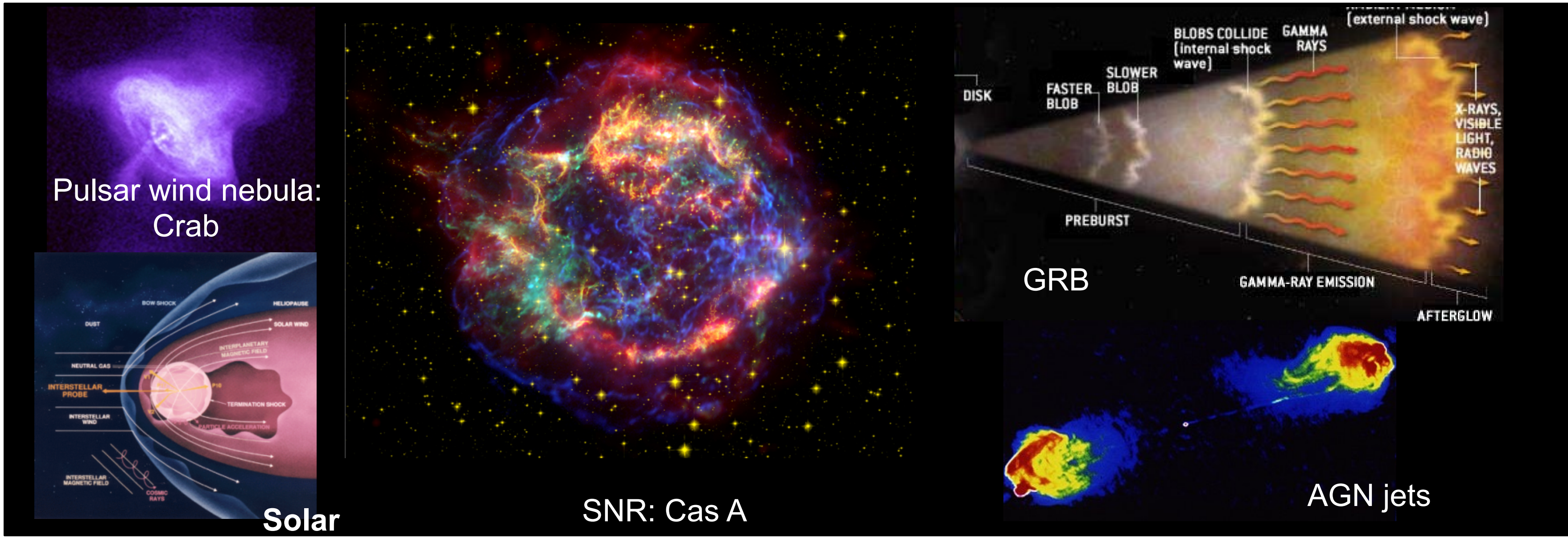

- **Shocks are typically created through the pile-up of pressure waves through collisions with a thickness ~λ_{mfp}**
- **In many astrophysical objects, λ_{mfp} >> scales of interest**
- **Some observed shocks are 'collisionless'…**

Collisionless shocks are mediated through scattering events with magnetic fields

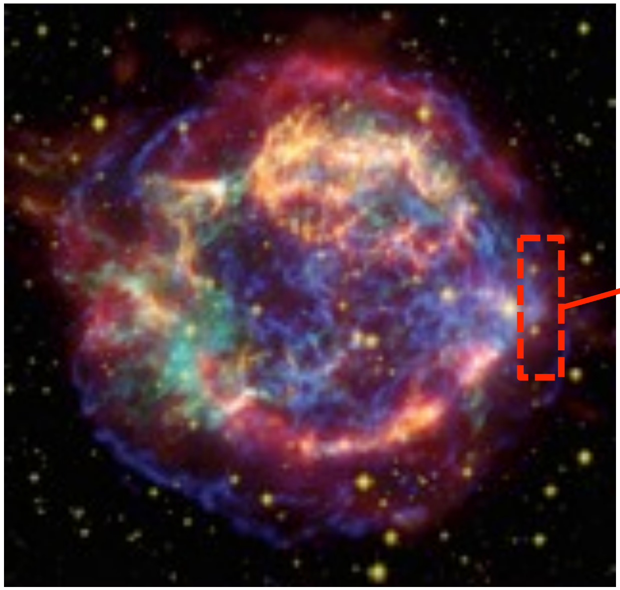

SNR Cassiopeia A

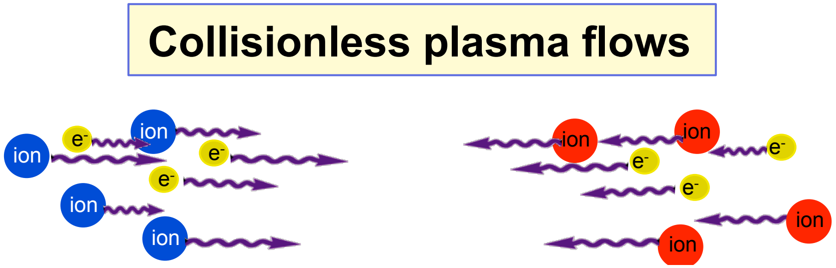

Collisionless shocks are mediated through scattering events with magnetic fields

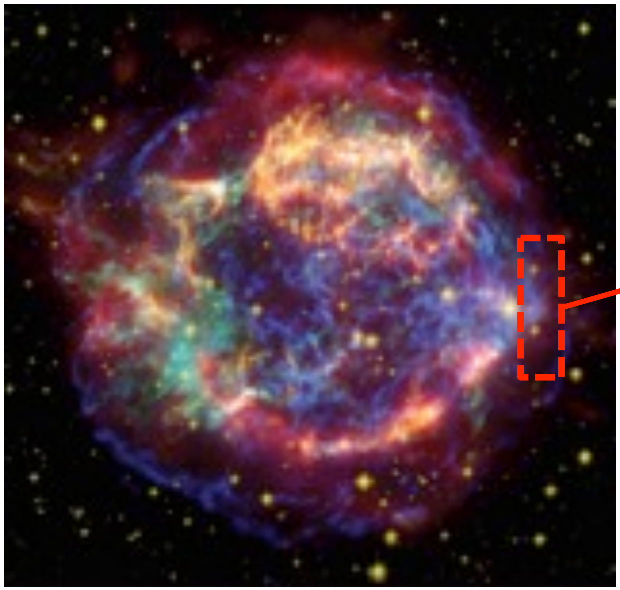

SNR Cassiopeia A

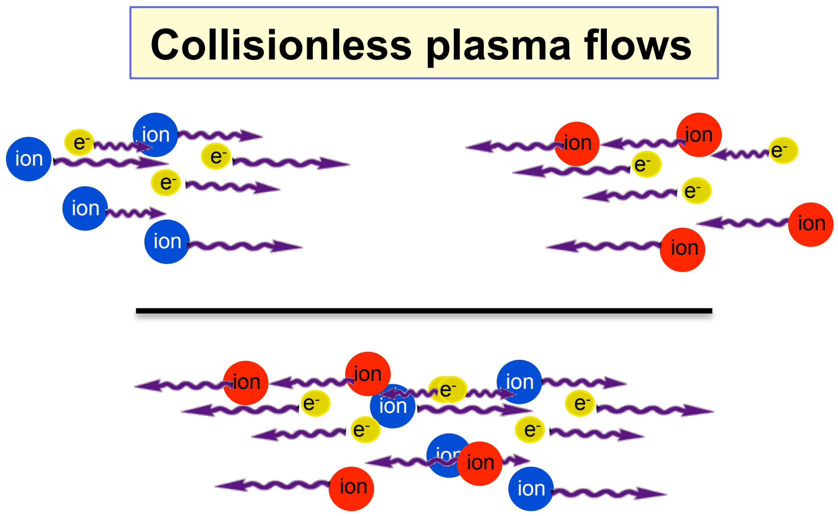

Do ions pass through without creating a shock?

Collisionless shocks are mediated through scattering events with magnetic fields

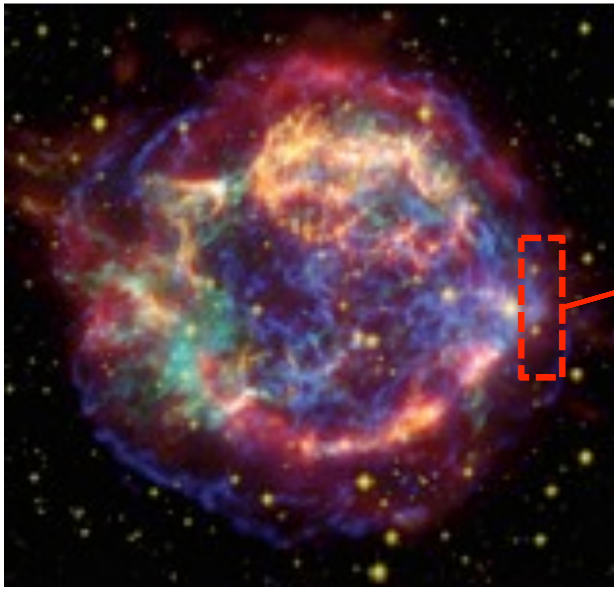

SNR Cassiopeia A

Collisionless plasma flows

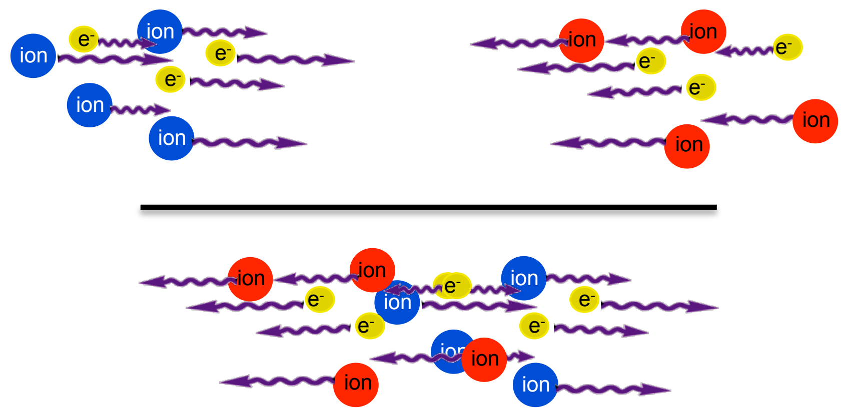

Do ions pass through without creating a shock?

Strong (scattering) fields may be self-generated or be created through compression of preexisting background fields.

Collisionless shocks are created when the Coulomb MFP is much larger than the characteristic interaction scale length

The conditions for generating a collision shock require:

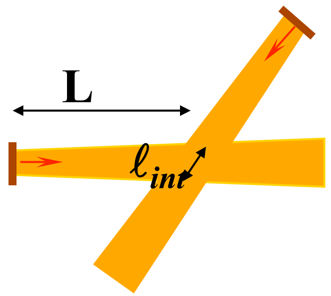

$\ell^* \ll \ell_{int} \ll \lambda_{mfp}$

ℓ^*, characteristic (electrostatic or electromagnetic) instability scale length
ℓ_{int}, intersection zone length
λ_{mfp}, Coulomb mean free path

$$\lambda_{mfp} \sim 5x10^{-13} \frac{A_Z^2}{Z^4} \frac{[v(cm/s)]^4}{n_z(cm^{-3})}$$ **For head-on collisions**

$$\ell^*_{ES} \sim K' \frac{v}{\omega_{pi}} \frac{W}{T_e} \qquad \ell^*_{EM} \sim K \frac{c}{\omega_{pi}} \qquad \omega_{pi} \sim Z\sqrt{\frac{n_i}{A}}$$

Ion plasma frequency

[D. Ryutov, PPCF, 2012]
[H. Park, HEDP, 2012]

Simulations suggest that self-generated B-fields can mediate shocks over long scale lengths (>100 c/ω_{pi})

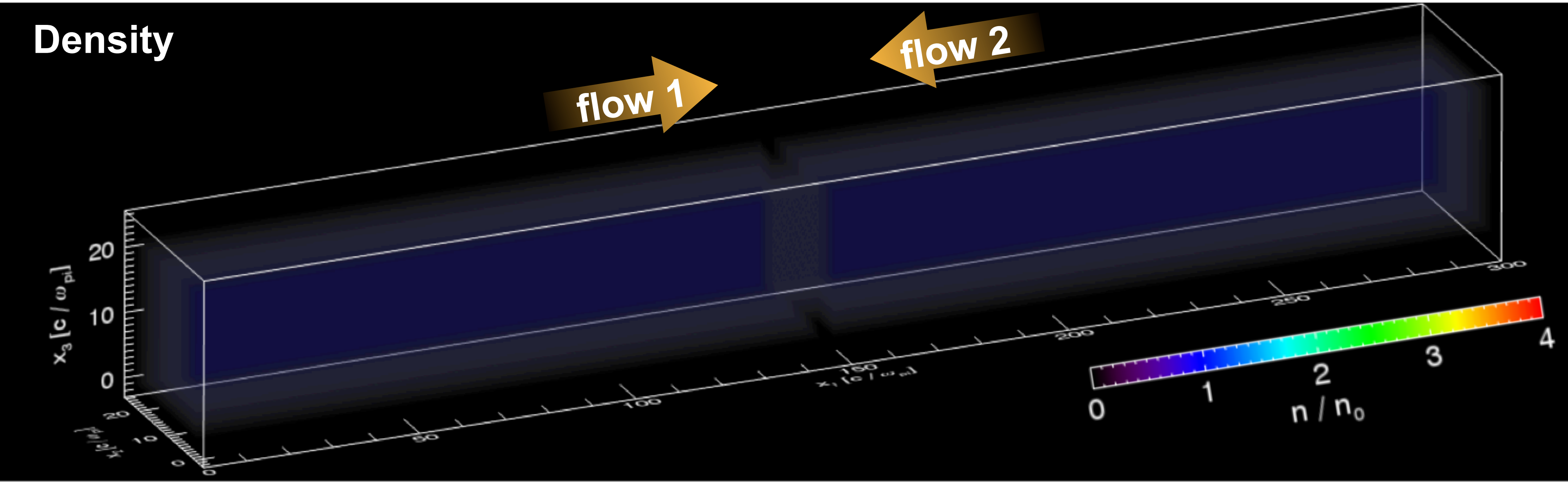

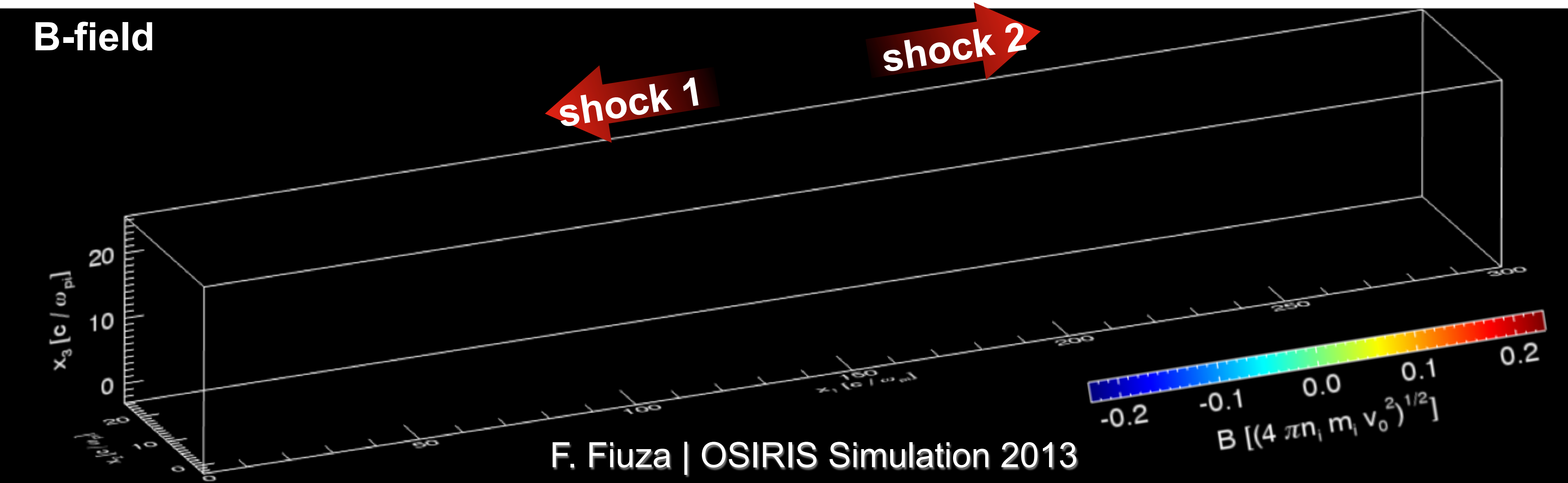

Simulations suggest that self-generated B-fields can mediate shocks over long scale lengths (>100 c/ω_{pi})

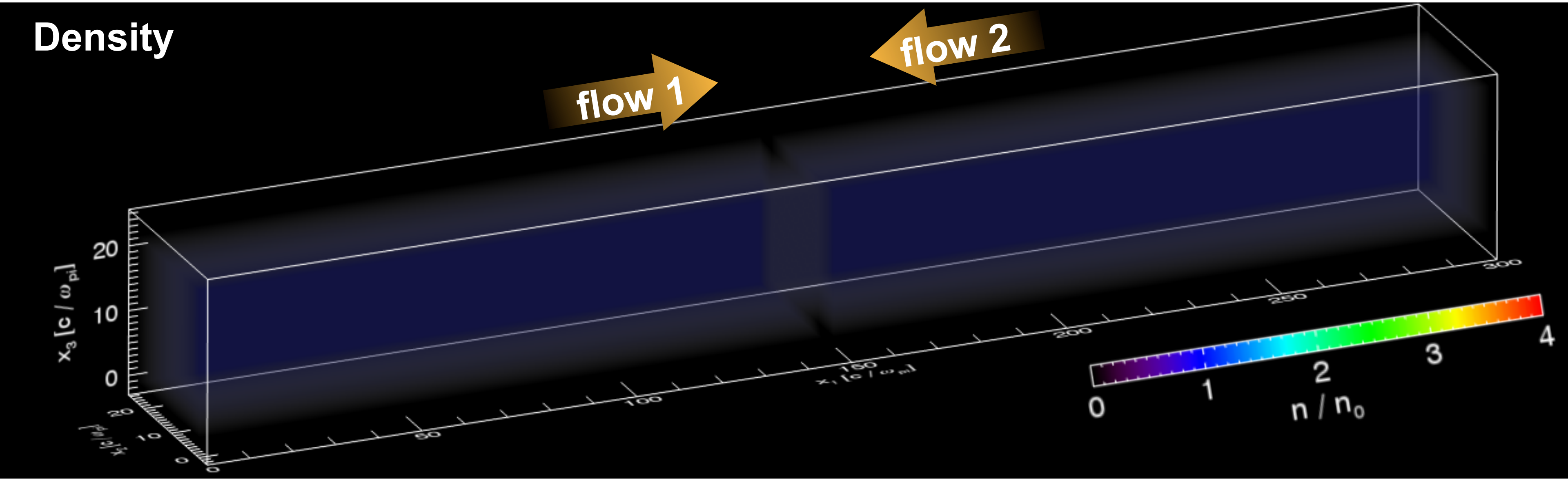

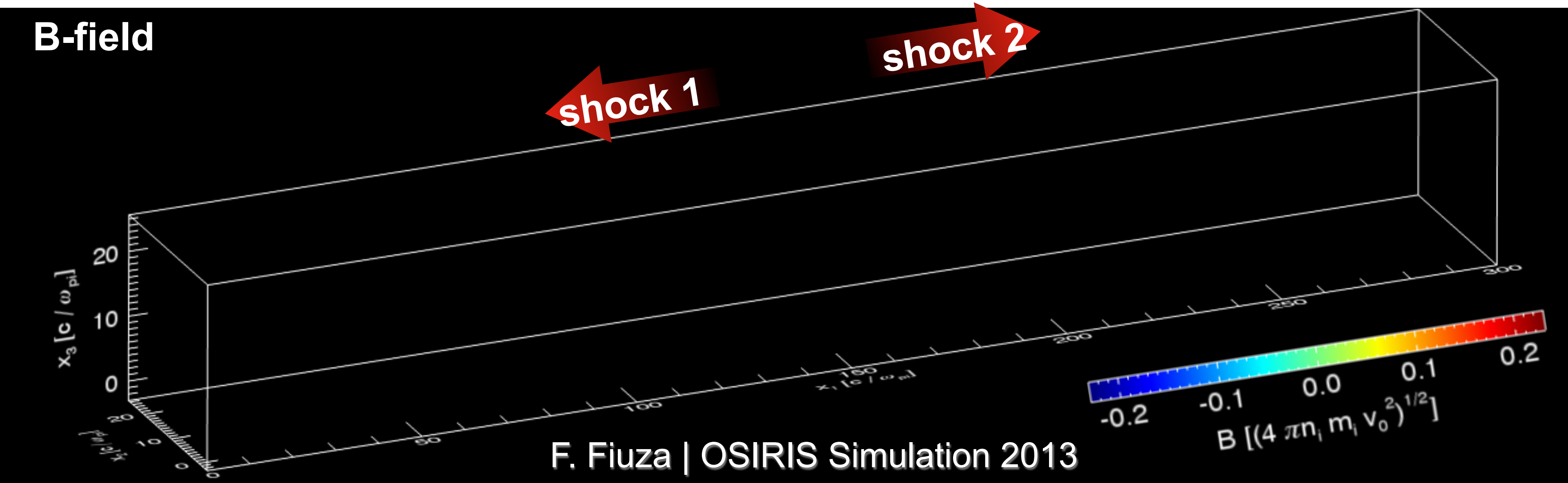

Proton imaging reproducibly shows self-organized B-fields in collisionless counter-streaming plasmas

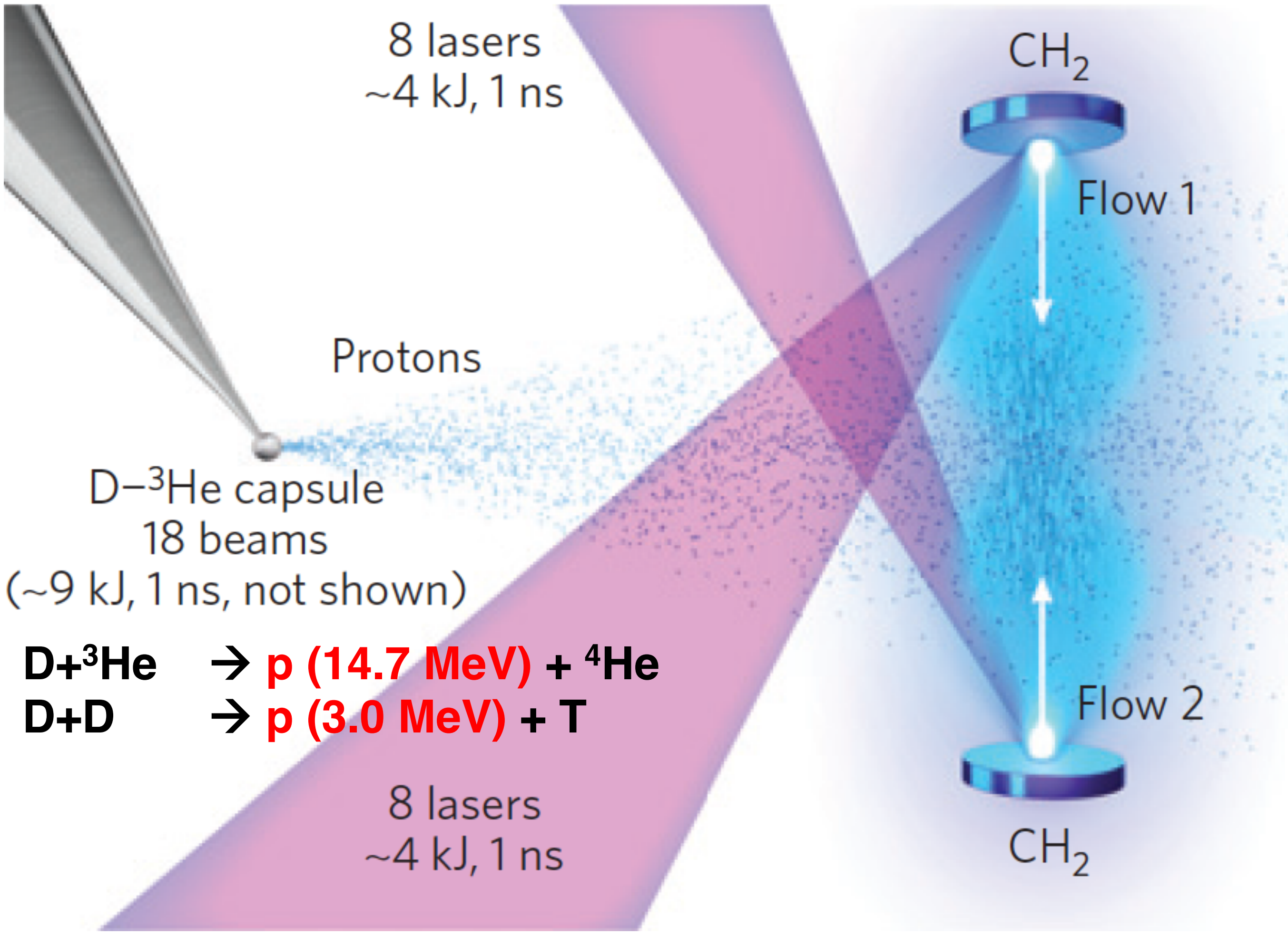

$D+{}^3He \rightarrow$ p (14.7 MeV) + ^4He

$D+D \rightarrow$ p (3.0 MeV) + T

C. M. Huntington et al, Nature Physics, 2015

Proton imaging reproducibly shows self-organized B-fields in collisionless counter-streaming plasmas

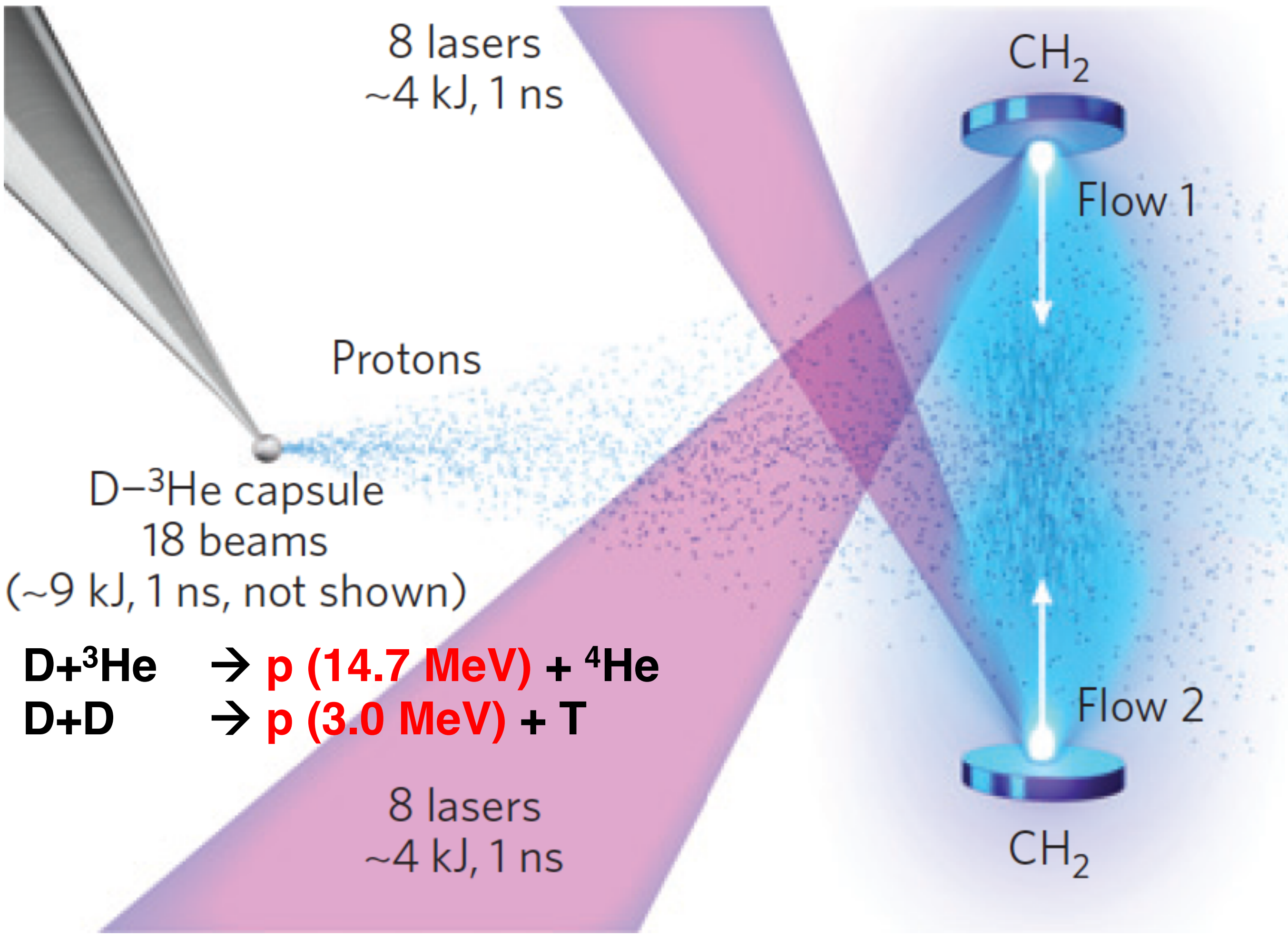

D+^{3}He → p (14.7 MeV) + ^{4}He

D+D → p (3.0 MeV) + T

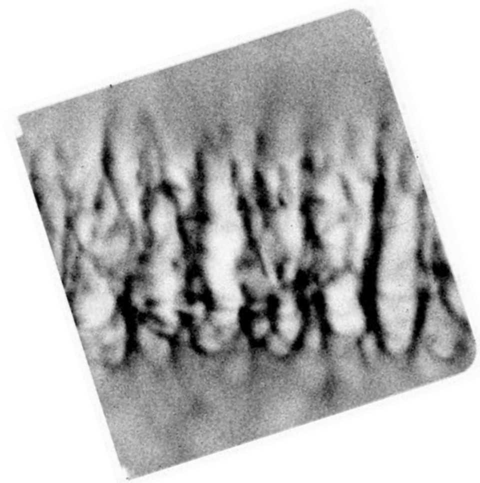

14.7-MeV proton image

C. M. Huntington et al, Nature Physics, 2015

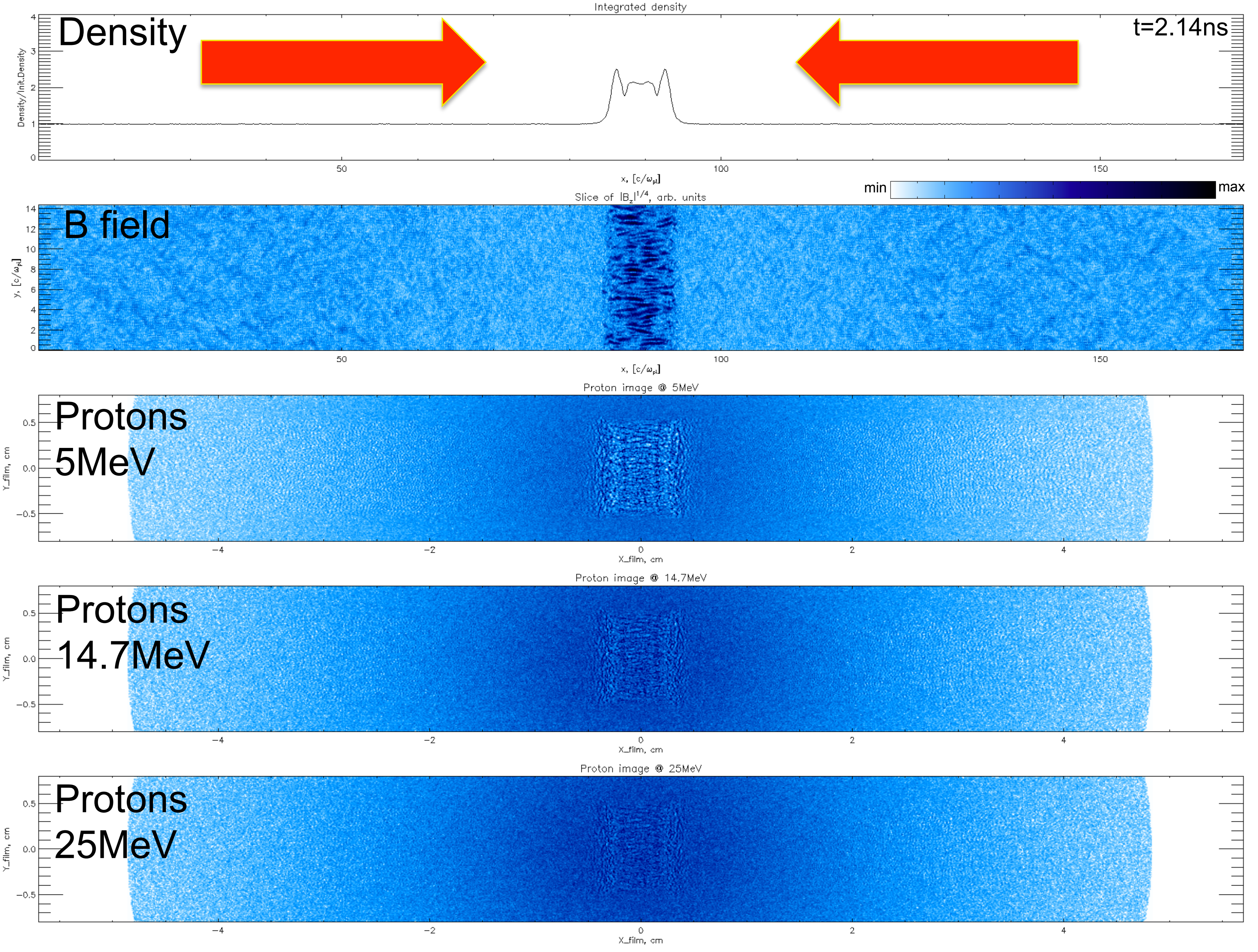

Integrated density
Density
t=2.14ns
Density/Init.Density
x, [c/ω_pi]
Slice of |B_z|^{1/4}, arb. units
min
max
B field
y, [c/ω_pi]
Proton image @ 5MeV
Protons
5MeV
Y_film, cm
X_film, cm
Proton image @ 14.7MeV
Protons
14.7MeV
Proton image @ 25MeV
Protons
25MeV

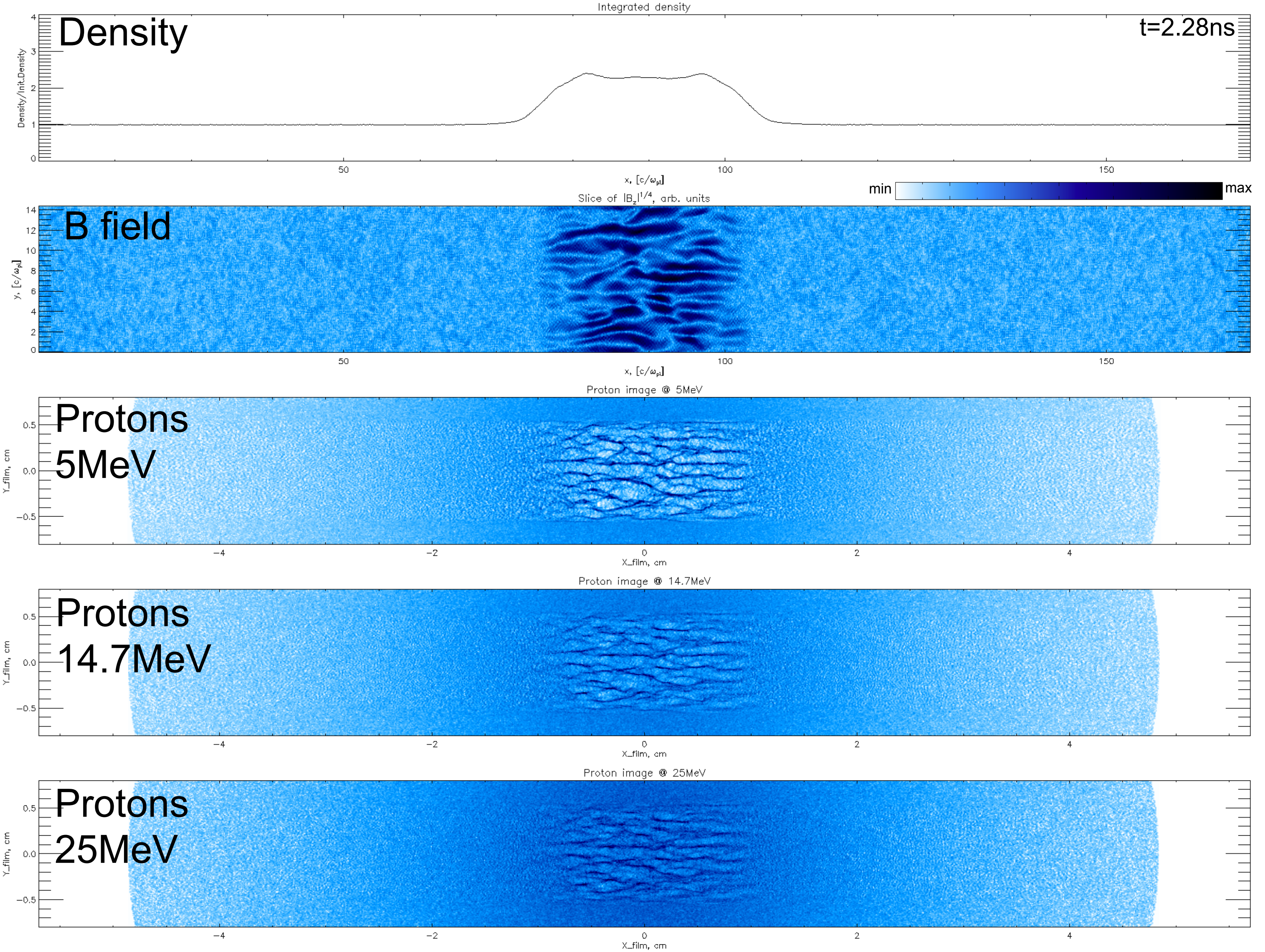
Integrated density
Density
t=2.28ns
Density/Init.Density
x, [c/ω_pi]
Slice of |B_z|^{1/4}, arb. units
min
max
B field
y, [c/ω_pi]
Proton image @ 5MeV
Protons
5MeV
Y_film, cm
X_film, cm
Proton image @ 14.7MeV
Protons
14.7MeV
Proton image @ 25MeV
Protons
25MeV

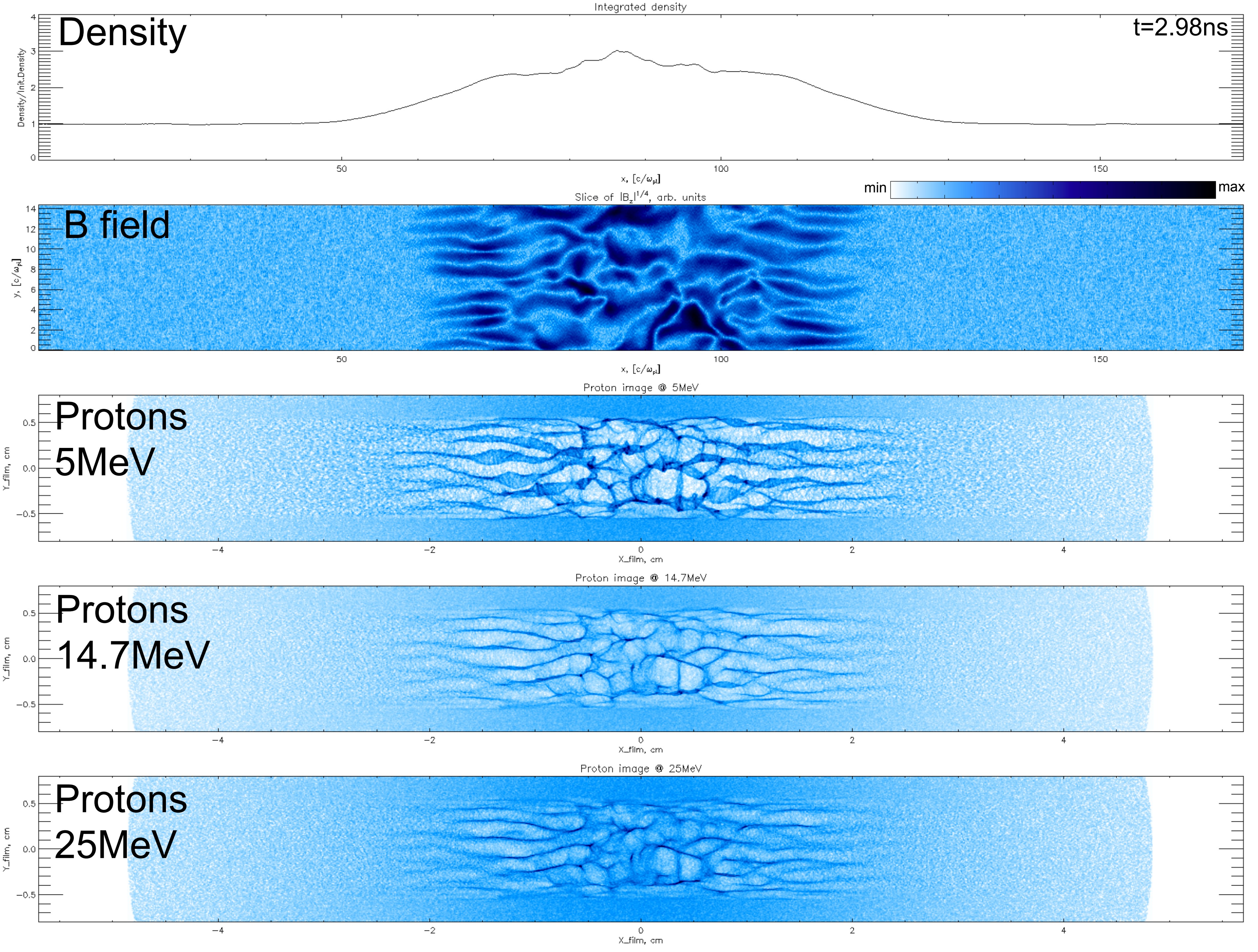

Integrated density
Density
t=2.98ns
Density/Init.Density
x, [c/ω_pi]
min
max
Slice of |B_z|^{1/4}, arb. units
B field
y, [c/ω_pi]
x, [c/ω_pi]
Proton image @ 5MeV
Protons
5MeV
Y_film, cm
X_film, cm
Proton image @ 14.7MeV
Protons
14.7MeV
Y_film, cm
X_film, cm
Proton image @ 25MeV
Protons
25MeV
Y_film, cm
X_film, cm

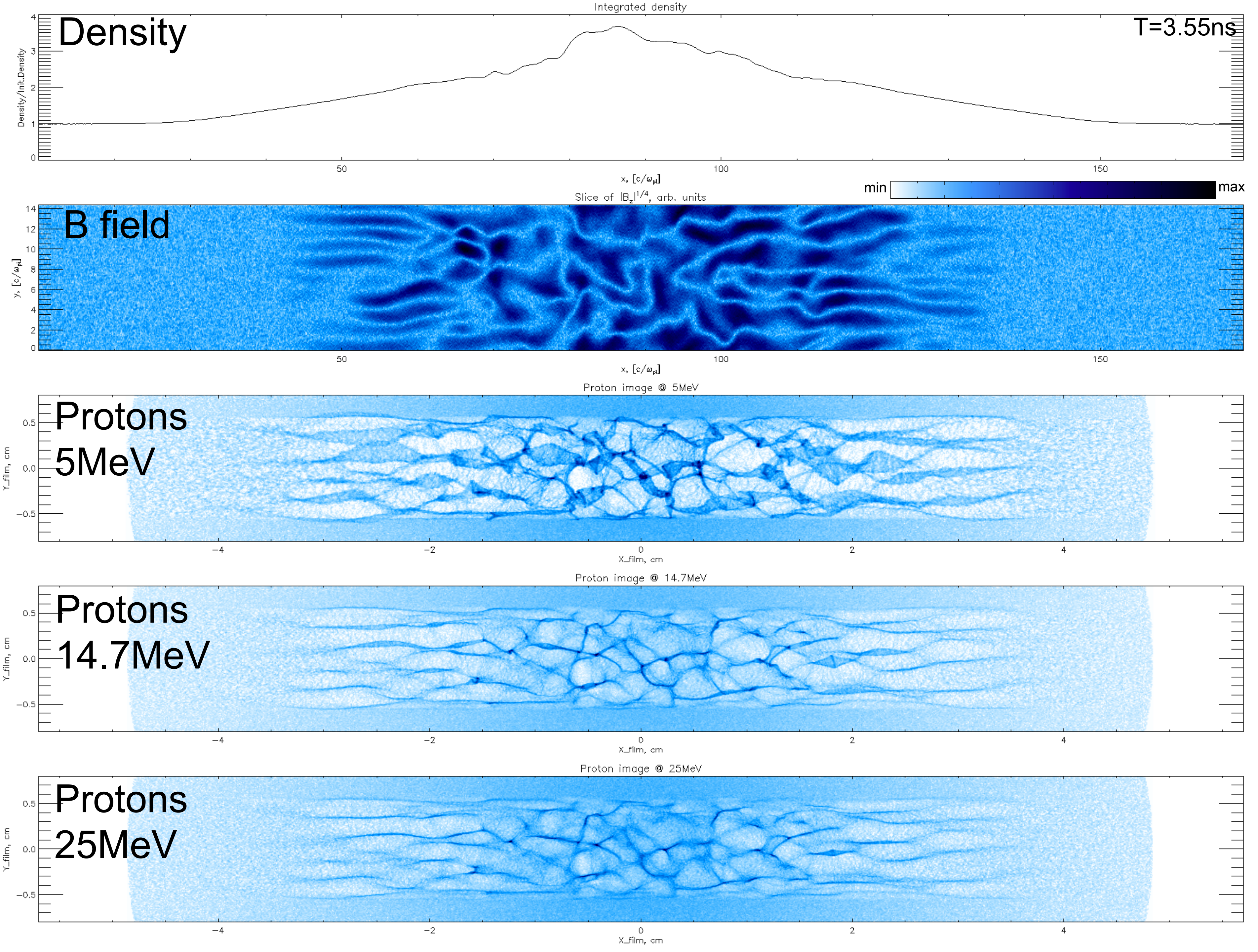

Integrated density
Density
T=3.55ns
Density/Init.Density
x, [c/ω_pi]
Slice of |B_z|^{1/4}, arb. units
min
max
B field
y, [c/ω_pi]
x, [c/ω_pi]
Proton image @ 5MeV
Protons 5MeV
Y_film, cm
X_film, cm
Proton image @ 14.7MeV
Protons 14.7MeV
Y_film, cm
X_film, cm
Proton image @ 25MeV
Protons 25MeV
Y_film, cm
X_film, cm

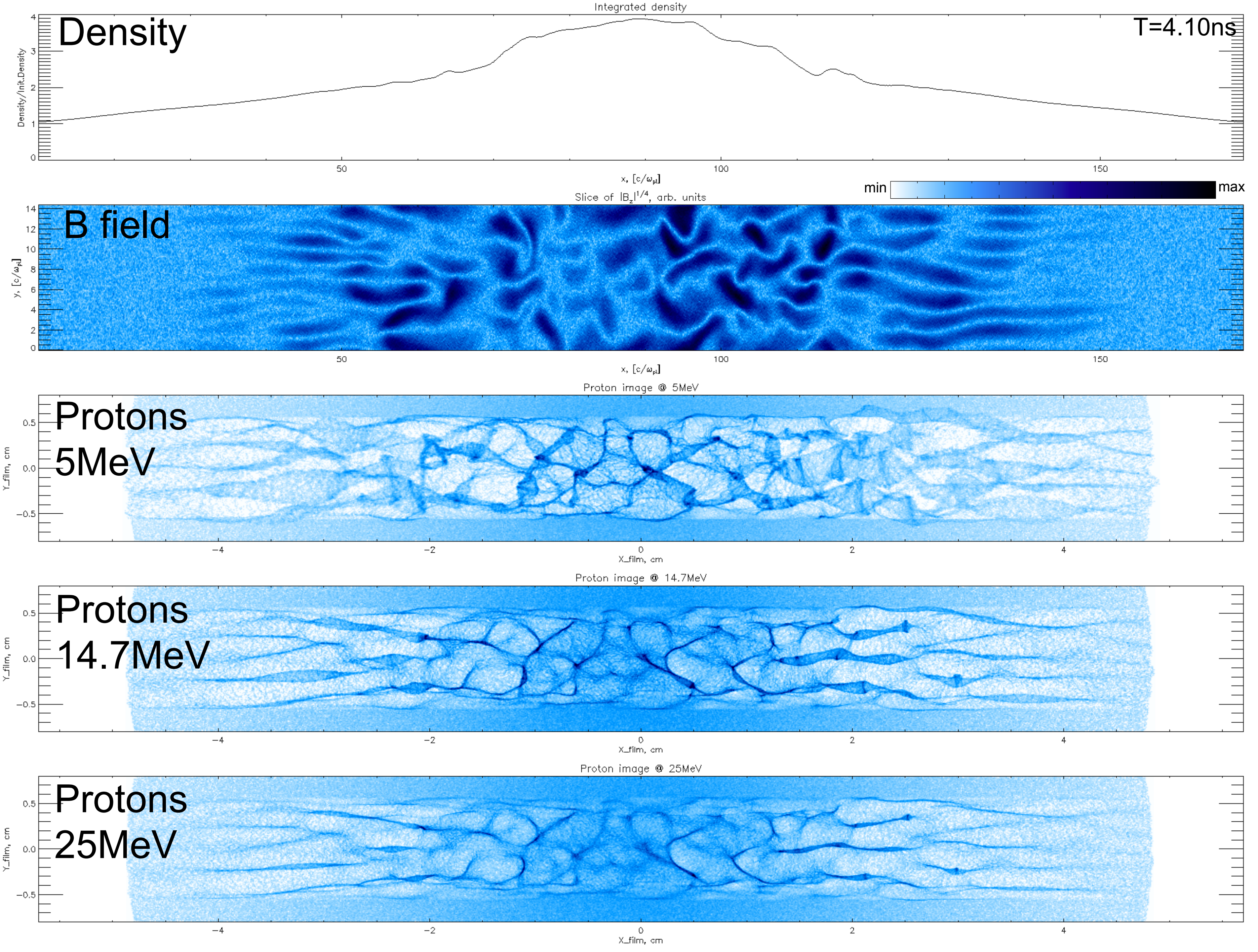

Integrated density
Density
T=4.10ns
Density/Init.Density
x, [c/ωpi]
min
max
Slice of |Bz|^1/4, arb. units
B field
y, [c/ωpi]
x, [c/ωpi]
Proton image @ 5MeV
Protons
5MeV
Y_film, cm
X_film, cm
Proton image @ 14.7MeV
Protons
14.7MeV
Y_film, cm
X_film, cm
Proton image @ 25MeV
Protons
25MeV
Y_film, cm
X_film, cm

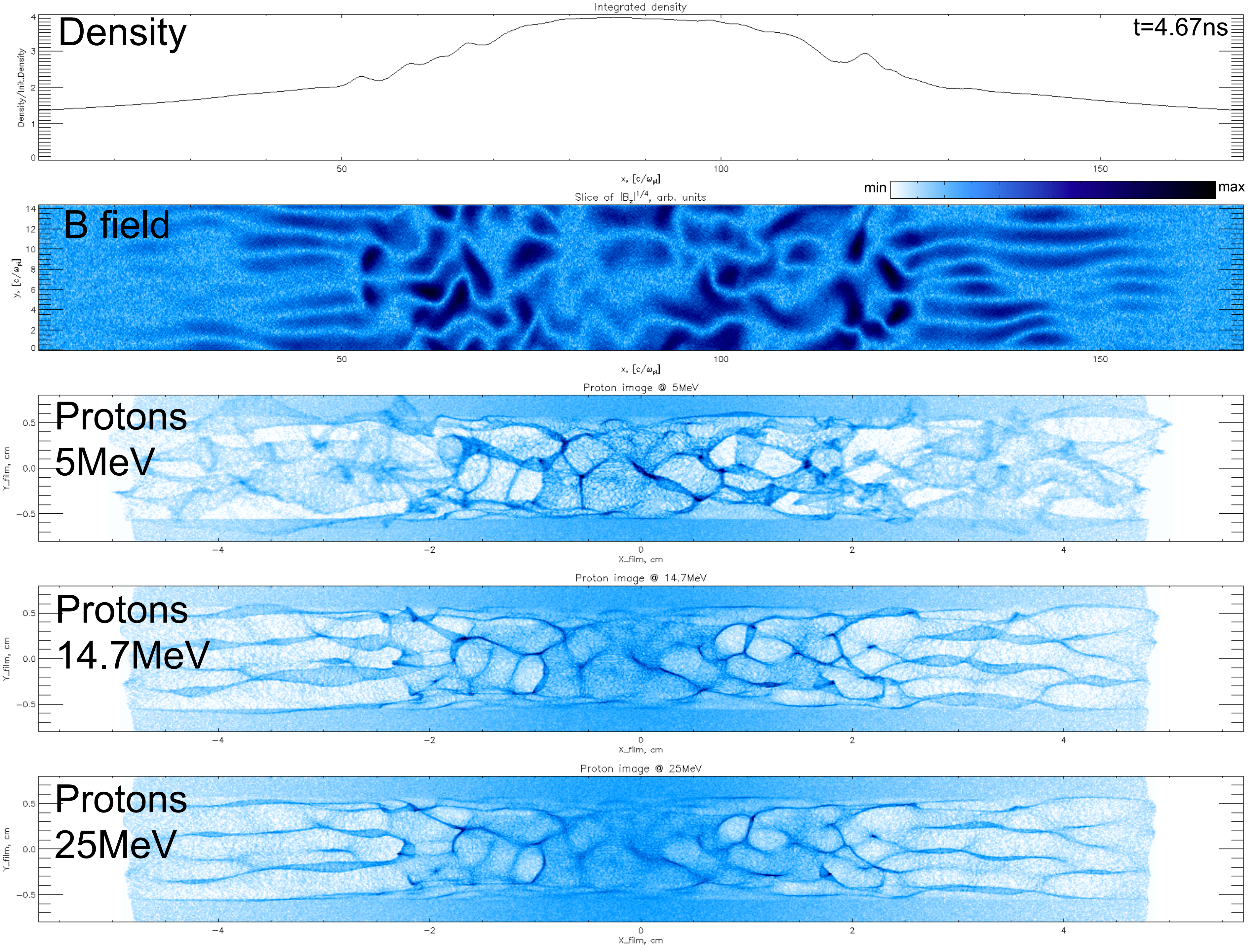

Integrated density
Density
t=4.67ns
Density/Init.Density
x, [c/ωpi]
min
max
Slice of |Bz|^1/4, arb. units
B field
y, [c/ωpi]
Proton image @ 5MeV
Protons
5MeV
Y_film, cm
X_film, cm
Proton image @ 14.7MeV
Protons
14.7MeV
Proton image @ 25MeV
Protons
25MeV

Proton images at different times illustrate B-field evolution

2.5 ns **3.5 ns** **4.5 ns** **5.5 ns**

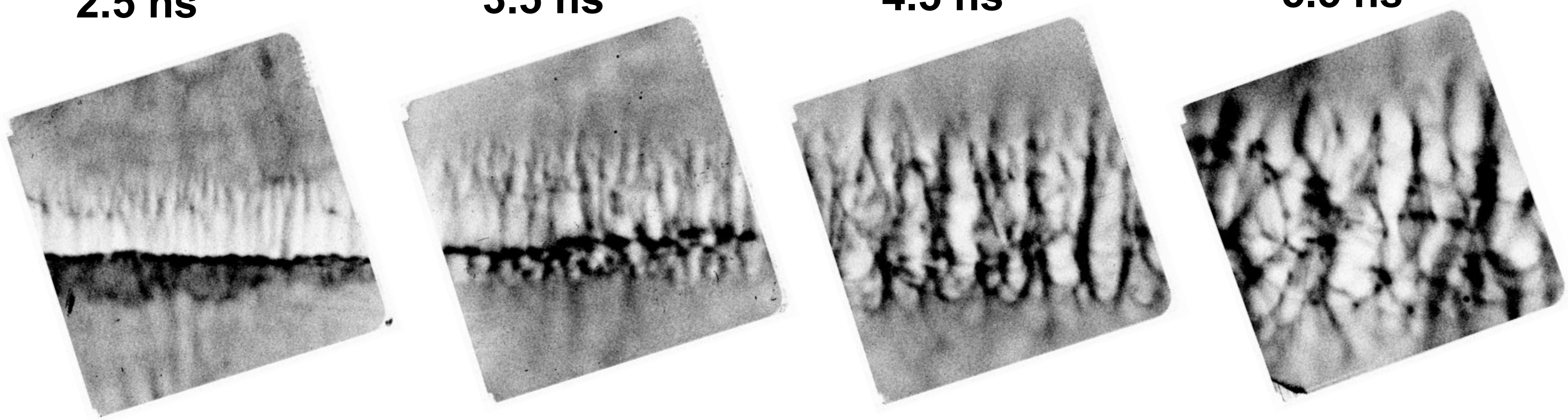

Very early time; only very fast and low n_e intercepts

Bulk of flow intercept; developing Weibel instability

Weibel growth matures

- **The flow velocity is ~1000 km/s and in collisionless regime**
- **The evolution of Weibel filaments is clearly observed in 14.7-MeV images**
- **Shock formation needs longer scale lengths!**

C. M. Huntington et al, Nature Physics, 2015; H. –S. Park et al., Phys. Plasmas, 2015; C. Huntington et al., Phys. Plasmas, 2017

NIF provides the means to achieve the necessary conditions to actually form the collionless shock

Experimental layout

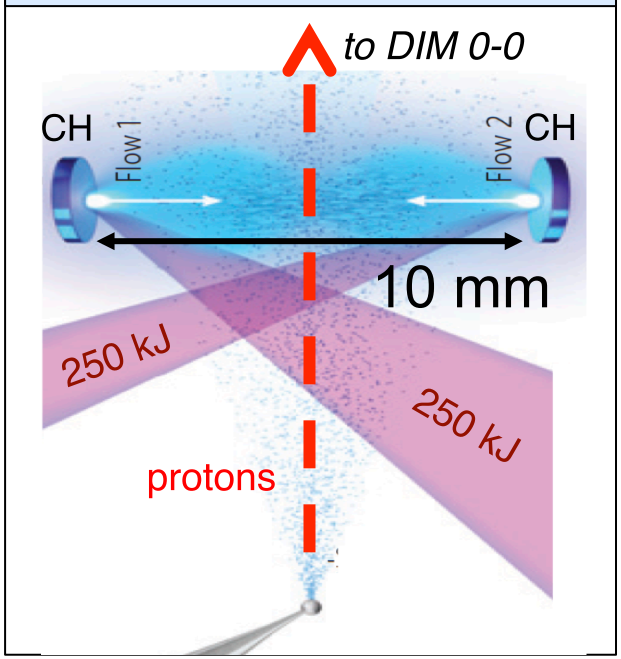

NIF target for N160329

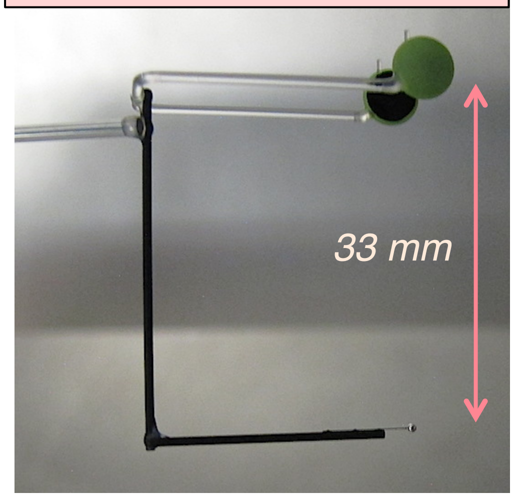

View from DIM 0-0

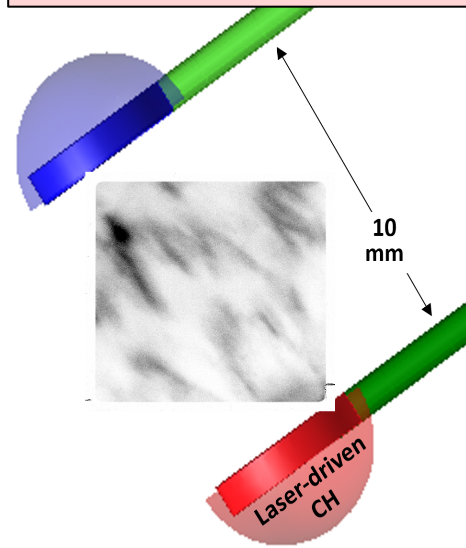

Proton radiography indicates strong magnetic field formation with evolving filamentary field structures

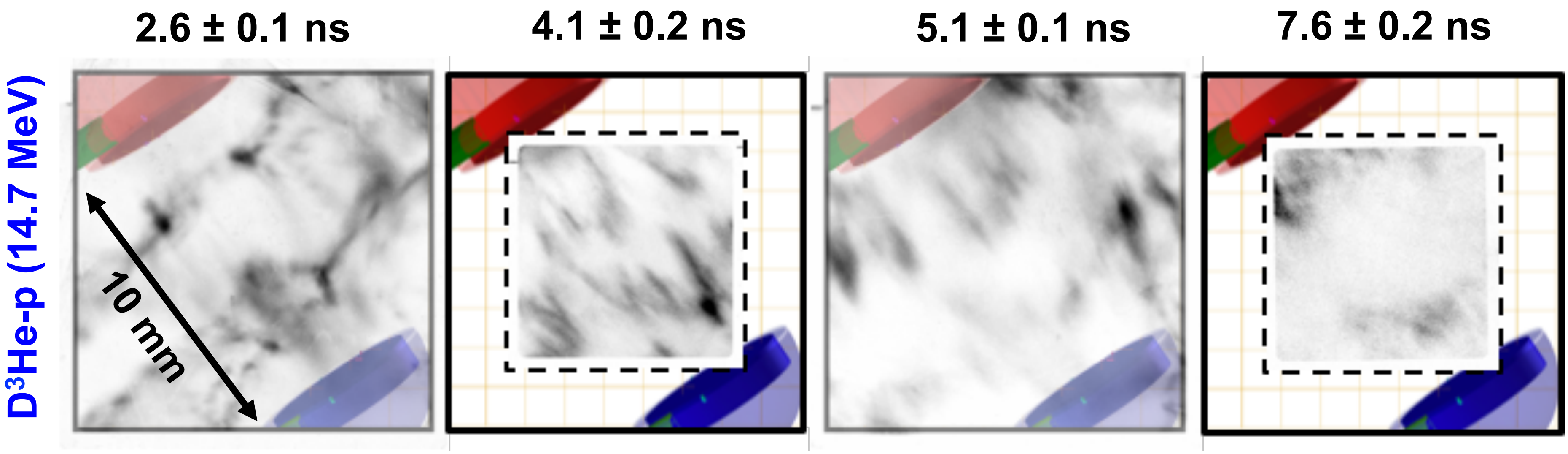

Biermann Battery Fields

Development and Merging of Weibel Filaments

Shock Development ??

- **Fluence normalized images show large deflection of protons**
- **NIF experiments show larger spatial features than the Omega observations: ~100 μm vs. ~1 mm**
- **B-field strength is 3~5 MG at saturation; filaments merge; more turbulent**

Outline

- High-Energy-Density (HED) Plasma
  - US facilities
- Plasma Nuclear Science using ICF-like implosions
  - p-p chain at relevant Gamow energies
  - Zylstra et al. (MIT)
- Laser-produced Magnetohydrodynamics
  - similarity conditions
  - Rayleigh-Taylor growth in core-collapse SNe
  - Drake, Kuranz et al. (UM)
- Laser-produced Jets
  - 'collisionless' shocks ← Park, Huntington et al. (LLNL)
  - supersonic jet dynamics → Manuel, Kuranz et al. (UM)
- Pair-Plasma Production
  - relativistic jets
  - Chen et al. (LLNL)
- Summary

Jets form during all stages of low-mass star formation

Collapsing pre-stellar dense core

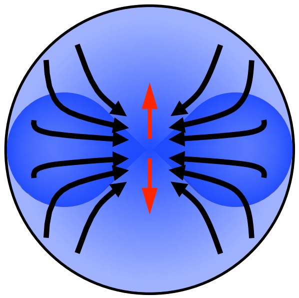

Time in Years **0** **~10^5** **~10^6**

beginning of an outflow

Cloud Radius	**~ 10^4 AU**
Cloud Mass	**~ few $M_\odot$**
Accretion Rate	**~ 10^{-4} $M_\odot$/year**

Jet/Outflow:
- **Young pre-stellar (adiabatic?) core**
- **Estimated age 200 years**
- **Slow, few km/s outflow**

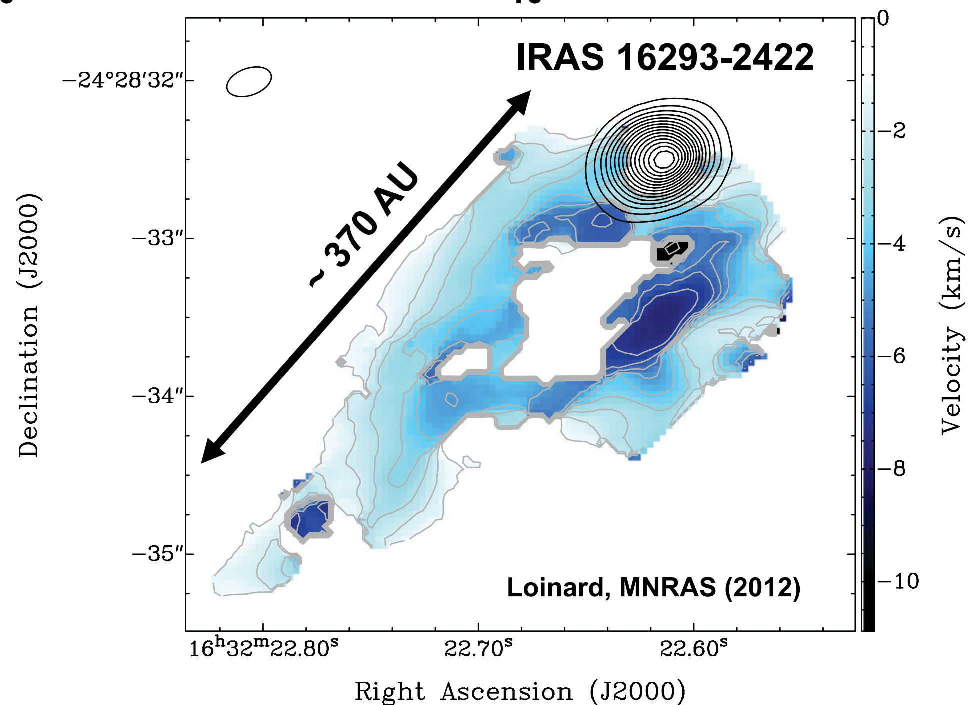

Jets form during all stages of low-mass star formation

Collapsing pre-stellar dense core

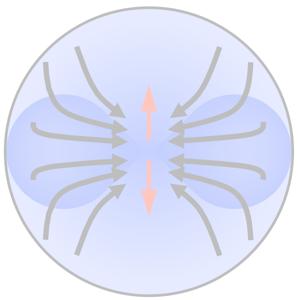

Class 0
Young Accreting Protostar

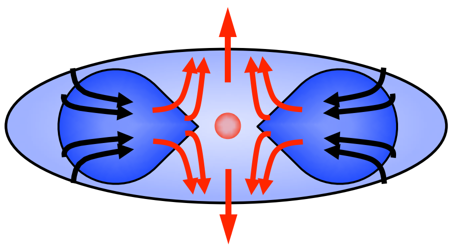

Time in Years 0 ~10^5

beginning of an outflow

jet/outflow ~ sub-pc scale

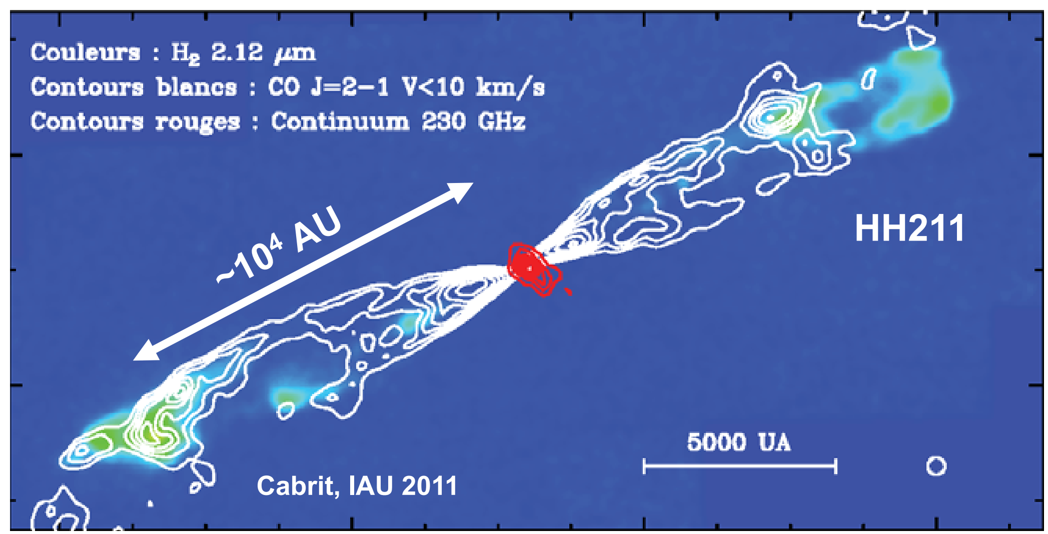

Envelope Radius ~ 10^3 AU
Envelope Mass > $M_\star$
Accretion Rate ~ 10^{-5} $M_\odot$/year

Jet/Outflow:

- Typically observed as molecular flows from the source
  - Slow (< 10 km/s) cavities
  - Fast (~10-100 km/s) jets

Jets form during all stages of low-mass star formation

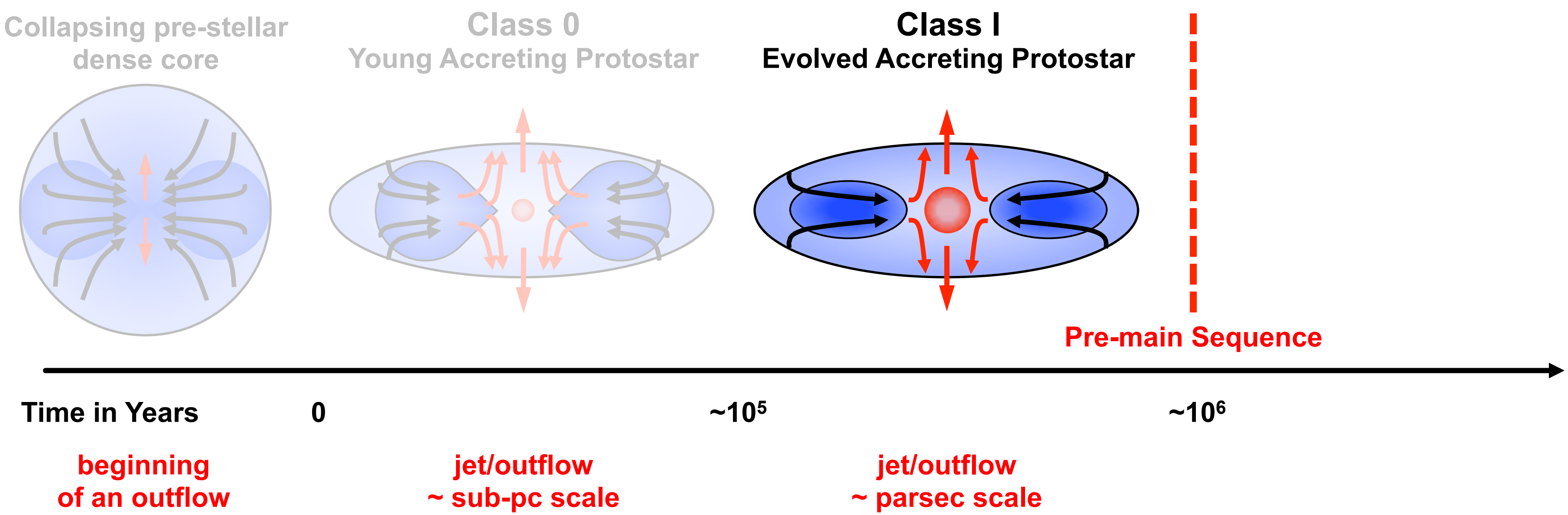

Envelope Radius ~ few $\times 10^2$ AU
Disk Mass < $M_\star$
Accretion Rate ~ 10^{-6} $M_\odot$/year

Jet/Outflow:

- ➢ Atomic jet traced to pc-scales
- ➢ Weaker swept up molecular flow
- ➢ Clear evidence of jet episodicity and variability

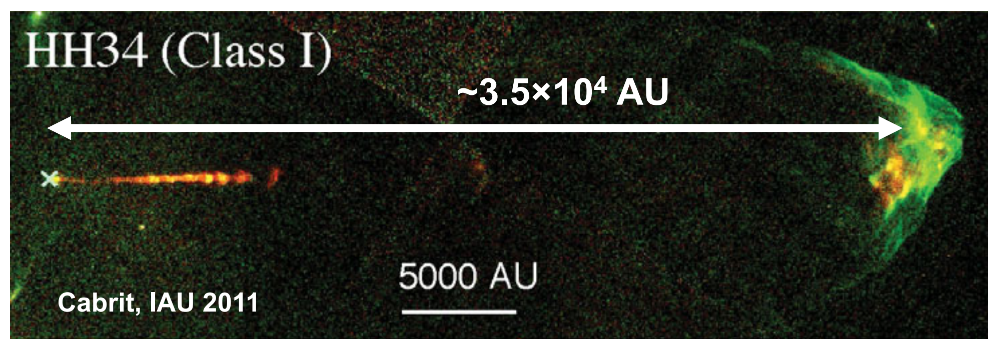

Jets form during all stages of low-mass star formation

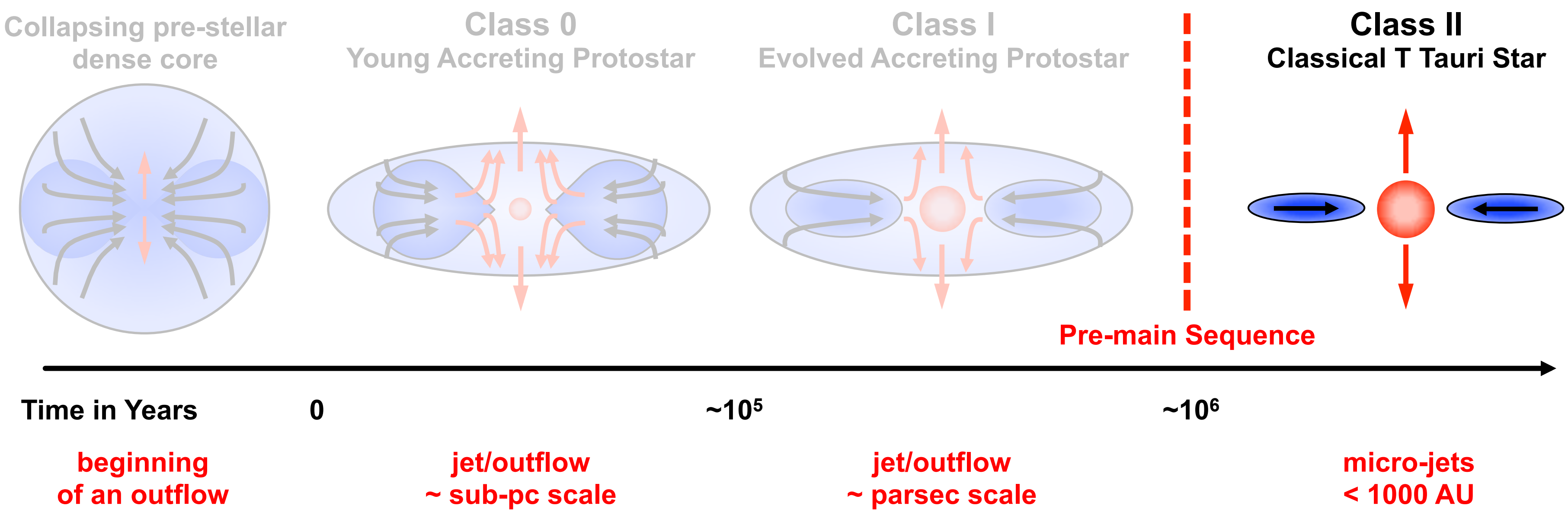

Disk Radius ~10^2 AU
Disk Mass << $M_\star$
Accretion Rate ~ 10^{-7} $M_\odot$/year

Jet/Outflow:
- Fast, few ×10^2 km/s atomic jets
- Wide-angle, slow H_2
- Rapid (few years) jet variability

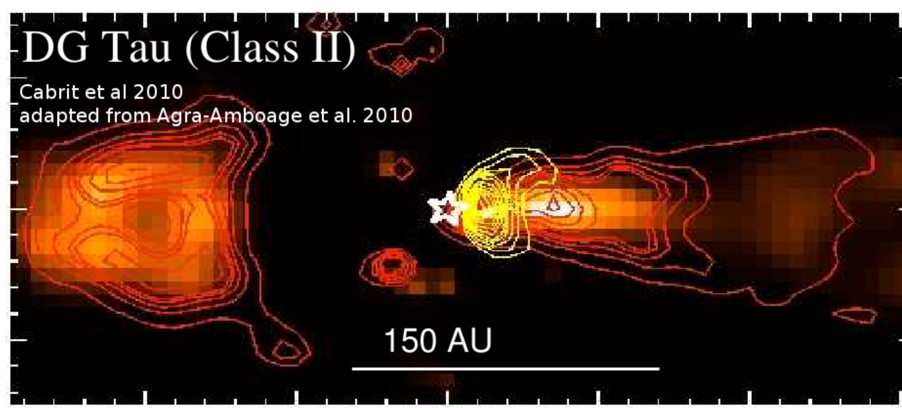

Jets form during all stages of low-mass star formation

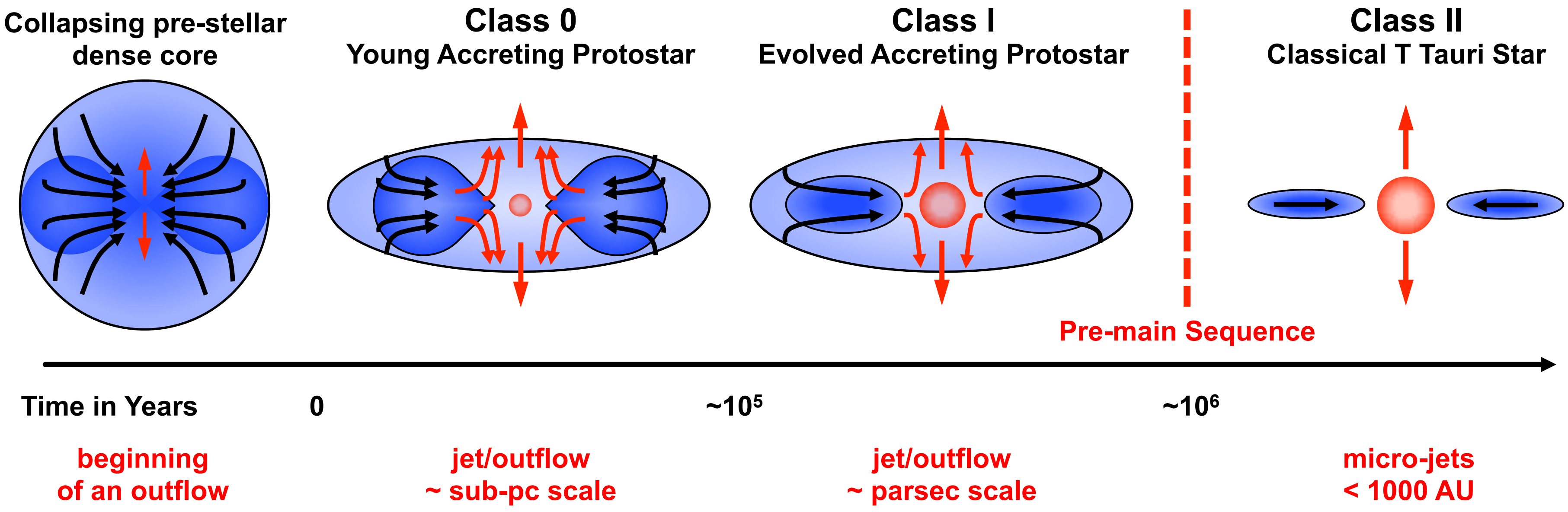

Jets form during all stages of evolution in accretion systems where $M_\star < 2\ M_\odot$

Cabrit, IAU (2011)

Magnetized plasma jets are prominent in young stellar objects with a wide range of parameters

Physical condition	Constraint	YSO Jets	Experiment
Viscosity plays minor role	Reynolds	$\sim10^3 - 10^7$	$\sim10^3 - 10^5$
Magnetic diffusion plays minor role	Magnetic Reynolds	$\sim10^{13} - 10^{17}$	$\sim10^{-1} - 10^2$
Supersonic flow	Mach number	$\sim10^1 - 10^2$	$\sim10^0$
Thermal compared to magnetic pressure	Thermal plasma β_{th}	$\sim10^{-3} - 10^1$	$\sim10^0 - 10^5$
Dynamic compared to magnetic pressure	Dynamic plasma β_{dyn}	$\sim10^{-3} - 10^1$	$\sim10^{-3} - 10^5$

Curran et al., MNRAS 382 (2007); Carrasco-Gonzalez et al., Science 330 (2010); Ferreira AA 452 (2006); Reipurth ARAA 39 (2001)

Jets are produced from laser-irradiated plastic targets and magnetized using a custom-built solenoid

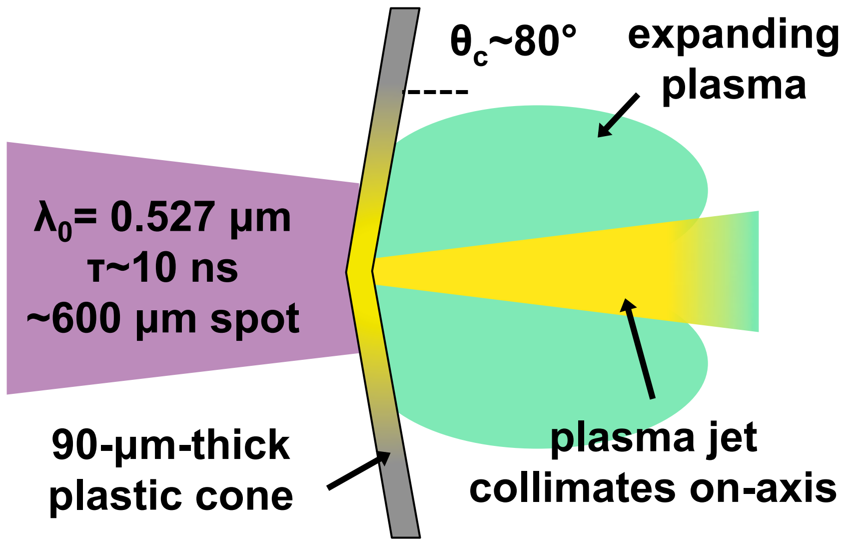

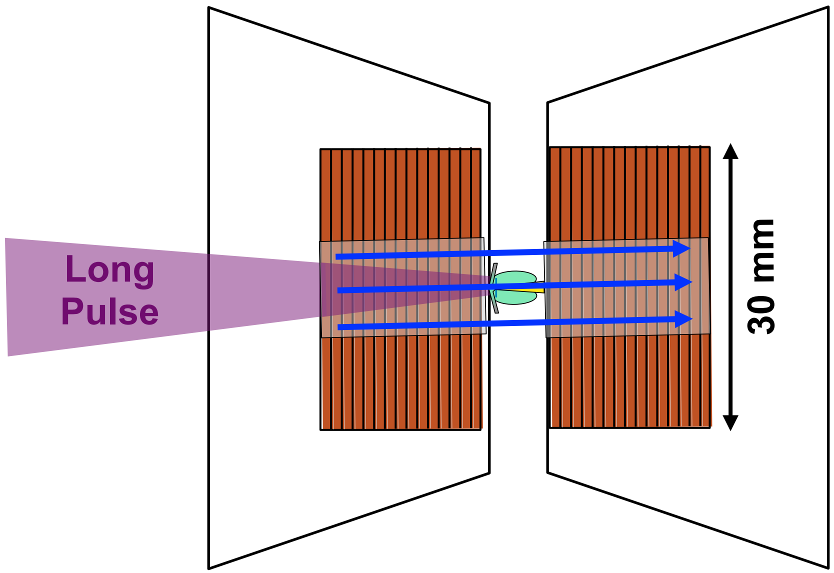

The 5 T point design generates thermal betas down to β~0.01-1 and dynamic betas down to to β~1-10 (n ~ 10^{18} cm^{-3}, T~1 eV, v~50-150 km/s)

Optical interferometry characterizes the spatial profile of inertially-confined plasma flows

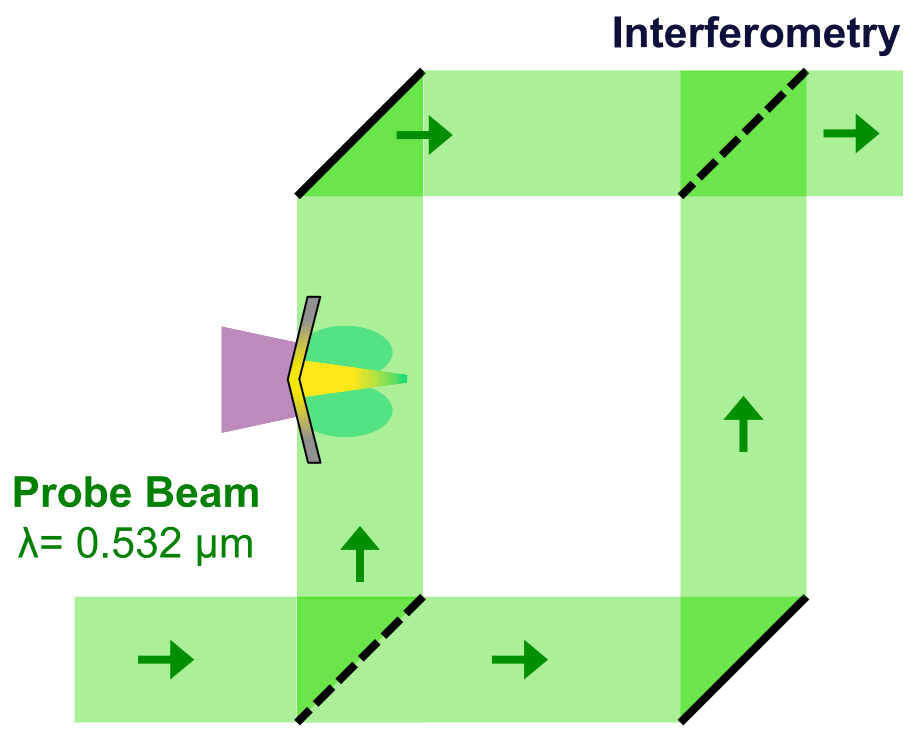

Optical interferometry characterizes the spatial profile of inertially-confined plasma flows

raw interferogram

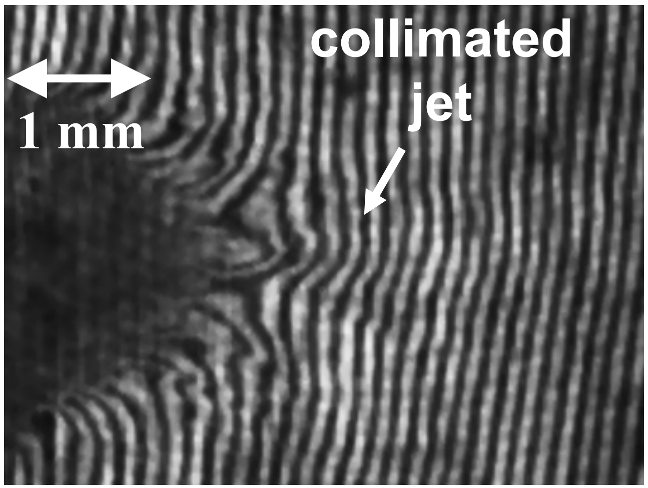

$$\Delta\varphi_{free} \approx \int \left(-\frac{n_e}{2n_{cr}}\right)\frac{\omega}{c}\,dl$$

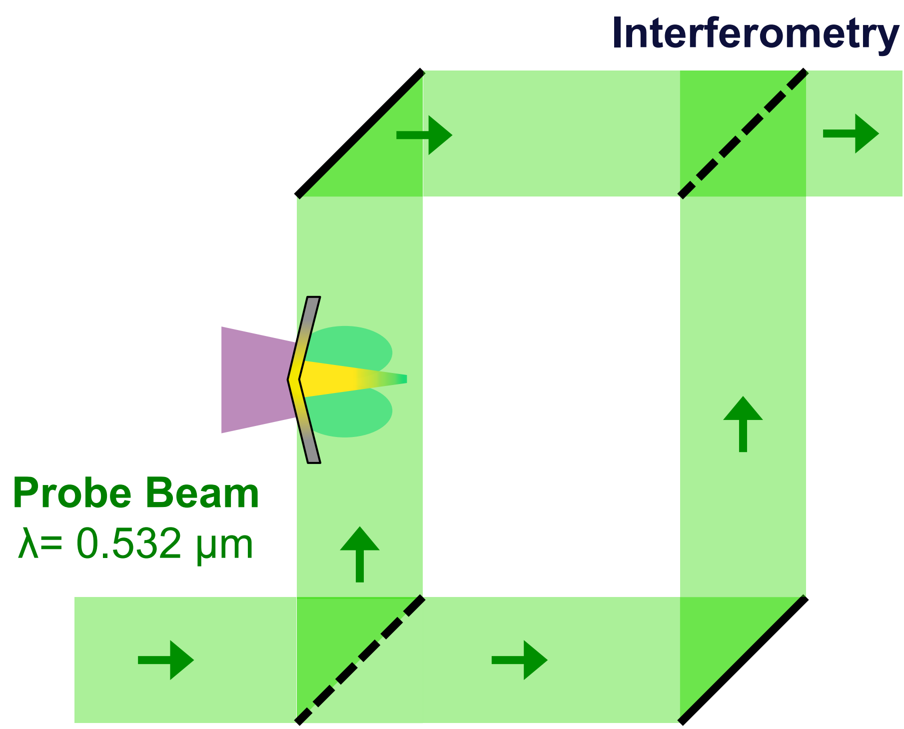

Processed interferograms show collimated flows when no axial B-field is applied

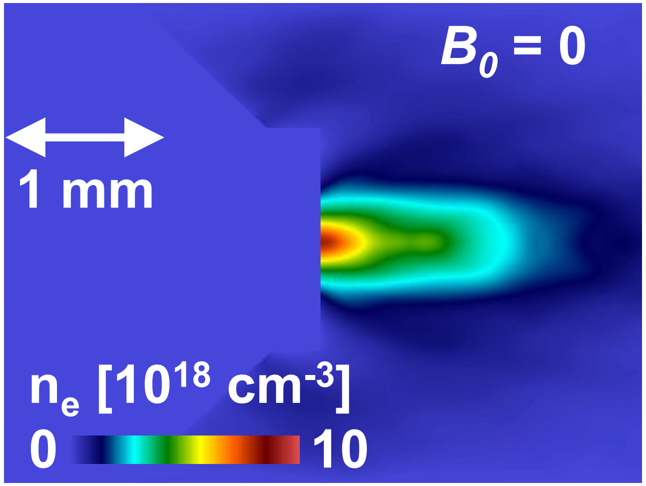

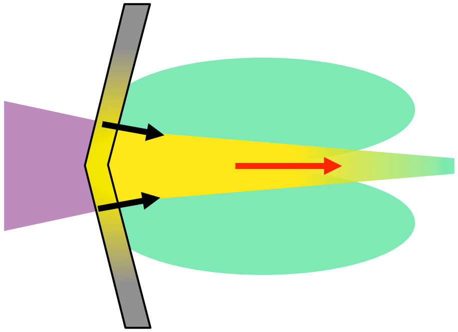

A 5-T B-field applied along the jet axis disrupts axial collimation

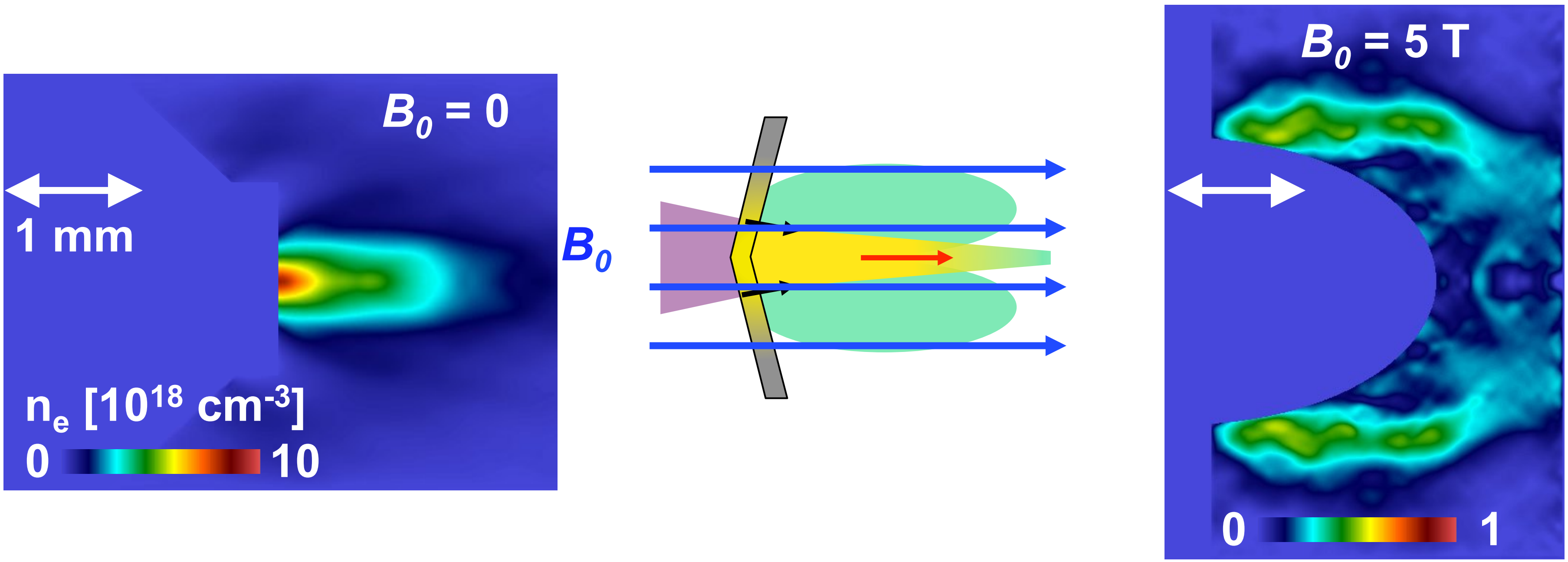

Jet-disruption effectiveness depends on the B-field strength

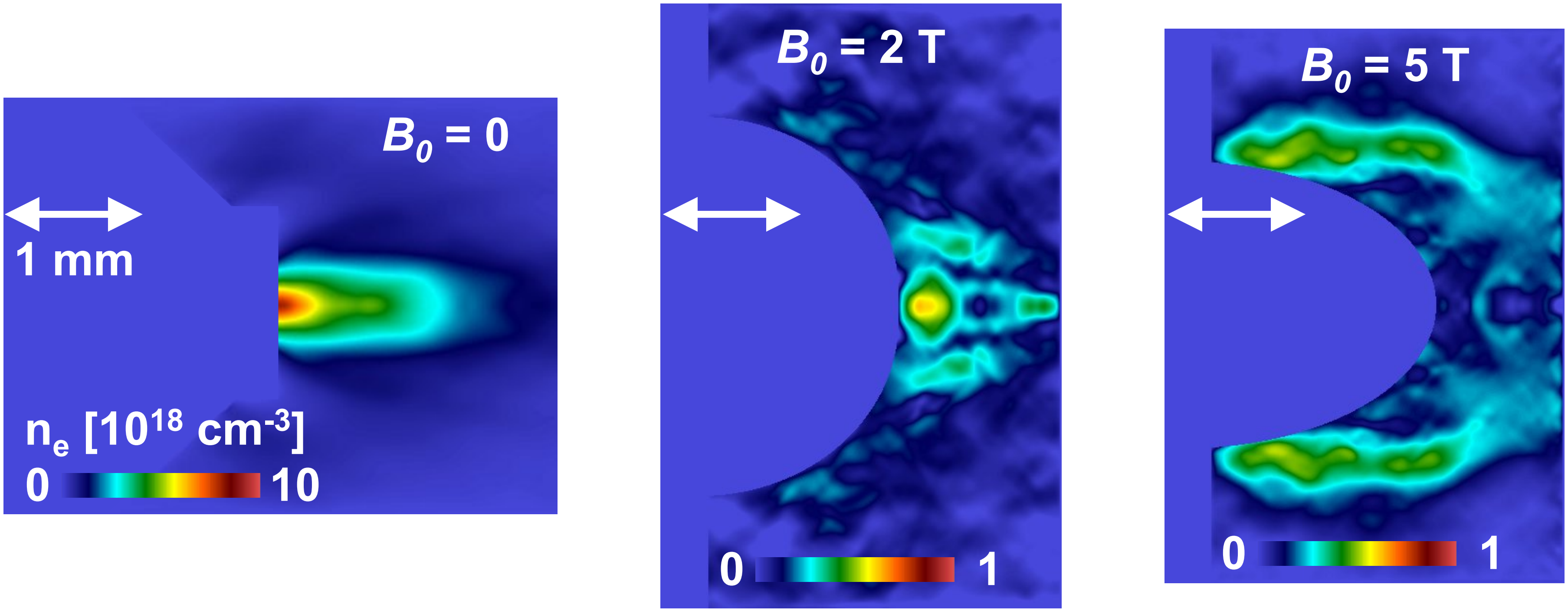

A 5-T axial B-field disrupts the inertially-collimated region of the flow, and magnetically collimates the radially expanding plasmas

A Lagrangian model* analytically accounts for B-field advection and diffusion in a converging cylindrical plasma

initial condition

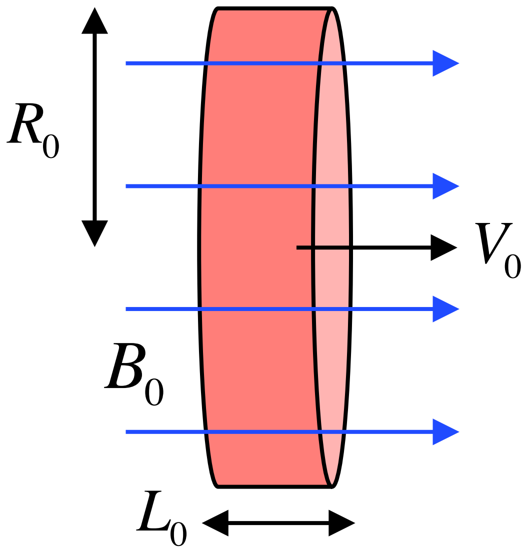

time *t* later

$R = R_0/\sqrt{\tau}$

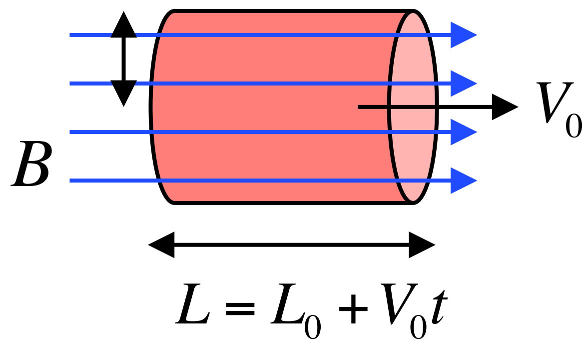

Dimensionless metric for time

$\tau \equiv L/L_0$

- **Uniform, incompressible, constant V_0**
- **Axial B-field B_0 penetrating the volume**
- **Elongation occurs in time due to collimation (dR/dt<0)**

---

*Fedorov CESW 41 (2005)

A Lagrangian model* analytically accounts for B-field advection and diffusion in a converging cylindrical plasma

$$B(r,\tau) = B_0 \tau e^{-\frac{\tau^2 - 1}{2\,\mathrm{Re}_m}}$$

$$\mathrm{Re}_m = \left(\frac{R_0}{4L_0}\right)\frac{V_0 R_0}{\eta / \mu_0}$$

Ratio of B-field advection to diffusion

*Fedorov CESW 41 (2005)

A Lagrangian model* analytically accounts for B-field advection and diffusion in a converging cylindrical plasma

$$B(r,\tau) = B_0 \tau e^{-\frac{\tau^2 - 1}{2\mathrm{Re}_m}}$$

Linear amplification

$$\mathrm{Re}_m = \left(\frac{R_0}{4L_0}\right)\frac{V_0 R_0}{\eta / \mu_0}$$

Ratio of B-field advection to diffusion

*Fedorov CESW 41 (2005)

A Lagrangian model* analytically accounts for B-field advection and diffusion in a converging cylindrical plasma

$$B(r,\tau) = B_0 \tau e^{-\frac{\tau^2 - 1}{2\,\mathrm{Re}_m}}$$

$$\mathrm{Re}_m = \left(\frac{R_0}{4L_0}\right)\frac{V_0 R_0}{\eta / \mu_0}$$

Linear amplification

Diffusion becomes more important with increasing τ (shrinking radius)

Ratio of B-field advection to diffusion

*Fedorov CESW 41 (2005)

A Lagrangian model* analytically accounts for B-field advection and diffusion in a converging cylindrical plasma

$$B(r,\tau) = B_0 \tau e^{-\frac{\tau^2 - 1}{2\mathrm{Re}_m}} \qquad \mathrm{Re}_m = \left(\frac{R_0}{4L_0}\right)\frac{V_0 R_0}{\eta / \mu_0}$$

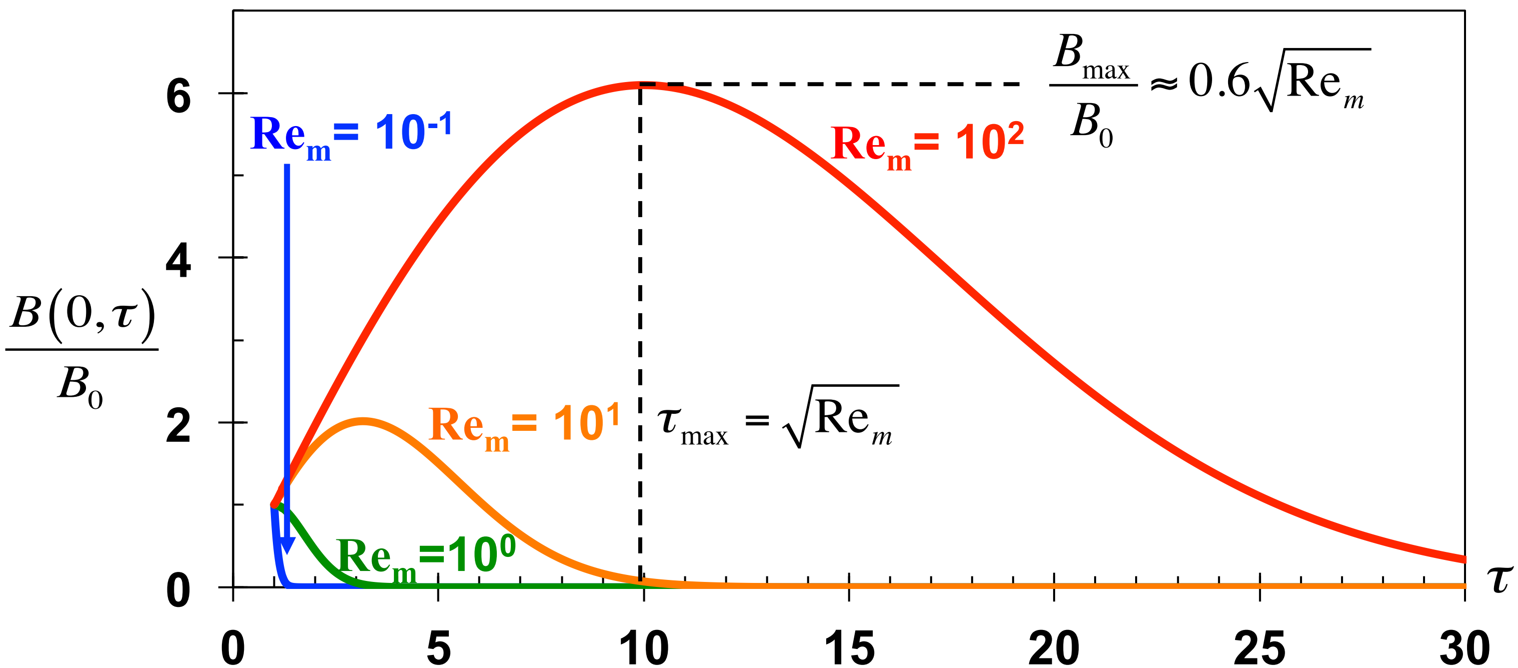

A collimation parameter (ψ) is derived from the on-axis pressure normalized to the magnetic pressure

$$\beta_{dyn} = \frac{\rho V_0^2}{B_0^2 / 2\mu_0}$$

$$\psi = \underbrace{\frac{1}{4}\left(\frac{R_0}{L_0}\right)^2 \frac{\beta_{dyn}}{\tau^3}}_{\text{Inertial Collimation}}$$

A collimation parameter (ψ) is derived from the on-axis pressure normalized to the magnetic pressure

$$\beta_{dyn} = \frac{\rho V_0^2}{B_0^2 / 2\mu_0}$$

$$\psi = \underbrace{\frac{1}{4}\left(\frac{R_0}{L_0}\right)^2 \frac{\beta_{dyn}}{\tau^3}}_{\text{Inertial Collimation}} - \underbrace{\frac{\beta_{th}}{\sqrt{\tau}}}_{\text{Thermal Expansion}}$$

Inertial Collimation

Thermal Expansion

A collimation parameter (ψ) is derived from the on-axis pressure normalized to the magnetic pressure

$$\beta_{dyn} = \frac{\rho V_0^2}{B_0^2 / 2\mu_0}$$

$$\psi = \underbrace{\frac{1}{4}\left(\frac{R_0}{L_0}\right)^2 \frac{\beta_{dyn}}{\tau^3}}_{\text{Inertial Collimation}} - \underbrace{\frac{\beta_{th}}{\sqrt{\tau}}}_{\text{Thermal Expansion}} - \underbrace{\tau^2 e^{-\frac{\tau^2 - 1}{\mathrm{Re}_m}}}_{\text{Magnetic Expansion}}$$

$$\mathrm{Re}_m = \left(\frac{R_0}{4L_0}\right)\frac{V_0 R_0}{\eta / \mu_0}$$

A collimation parameter (ψ) is derived from the on-axis pressure normalized to the magnetic pressure

$$\beta_{dyn} = \frac{\rho V_0^2}{B_0^2 / 2\mu_0}$$

$$\psi = \underbrace{\frac{1}{4}\left(\frac{R_0}{L_0}\right)^2 \frac{\beta_{dyn}}{\tau^3}}_{\text{Inertial Collimation}} - \underbrace{\frac{\beta_{th}}{\sqrt{\tau}}}_{\text{Thermal Expansion}} - \underbrace{\tau^2 e^{-\frac{\tau^2 - 1}{\mathrm{Re}_m}}}_{\text{Magnetic Expansion}}$$

$$\mathrm{Re}_m = \left(\frac{R_0}{4L_0}\right)\frac{V_0 R_0}{\eta / \mu_0}$$

$\psi < 0$: Jet Disruption

$\psi > 0$: Jet Formation

The Lagrangian-cylinder model describes observations well in a semi-quantitative manner at 50 ns (τ~25)

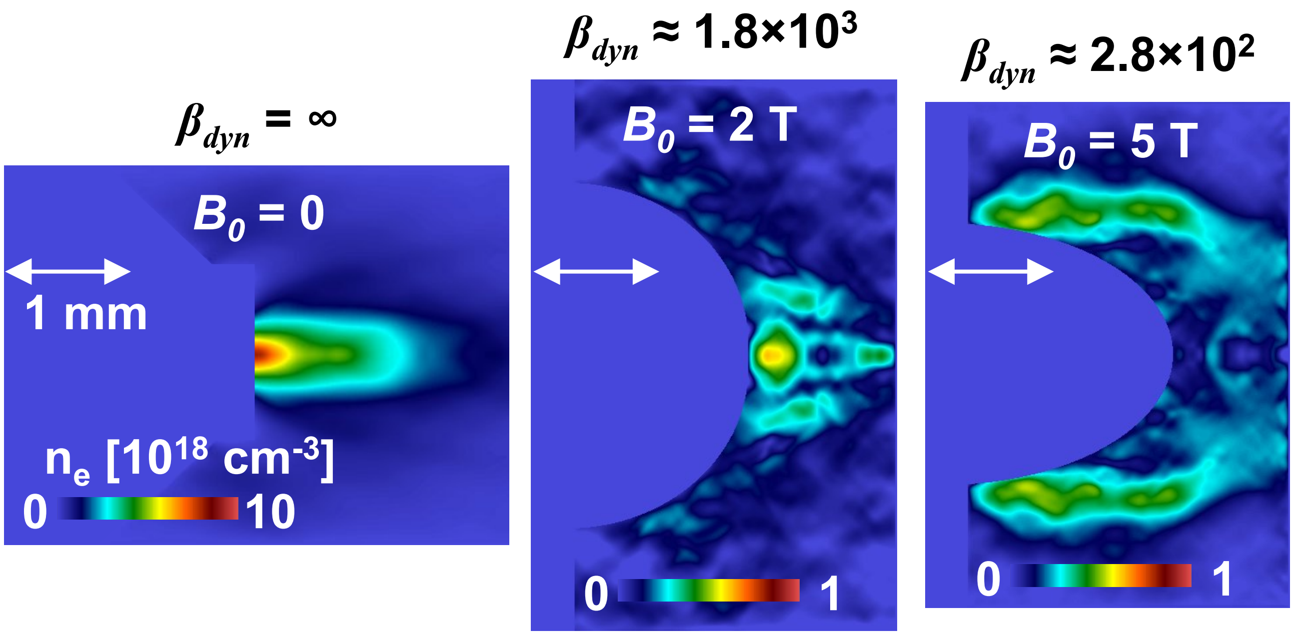

The Lagrangian-cylinder model describes observations well in a semi-quantitative manner at 50 ns (τ~25)

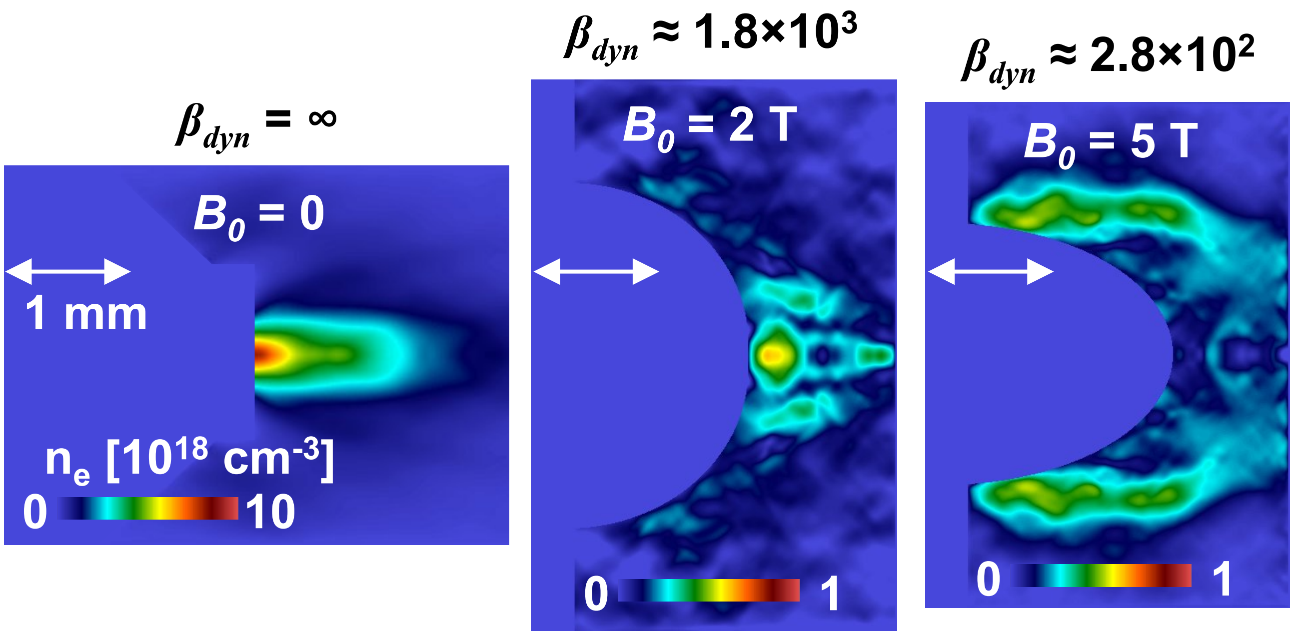

Re_m = 20

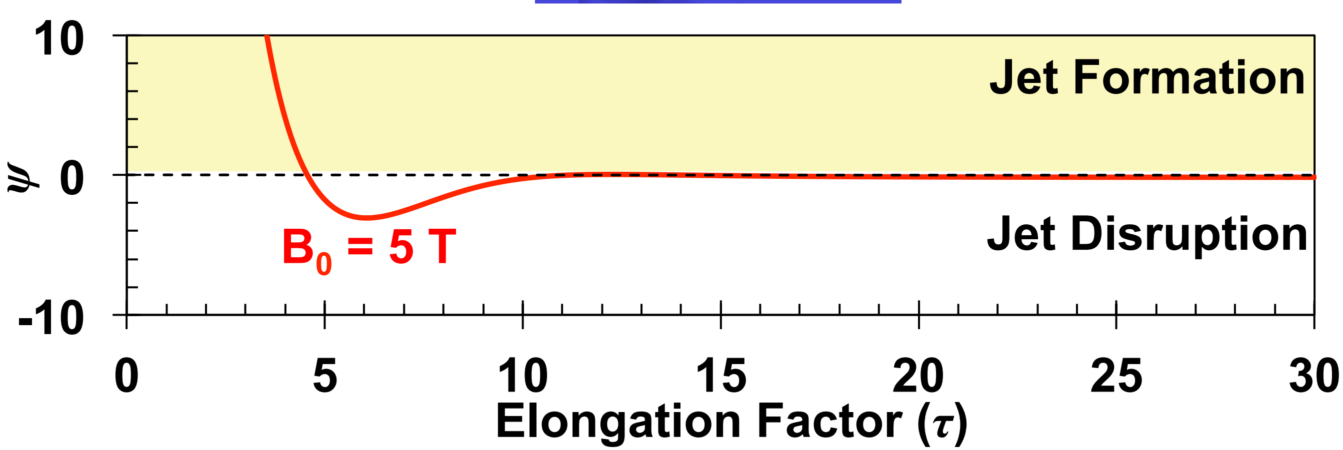

The Lagrangian-cylinder model describes observations well in a semi-quantitative manner at 50 ns (τ~25)

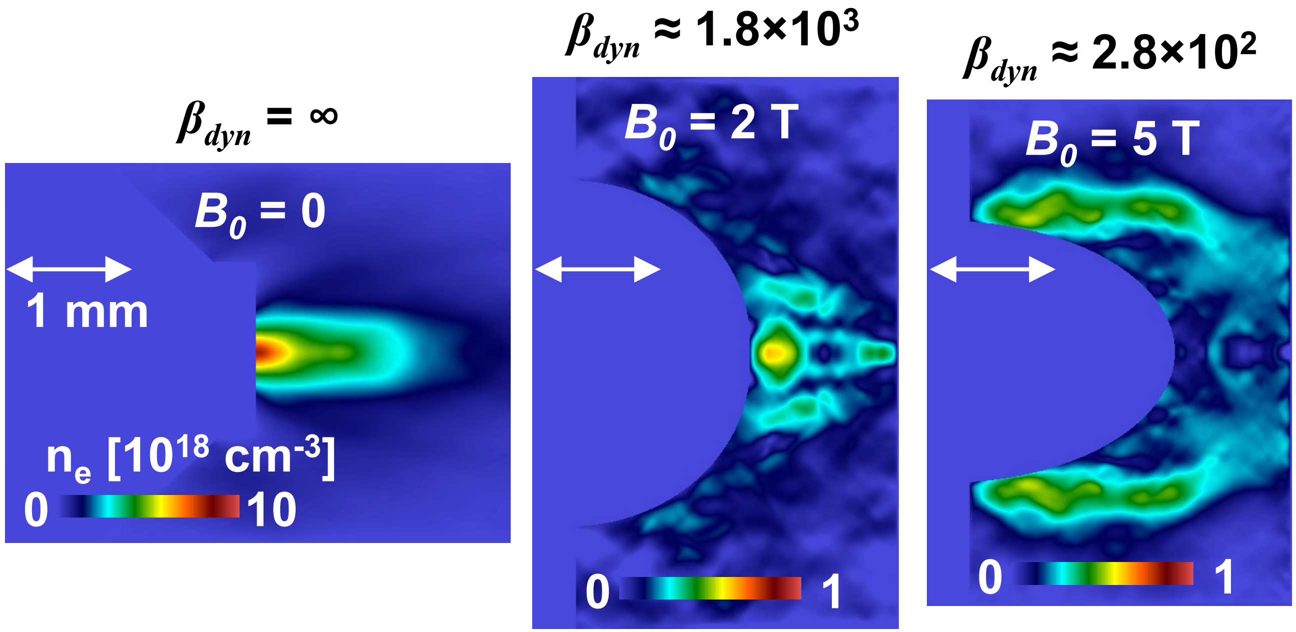

$Re_m = 20$

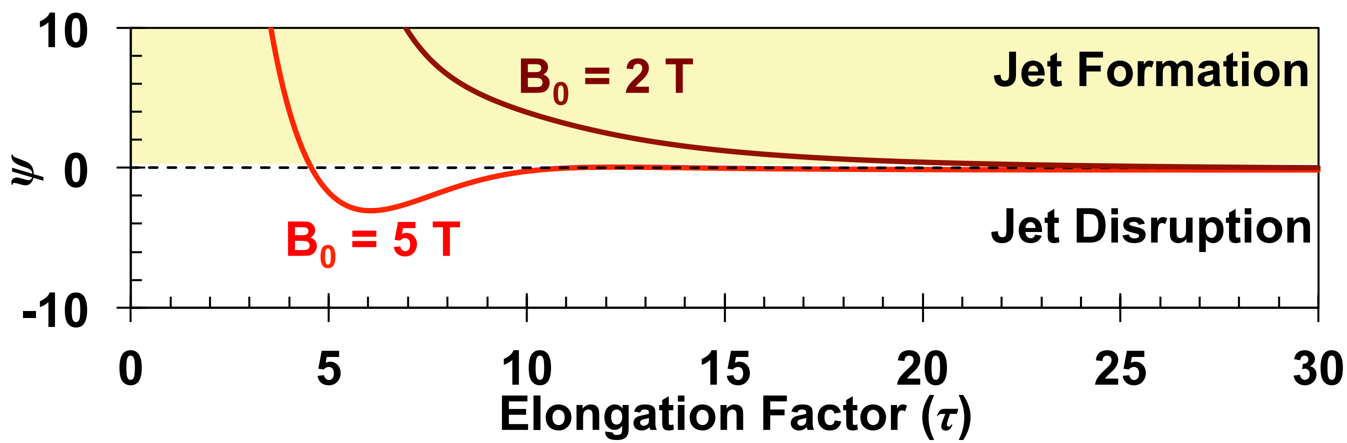

Similar behavior is observed* in magnetized shaped charges

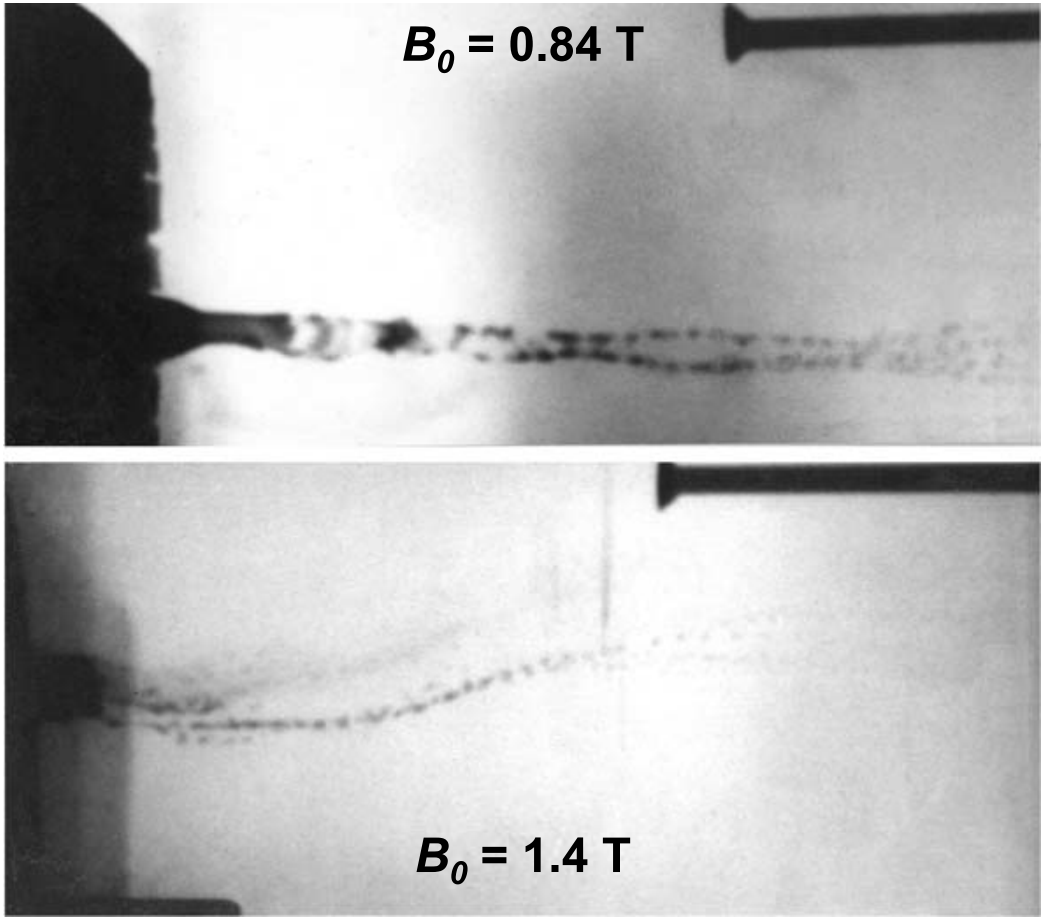

*Fedorov JAMTP 48 (2007)

B-field amplification can quickly cause jet disruption at high enough magnetic Reynolds numbers

$Re_m = 10^{-1}$

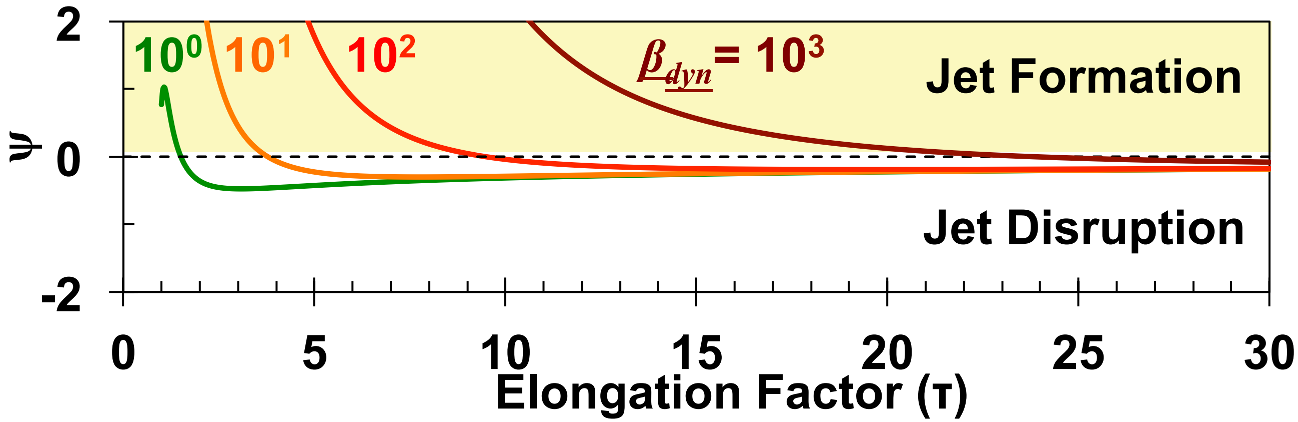

B-field amplification can quickly cause jet disruption at high enough magnetic Reynolds numbers

$Re_m = 10^{-1}$

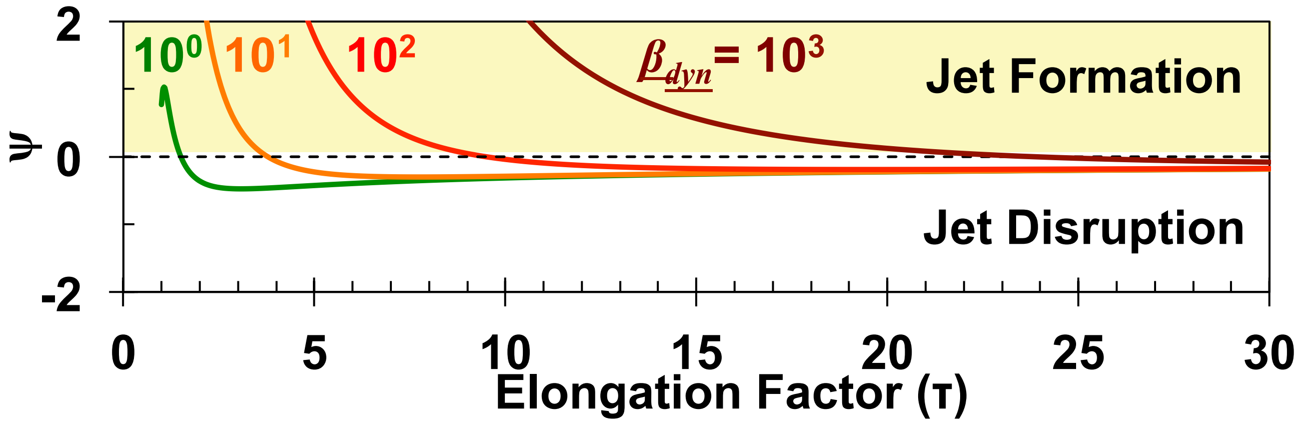

Higher Re_m pushes $\psi < 0$ at earlier τ

$Re_m = 10^2$

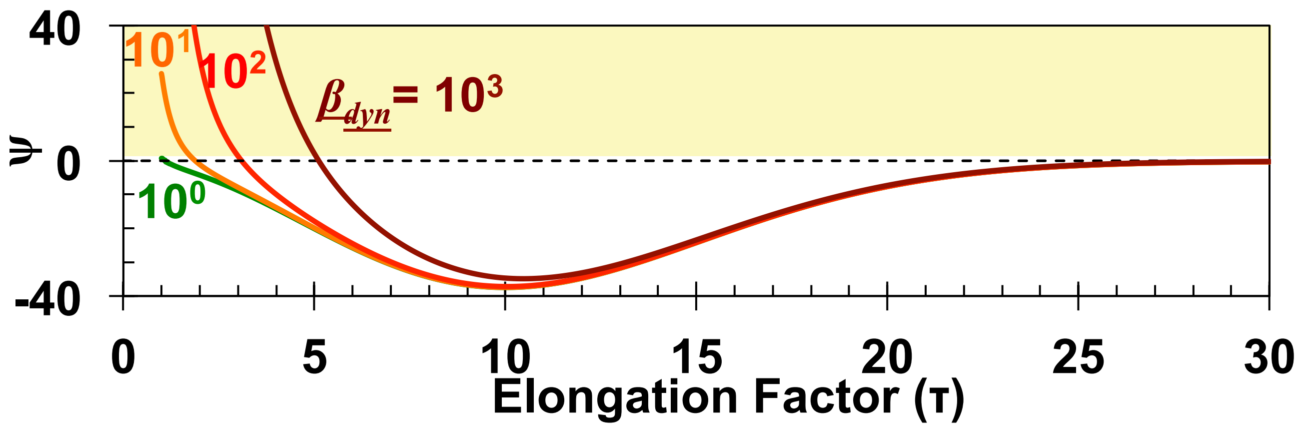

B-field amplification can quickly cause jet disruption at high enough magnetic Reynolds numbers

- **The presence of even a weak axial B-field in a hydrodynamically converging system will disrupt collimation at high enough Re_m**
- **In astrophysical accretion systems $Re_m > 10^{10}$, observations of a weak B-field parallel to the outflow* precludes inertial-collimation as a source**

$Re_m = 10^2$

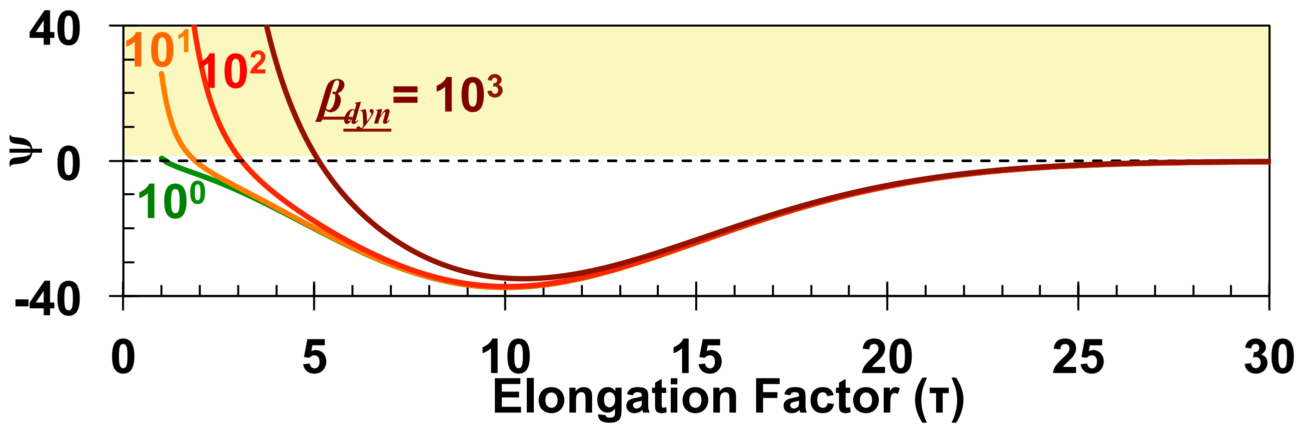

* Targon ApJ 743 (2011)

Outline

- High-Energy-Density (HED) Plasma
  - US facilities

Zylstra et al. (MIT)

- Plasma Nuclear Science using ICF-like implosions
  - p-p chain at relevant Gamow energies

Drake, Kuranz et al. (UM)

- Laser-produced Magnetohydrodynamics
  - similarity conditions
  - Rayleigh-Taylor growth in core-collapse SNe

Park, Huntington et al. (LLNL) ← 'collisionless' shocks

Manuel, Kuranz et al. (UM) ← supersonic jet dynamics

- Laser-produced Jets
  - 'collisionless' shocks
  - supersonic jet dynamics

Chen et al. (LLNL)

- Pair-Plasma Production
  - relativistic jets

- Summary

Relativistic plasmas can be created using high-power-laser facilities

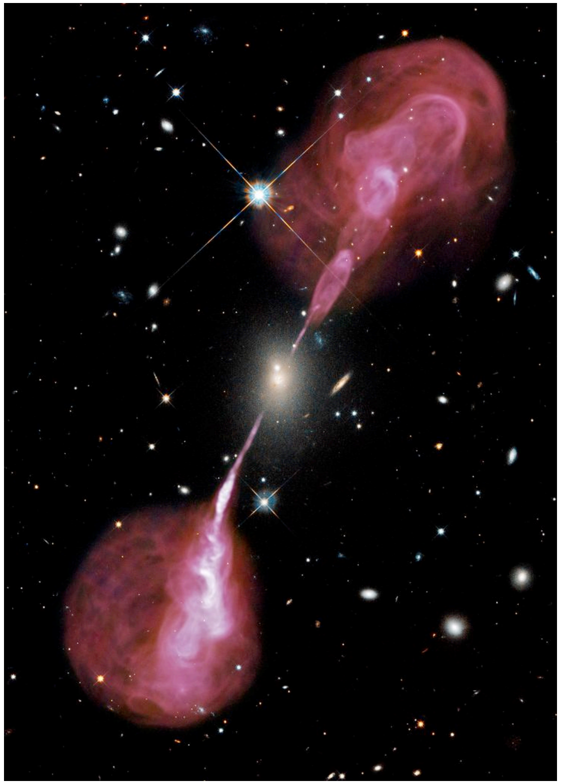

Unique features of these pair plasmas:

- **Positron acceleration**
- **Quasi monoenergetic positrons**
- **Relativistic electron-positron jets**
- **Scaling against laser energy**
- **Collimation**

Can we create and study relativistic jet dynamics in the lab?

At high laser intensities, photon-particle and particle-particle interactions become relativistic

10^{12} 10^{14} 10^{16} 10^{18} 10^{20} 10^{22} 10^{24} 10^{26} 10^{28} W/cm^2

- **atomic processes**
- **collisional absorption**
- **non-linear optics**

- **relativistic electrons**
- **nuclear processes**
- **γ-production**
- **e^+e^- plasmas**

- **pion production**
- **relativistic protons**
- **QED**

Typical parameters	> 10^{20} W/cm^2
Electric fields	10^{12} V/m
Magnetic fields	100's MG
Pressure	Gbar
Temperature	keV or 10^7 K
Acceleration	10^{21} g
Density	Nc or solid

Lasers create positrons indirectly through two processes using targets with high atomic numbers

Bethe-Heitler Process

$$\sigma_{BH} \propto Z^4$$

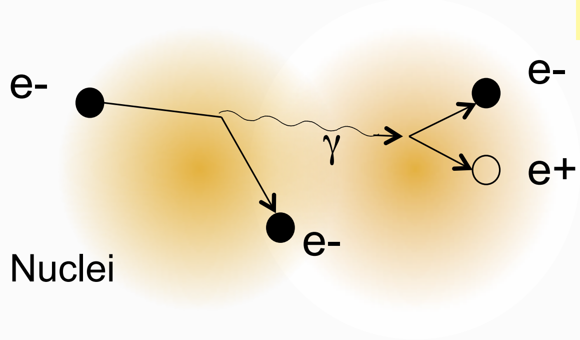

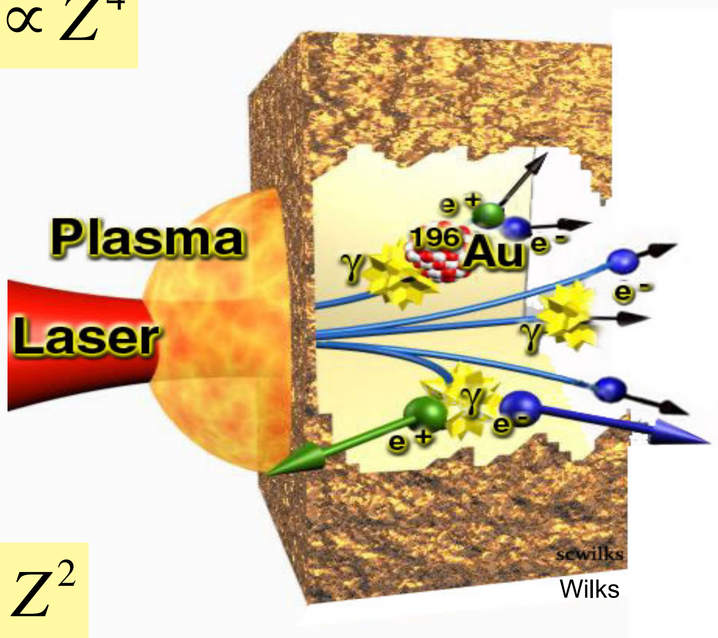

Trident process

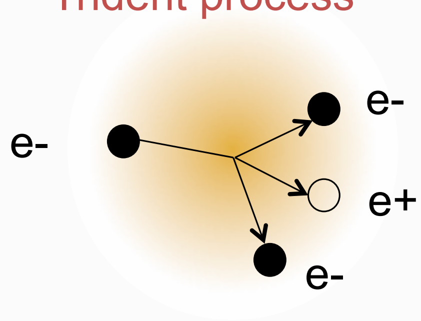

$$\sigma_{Tri} \propto Z^2$$

Heitler, 1954

Pair production probability is greatly enhanced by the nuclear field as momentum conservation is more easily preserved.

Laser-produced relativistic particles form jets at the back of the target

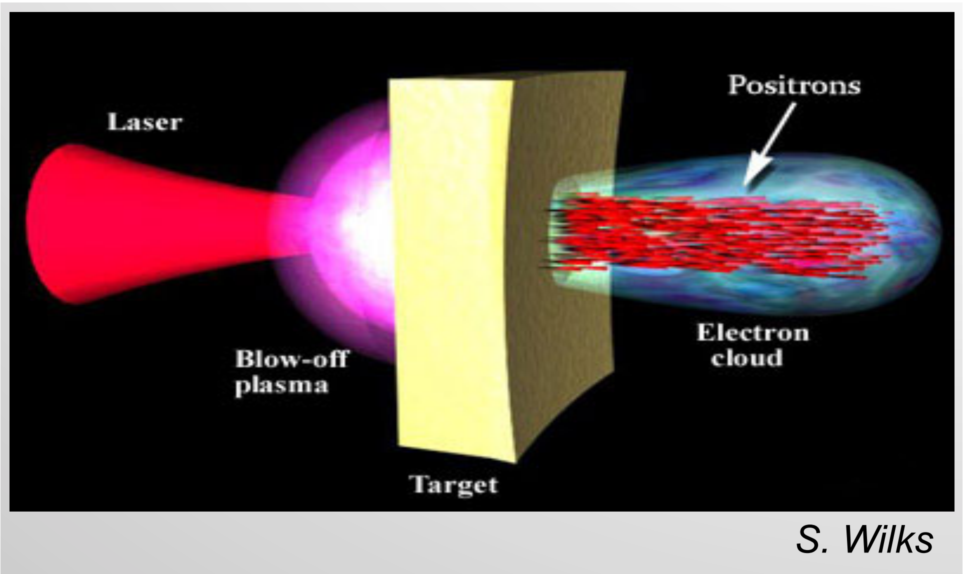

S. Wilks

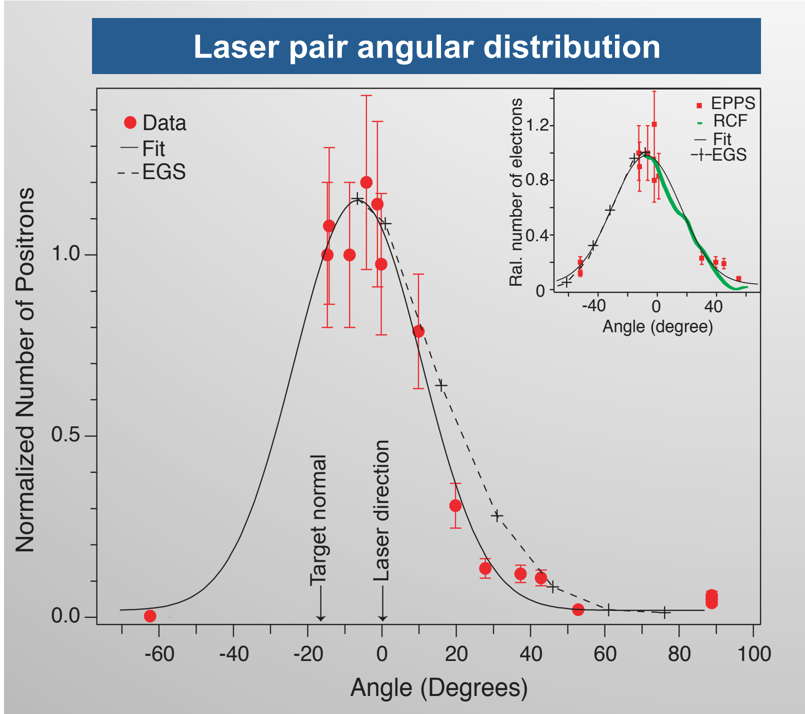

Chen *et al.*, PRL 2010

Jet angular spread is ~20°-30° and is shaped by electromagnetic fields in the target.

A non-linear scaling was found in positron data from Titan, EP and Orion experiments

Positron number ~ E^2

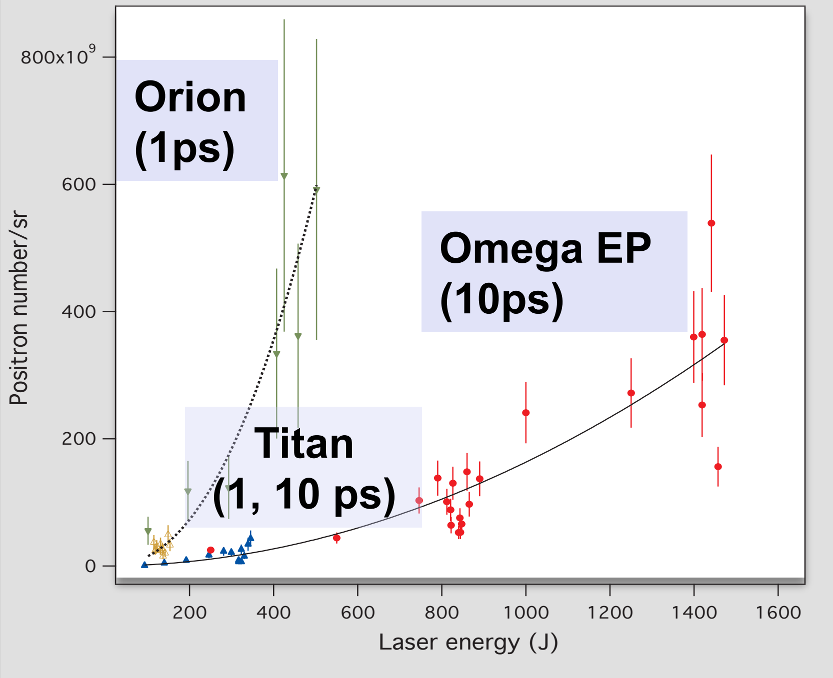

Norm. positrons ~ $I_{laser}^{1.1}$

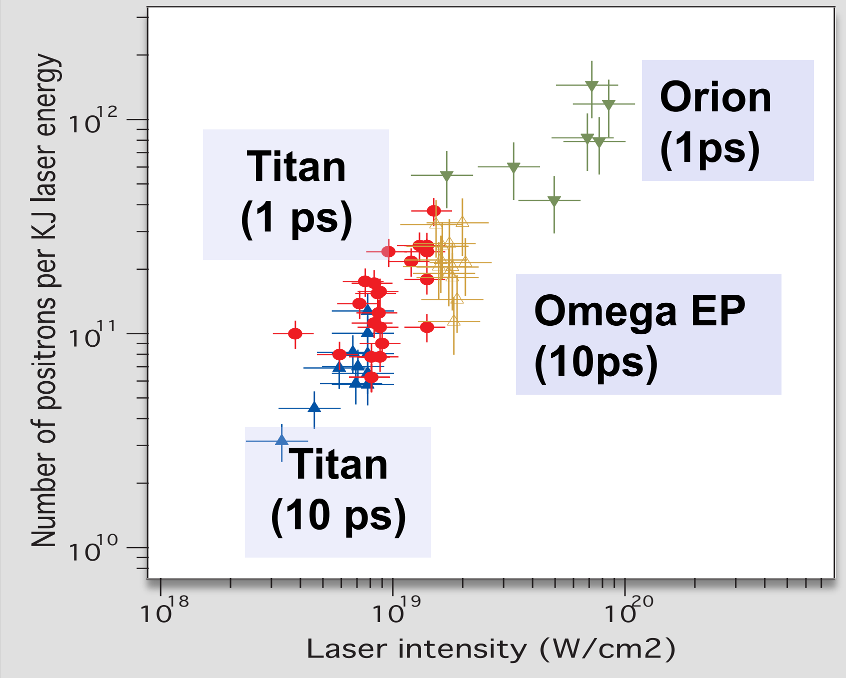

Chen, Fiuza, Sentoku et al. PRL, 2015

Myatt, et al. PRE 2009

Positron number shows a ~E^2 dependence for both 1 ps and 10 ps shots.

Laser-produced pair jets are approaching those needed for laboratory astrophysics experiments

Parameter	Exp. Value*	Desired for astro. relevant exp.**	
$T_{//}$	0.5 - 4 MeV	~ MeV	✔
$T_{\perp}$	0.2-1 MeV	~ MeV	✔
n_{e+}	$\sim 10^{11-13}$ cm^{-3}	$>10^{14-16}$ cm^{-3}	
n_{e-}	$\sim 10^{12-15}$ cm^{-3}	$>10^{14-16}$ cm^{-3}	✔
τ_{Jet}	5 – 30 ps	10-100 ps	✔

*Chen, et al. PRL 2010; HEDP 2011; POP 2014

**Fiuza et al., in preparation

The most obvious needs are to (1) increase the density of the pair jets and (2) reduce the electron/positron density ratio

Relativistic particles can be further collimated by applying an external magnetic field

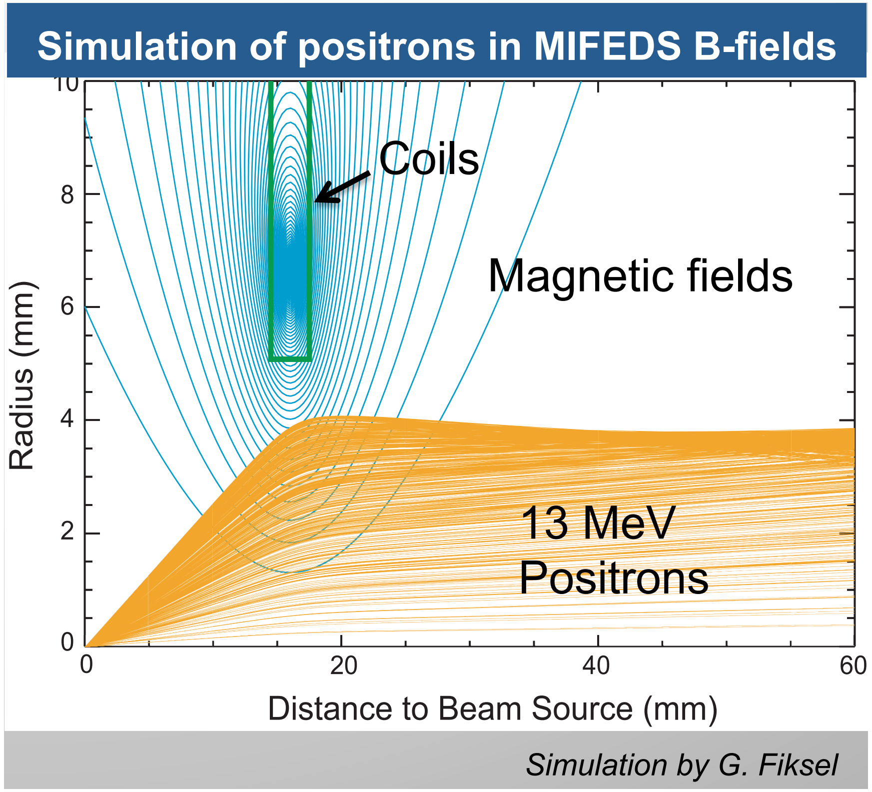

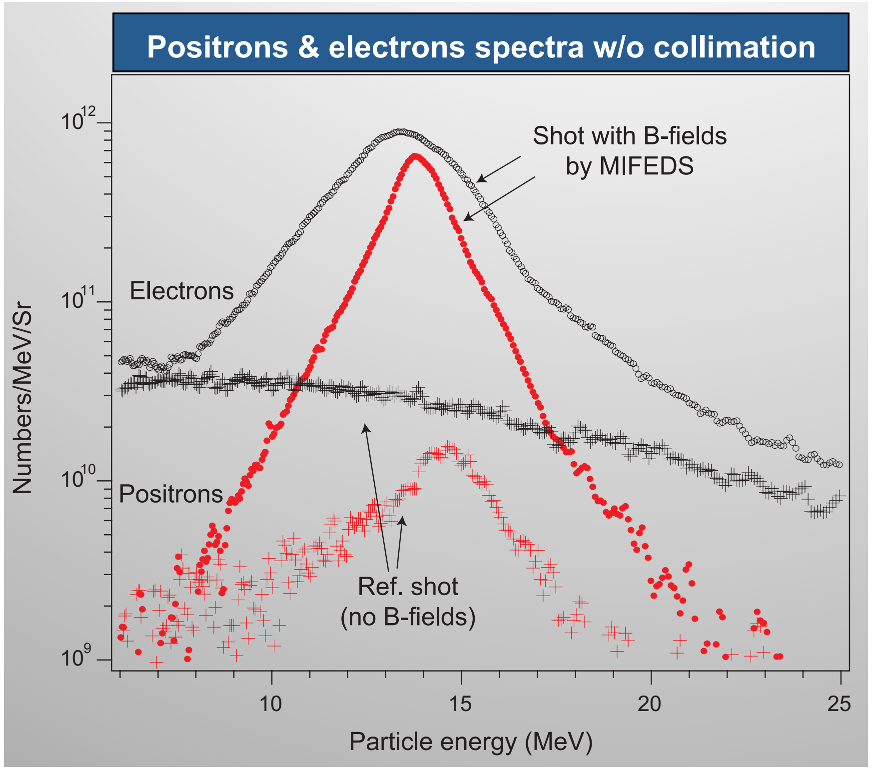

The effective divergence is reduced to 5° and the charge ratio (e-/e+) has reduced from ~100 to ~5

Outline

- High-Energy-Density (HED) Plasma
  - US facilities

Zylstra et al. (MIT)

- Plasma Nuclear Science using ICF-like implosions
  - p-p chain at relevant Gamow energies

Drake, Kuranz et al. (UM)

- Laser-produced Magnetohydrodynamics
  - similarity conditions
  - Rayleigh-Taylor growth in core-collapse SNe

Park, Huntington et al. (LLNL)

- Laser-produced Jets
  - ‘collisionless’ shocks
  - supersonic jet dynamics

Manuel, Kuranz et al. (UM)

Chen et al. (LLNL)

- Pair-Plasma Production
  - relativistic jets

- Summary

Laboratory experiments provide a complimentary technique to investigate some astrophysical systems

- High-power laser facilities provide a versatile environment to generate physical conditions similar to those in multiple astrophysical systems

- Laboratory results are directly scalable when similarity and geometric conditions hold between the two systems

- Experiments also allow for detailed benchmark comparisons with numerical calculations in relevant dynamic regimes

The Discovery Science Program allows basic science to be studied on the NIF

Stellar reaction rates

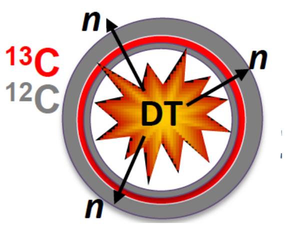

Dawn Shaughnessy
(LLNL)

Laser driven proton beams

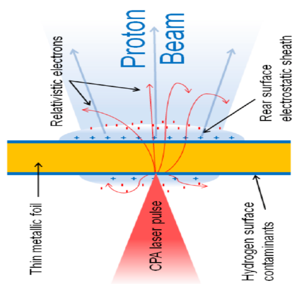

Tammy Ma
(LLNL)

High pressure, compressed carbon

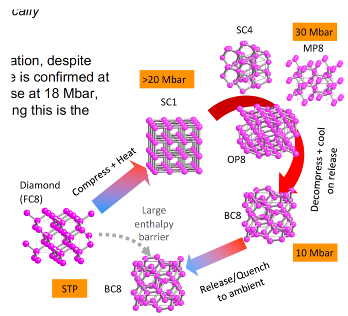

Justin Wark
(Univ. Oxford)

Planar direct drive hydrodynamics

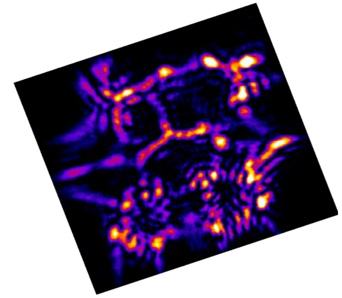

Alexis Casner
(CEA)

Particle acceleration from turbulence

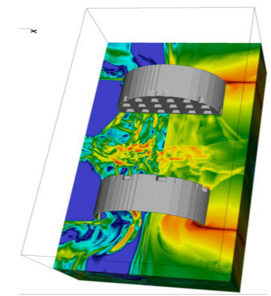

Gianluca Gregori
(Univ. Oxford)

Collisionless shock particle acceleration

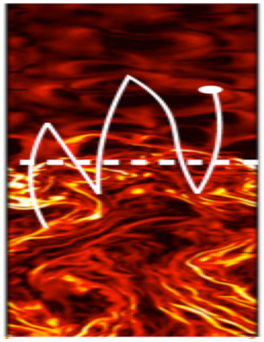

Frederico Fiuza
(SLAC)

Brown dwarf interiors: high-P properties of Be

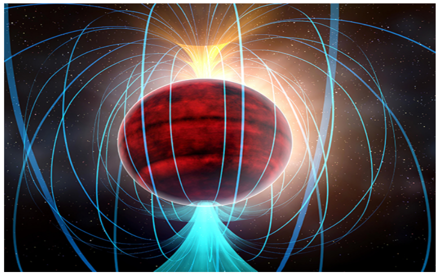

Ronald Redmer
(U. Rostock)

Charged particle stopping powers

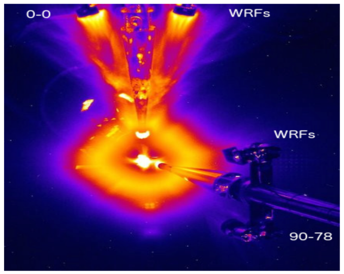

Alex Zylstra
(LANL)

Low-Z elements at Gbar pressures

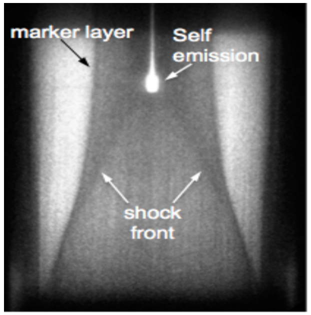

Roger Falcone
(UC Berkeley)

Dense hydrogen near the melt curve

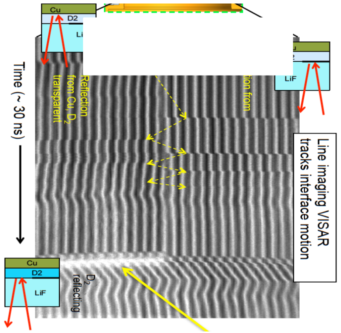

Raymond Jeanloz
(UC Berkeley_

Questions?

Backup Slides

To understand stars we must understand how fast they burn by measuring reactivity <**σv**> or cross section **σ**

$$\langle \sigma v \rangle \propto \int_0^\infty E e^{-E/T} \; \sigma(E)\, dE$$

The astrophysical S-factor parameterizes the slowly varying portion of the nuclear reaction cross section

$$\sigma(E) = \frac{1}{E} e^{-\sqrt{E_G/E}} S(E)$$

Geometric

Barrier Penetrability

$$\langle \sigma v \rangle \approx \sqrt{\frac{2\,\tau}{m_r T}\,\frac{4}{3}}\;\; S(E_0)\, \left(1 + \frac{5}{12\tau}\right) e^{-\tau}$$

NIF experiments allow measurements at lower Gamow energies closer to the solar Gamow peak

$$\langle \sigma v \rangle \propto \int_0^\infty E e^{-E/T} \; \sigma(E)\, dE$$

$$\sigma(E) = \frac{1}{E} e^{-\sqrt{E_G/E}} S(E)$$

$$\langle \sigma v \rangle \approx \sqrt{\frac{2\,\tau}{m_r T}} \; \frac{4}{3} \; S(E_0) \left(1 + \frac{5}{12\tau}\right) e^{-\tau}$$

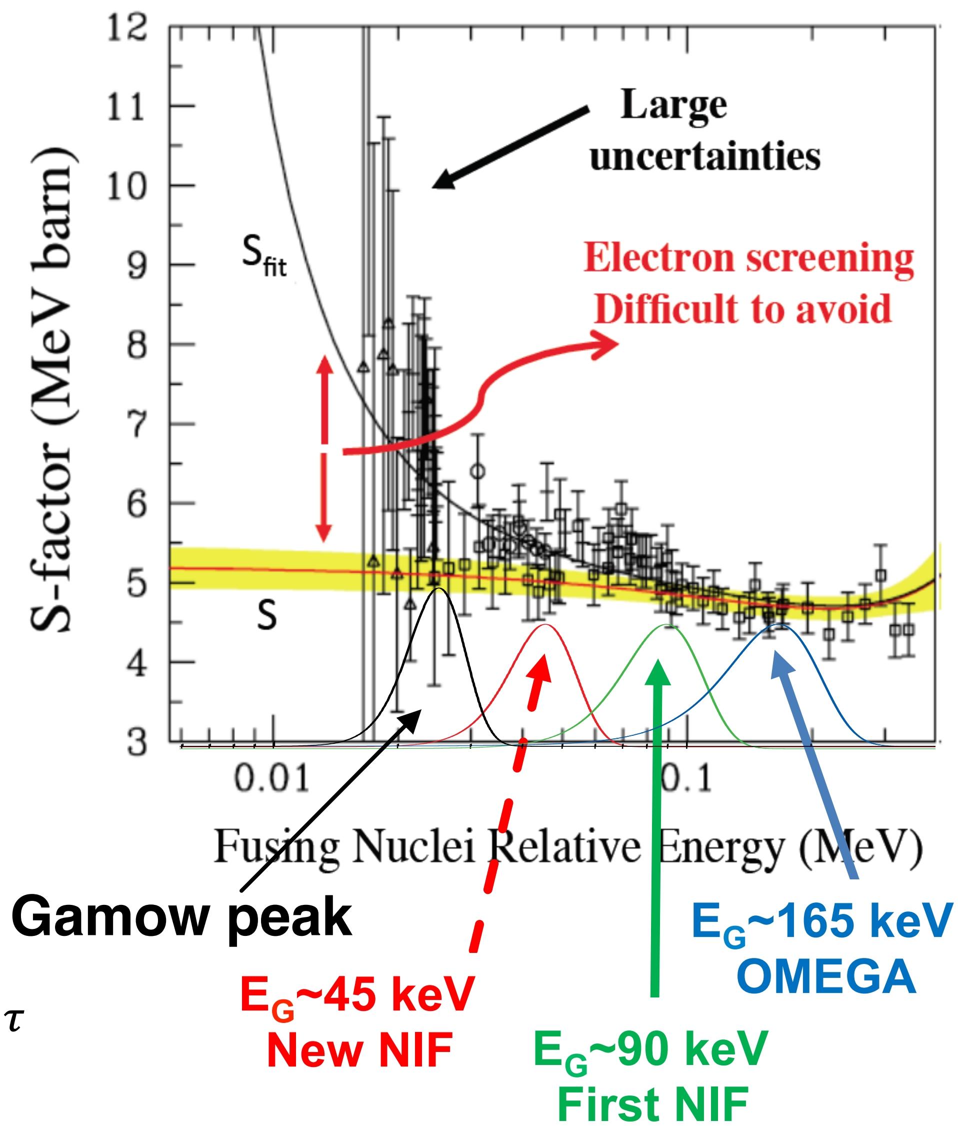

Recent experiments implemented a Gamma Cerenkov Detector (GCD) to measure D+p 5.5 MeV γ-rays

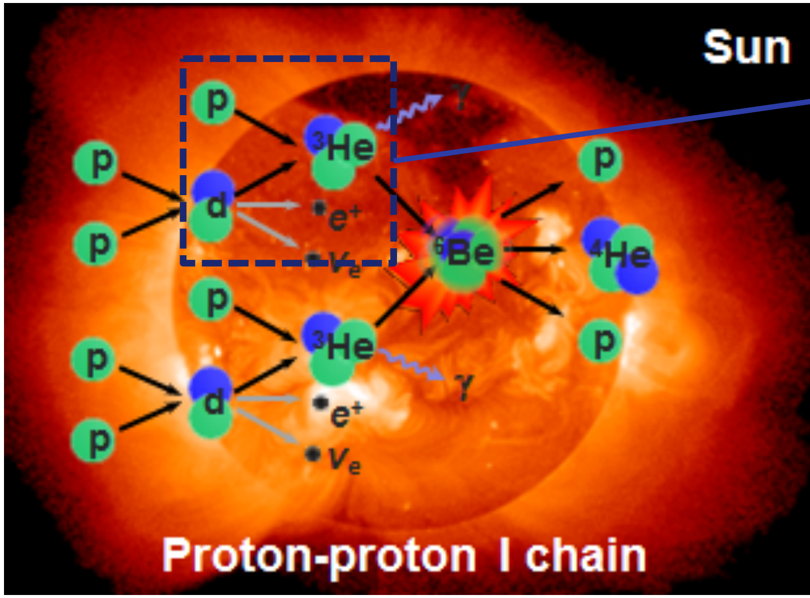

T_i ~ 5-12 keV

E_G ~ 10-30 keV

D + p → ^{3}He + γ (5.5 MeV)

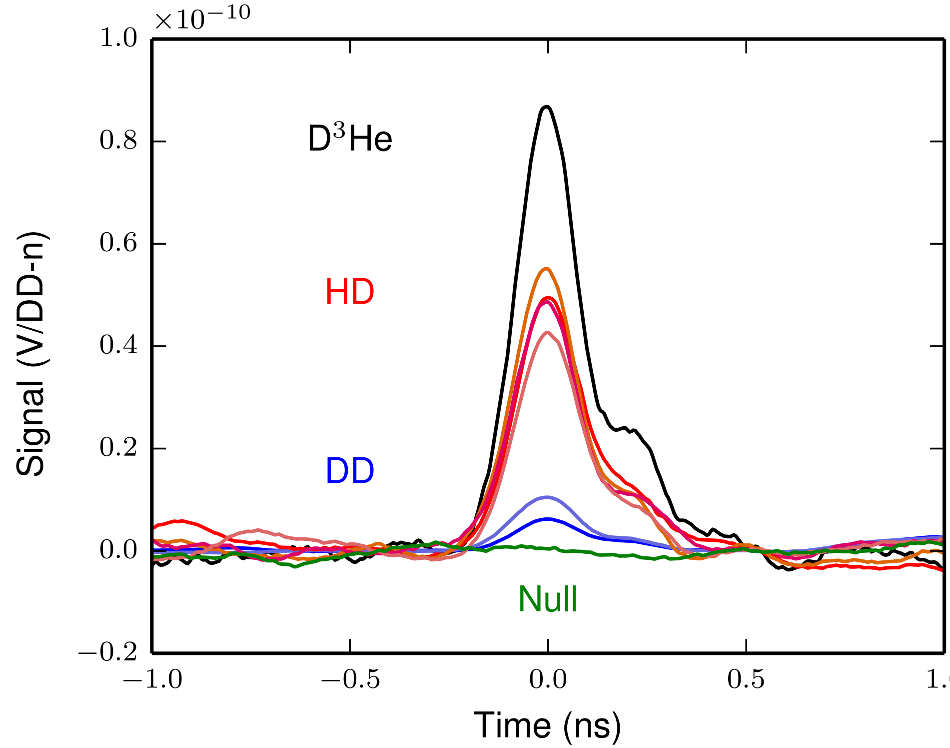

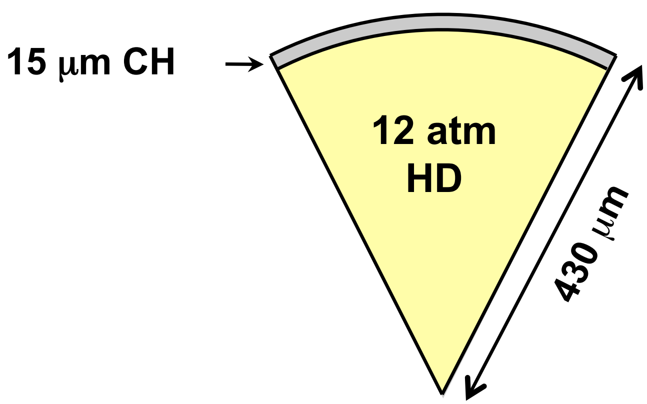

Precise understanding of this reaction at low Gamow energy is important for protostars and brown dwarfs.

Using inertial fusion plasmas to study nuclear physics reactions is a growing topic with several high-profile recent results

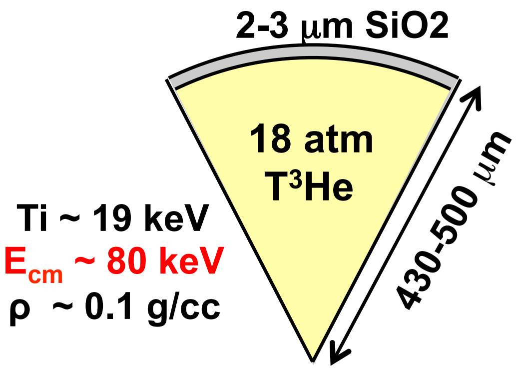

Glass capsule driven by the OMEGA laser, spherically-converging shock generates ~20keV ion temperature plasma

Gammas measured with Cherenkov detector[3]

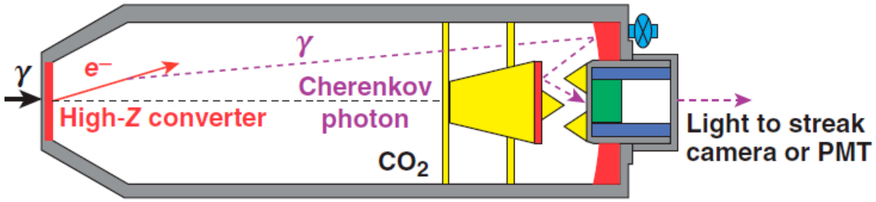

A.B. Zylstra et al., Phys. Rev. Lett. 117, 035002 (2016)

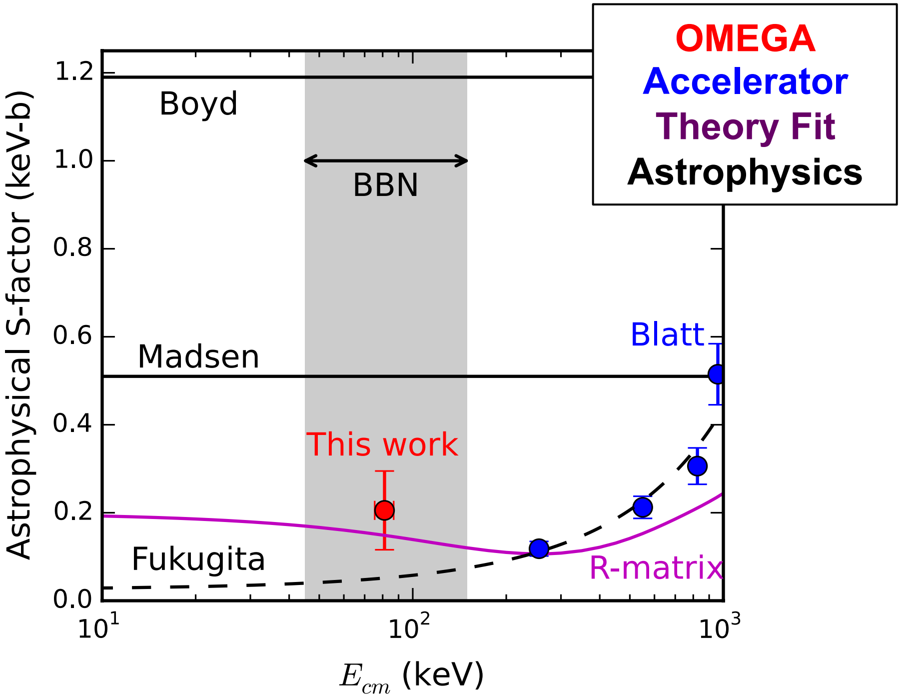

This reaction rate cannot explain high ^6Li levels in primordial material.

J. Mack et al., NIMA 513, 566 (2003)
S.L. Blatt et al., Phys. Rev. (1968)
Fukugita et al., PRD (1990)
Madsen et al., PRD (1990)
Boyd et al., PRD (2010)

NIF Rad-SNRT Team

Principal Investigator: Carolyn Kuranz
Liaison scientist: Hye-Sook Park (LLNL)

University of Michigan Participants

Carolyn Kuranz (Research Scientist, PI)
Paul Drake (Professor)
Carlos Di Stefano (Graduate Student)
Willow Wan (Graduate Student)
Sallee Klein (Research Engineer)

Additional Participants

Bérénice Loupias (CEA)
Tomasz Plewa (Florida State),
David Arnett (Univ. of Arizona)
Craig Wheeler (Univ. of Texas)
Jon Larsen (Cascade Sciences)

LLNL/GA/LANL Participants

Hye-Sook Park (experiment, RI)
Chan Huntington (experiment)
Dan Kalantar (experiment)
Steve MacLaren (design)
Aaron Miles (design)
Kumar Raman (design)
Bruce Remington (science)
Harry Robey (design)
Shon Prisbrey (design)

Forrest Doss (LANL, design)
Kirk Flippo (LANL, experiment)
John Kline (LANL, science)
George Kyrala (LANL, science)

Emilio Giraldez (GA, target)
Alex Hamza (target)
Abbas Nikroo (GA, target)
Russell Wallace (TFE)
Joe Kilkenny
Mike Farrell (GA, target)

We completed 3 shot day campaign each improving data quality

N150111-001
Low drive, 26 ns

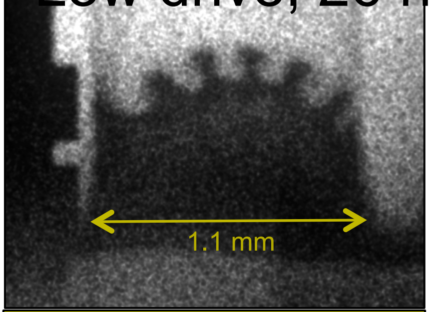

Good data but non-

N150406-001
Low drive, 28 ns

N150406-002
High-drive, 17 ns

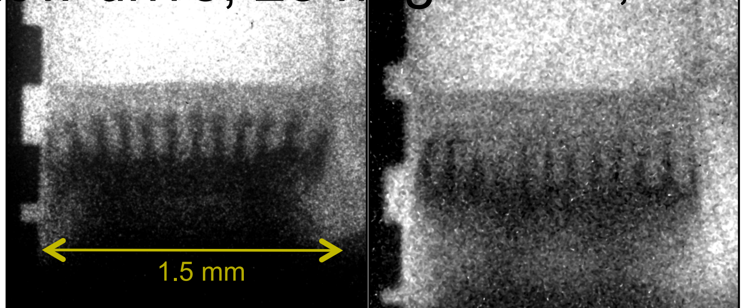

Planarity achieved; but low SNR for high-drive

N150601-004
High-drive, 15 ns

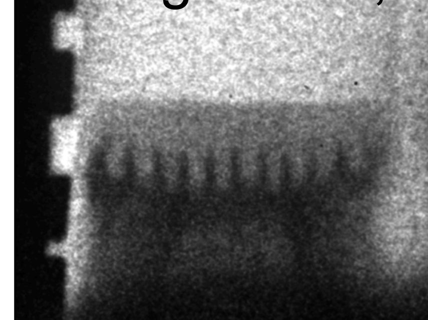

Good SNR for high-drive

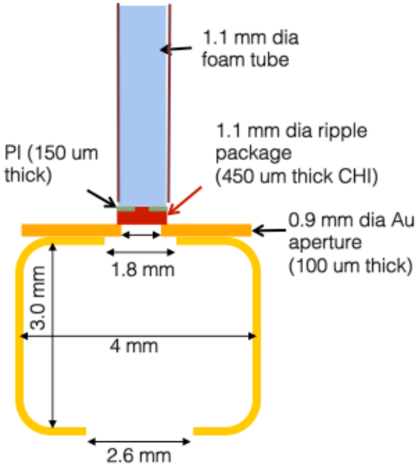

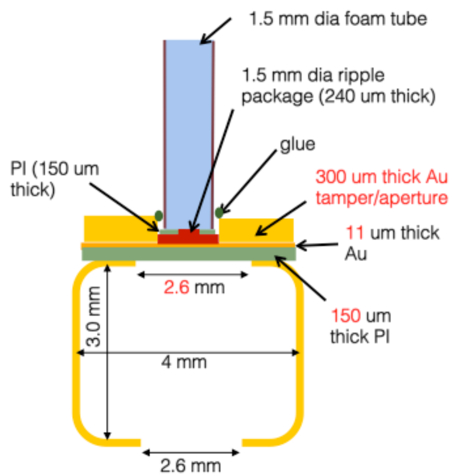

0.5mm Au
+0.5 mm CH

RSNRT Full Data Set Complete: April + S08, S09 and S10 (fired June 1, 2015)

Low-Drive 230 eV

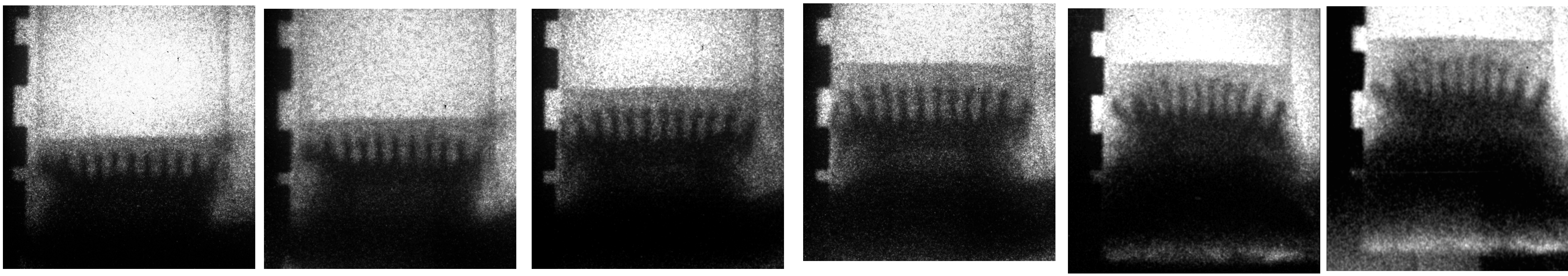

23ns 25ns 28ns 30ns 32ns 34ns

April

S09

High-Drive 325 eV

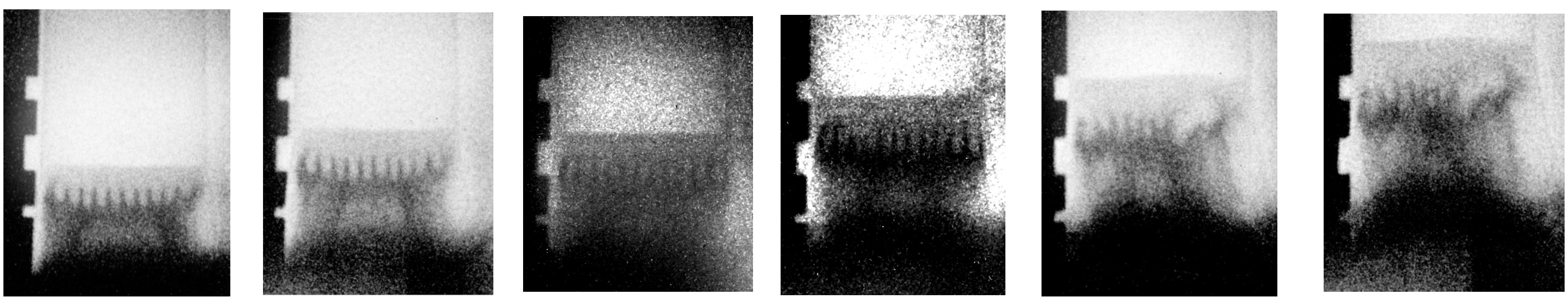

13 ns 15 ns 15 ns 17 ns 18 ns 20ns

S10

April

S08

NIF

Preshot simulation over-predicts the shock velocity and interface position

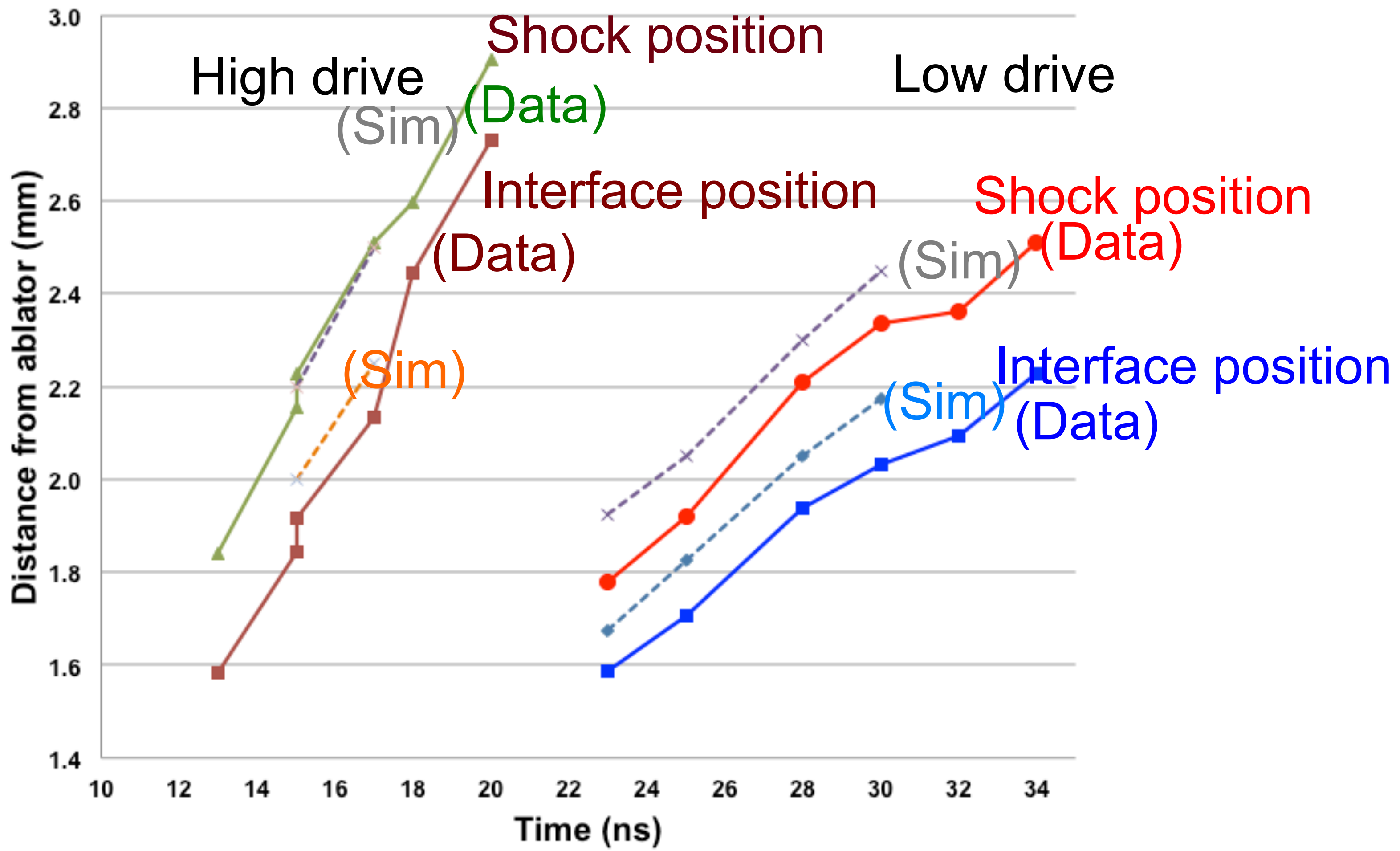

- Measurement at a same time repeated within the error
- Data analysis in progress
- Post-shot simulation in progress

International team (ACSEL collaboration):

Princeton University (USA):	<u>A. Spitkovsky</u>
LLNL (USA):	C. Huntington, H.-S. Park, C. Plechaty, S. Ross, B. Remington, D. Ryutov
LLE, Univ. of Rochester (USA):	G. Fiksel, P.-Y. Chang, D. Froula, J. Knauer
Osaka University (Japan):	Y. Sakawa, H. Takabe, Y. Kuramitsu, T. Morita
Oxford University (UK):	G. Gregori, J. Meinecke, A. Bell
LULI (France):	M. Koenig, A. Ravasio, A. Pelka, T. Vinci, C. Riconda, R. Yurchak
ETH Zurich (Switzerland):	F. Miniati
York University (UK):	N. Woolsey
Rice University (USA):	E. Liang, M. Levy
University of Michigan (USA):	R. P. Drake, M. Grosskopf, C. Kuranz, E. Rutter

Numerical modeling suggests that both scattering mechanisms may produce shocks

self-generated magnetic fields (filamentation/Weibel instability)

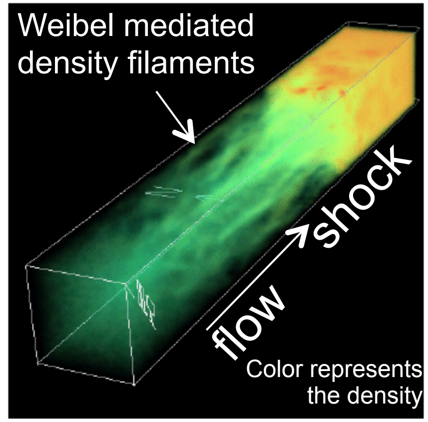

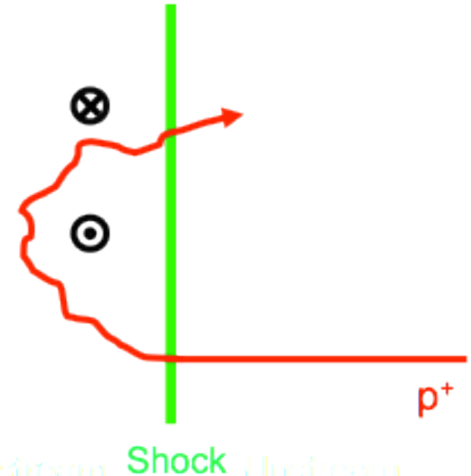

Compressed pre-existing fields

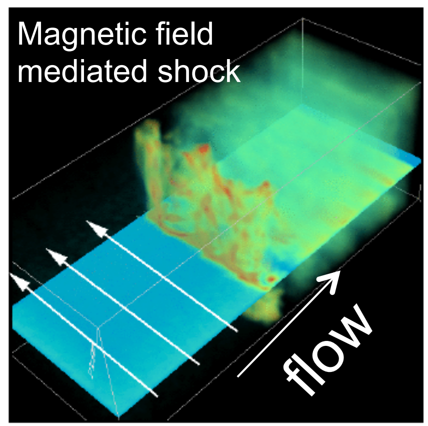

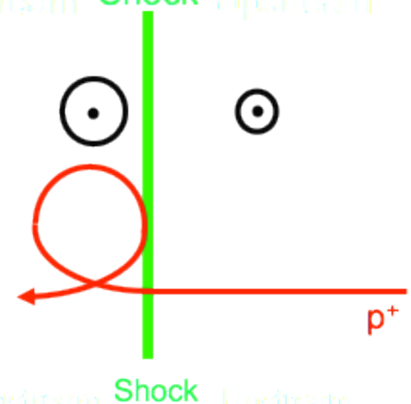

Proton images at different times illustrate B-field evolution

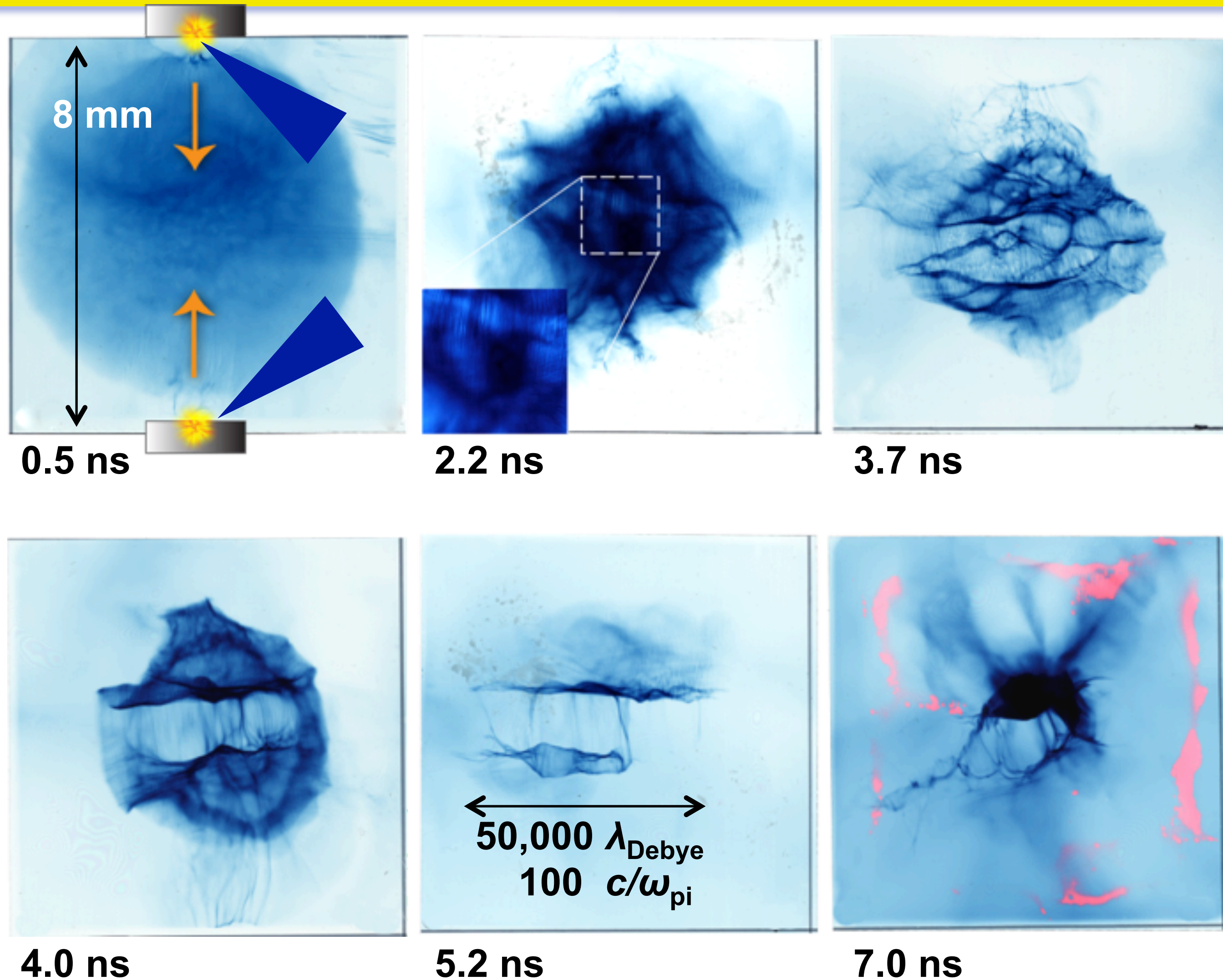

Proton images side-on view 7 to 8 MeV

Further work is needed to extend the spatial scales to allow for collisionless shock formation

Future NIF experiments to create optimal condition for creating fully-formed collisionless shocks

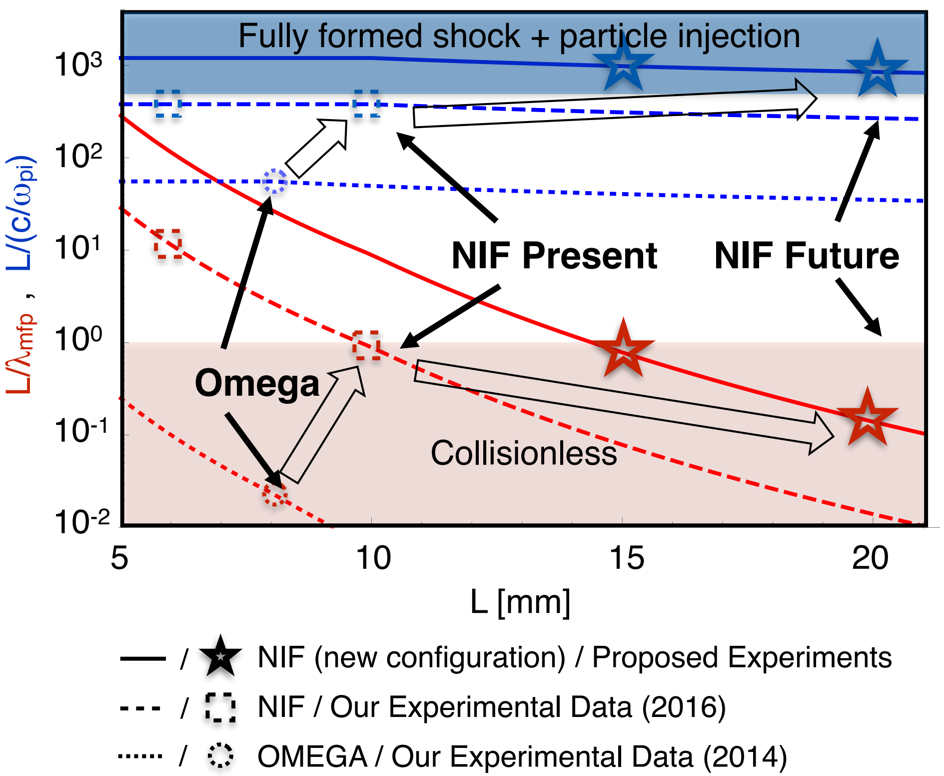

Weibel Instability Scale length

$$\frac{c}{\omega_{pi}} \propto \frac{1}{\sqrt{n_i}} \frac{\sqrt{A}}{Z}$$

Collisional Mean-free-path

$$\lambda_{mfp} \propto \left(\frac{A}{Z}\right)^2 \frac{\Delta v^4}{Z^2 n_i}$$

Need to increase $L/(c/\omega_{pi})$
Need to decrease L/λ_{mfp}

- Future collisionless shock experiments optimizes the flow velocity and density
- Optical Thomson Scattering and particle spectrometers will be the main diagnostics

A custom-designed ~1-mm^3 B-dot probe spatially resolved the axial magnetic-field strength in the solenoid gap

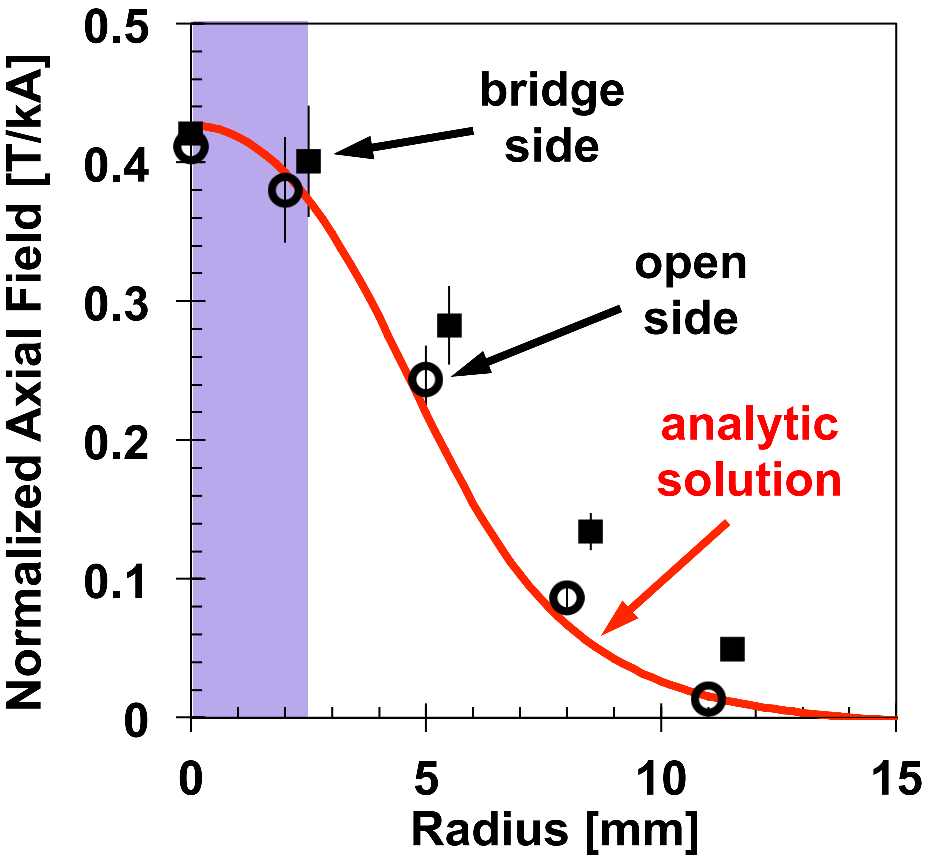

Top View

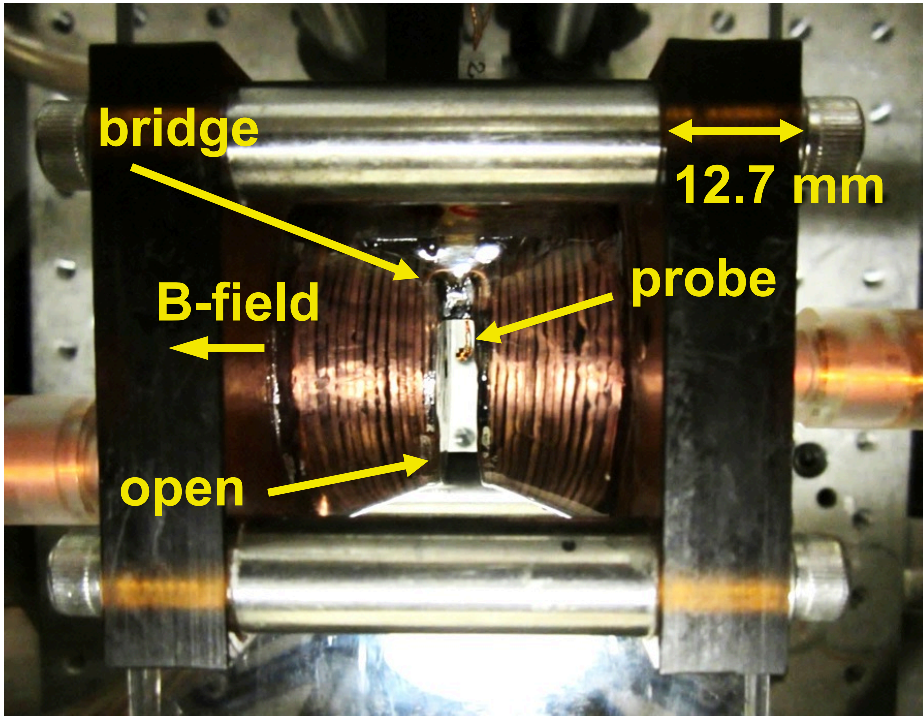

B-field measurements demonstrate a <5% spatial variation within a 2.5 mm radius of the gap center.

Radiation-hydrodynamic calculations predict inertial collimation in the breakout plasma of conical targets

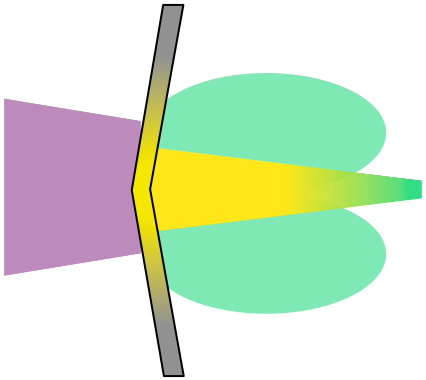

Schematic

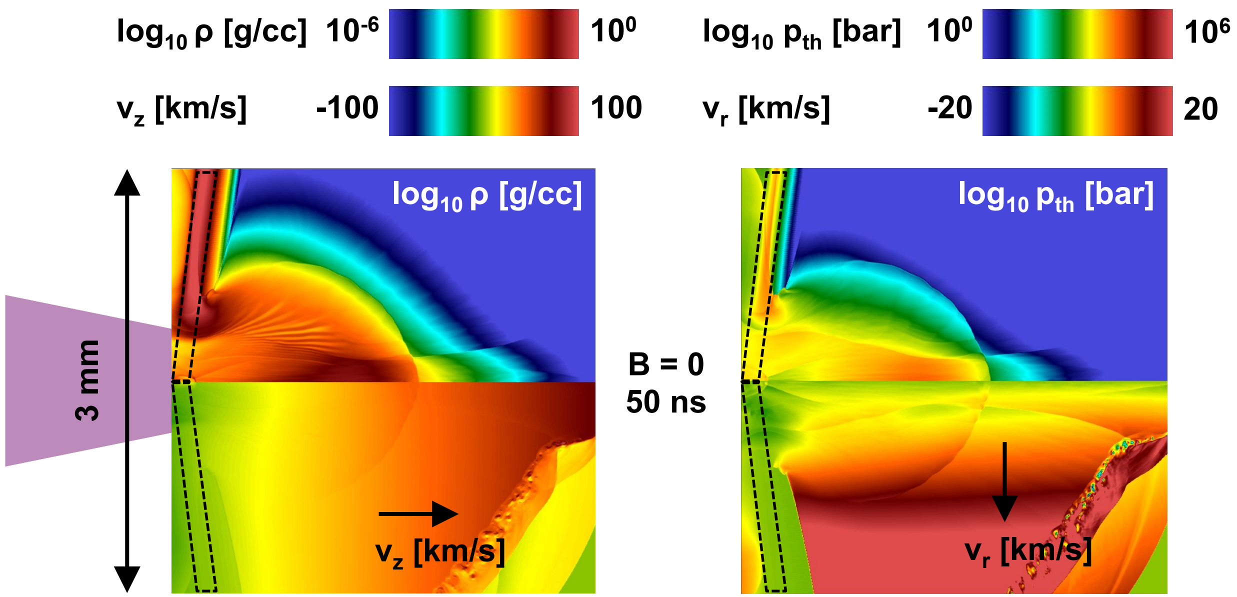

FLASH Results

Pinching in this geometry is proposed as a mechanism that can form astrophysical jets from isotropic, stellar outflows

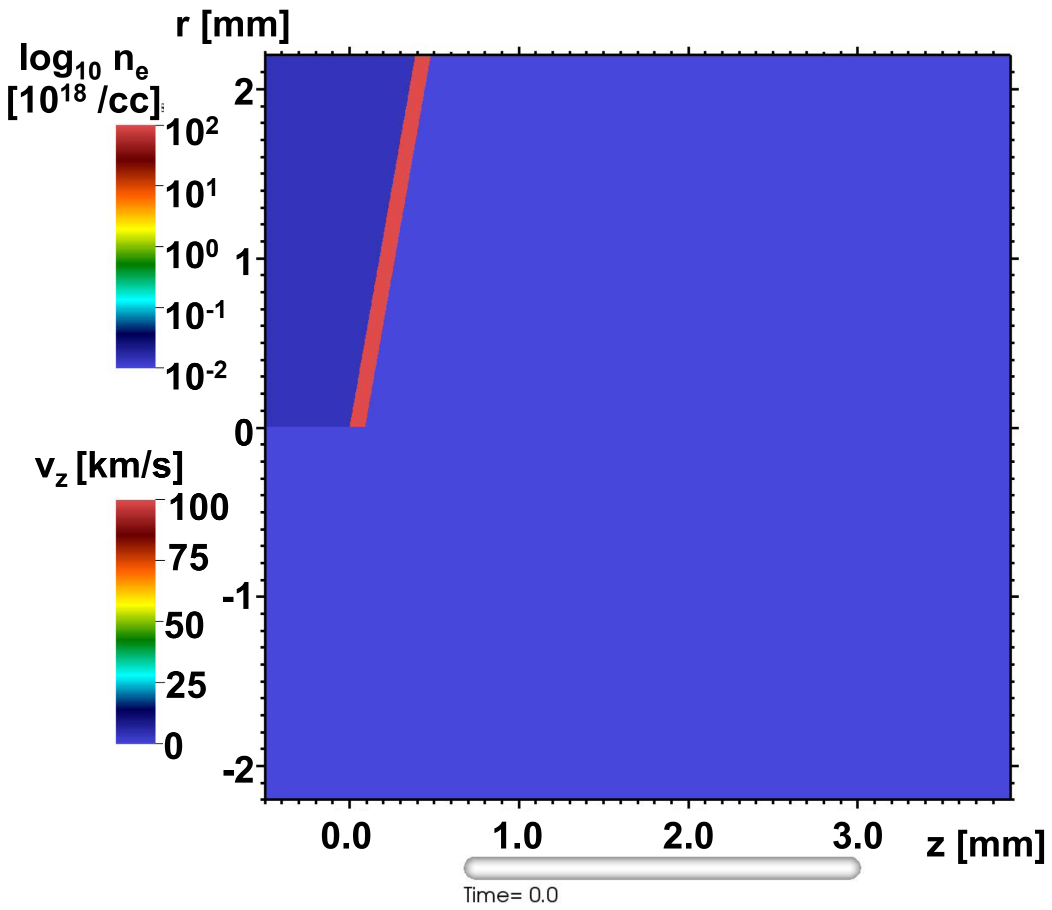

Pair production was shown to be primarily made through the Bethe-Heitler process

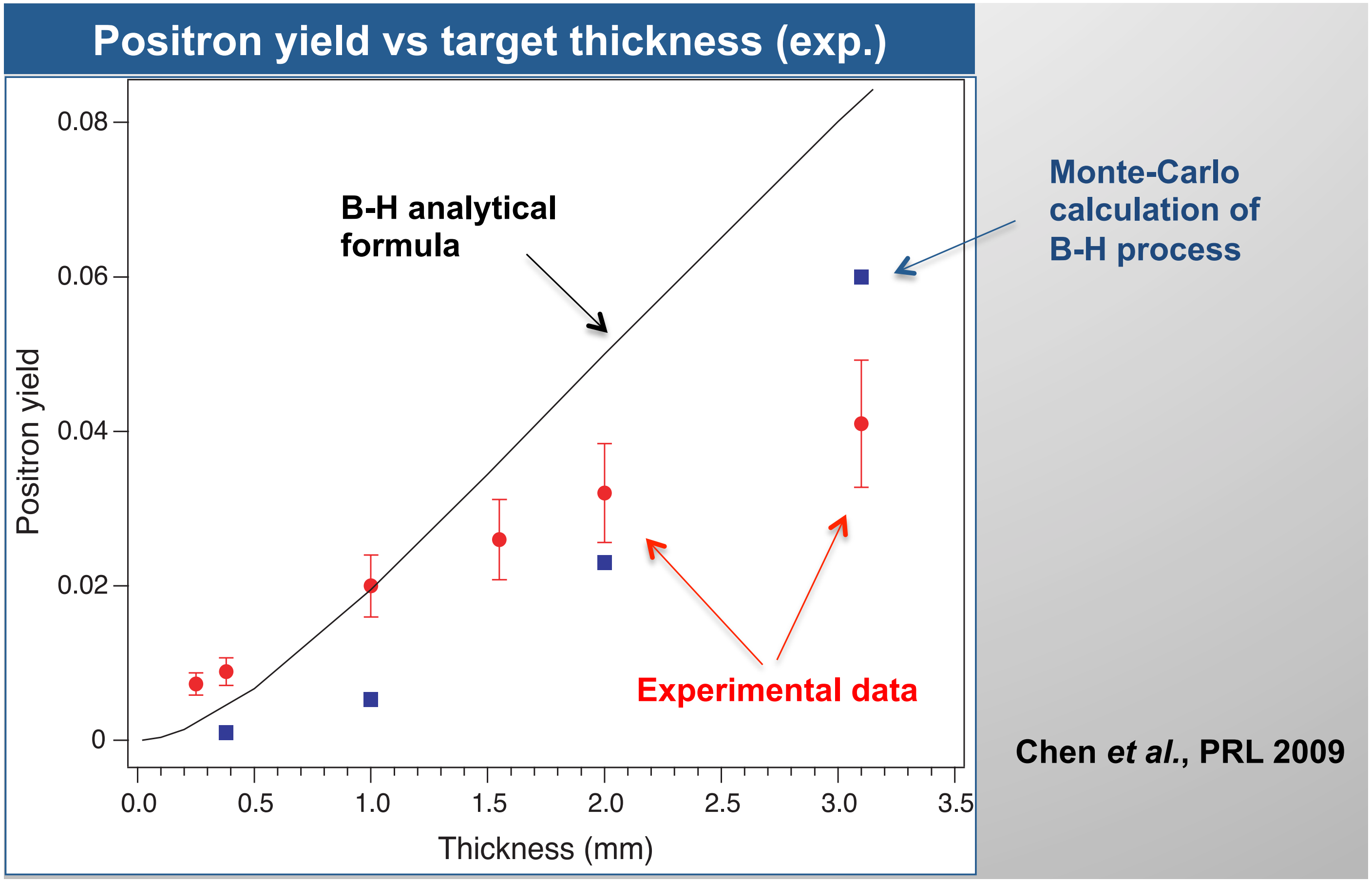

Due to the Z^4 dependence and necessity for 2 reactions for BH pair production, BH dominates for thicker targets (>20 μm).